AD-A173 255 DELAMINATION FRACTURE IN GRAPHITE/EPOXY MATERIALS(U) 1/2
TEXAS A AND M UNIV COLLEGE STATION DEPT OF MECHANICAL
ENGINEERING W L BRADLEY JUN 86 AFOSR-TR-86-0941
UNCLASSIFIED AFOSR-84-0064 F/G 11/4 NL

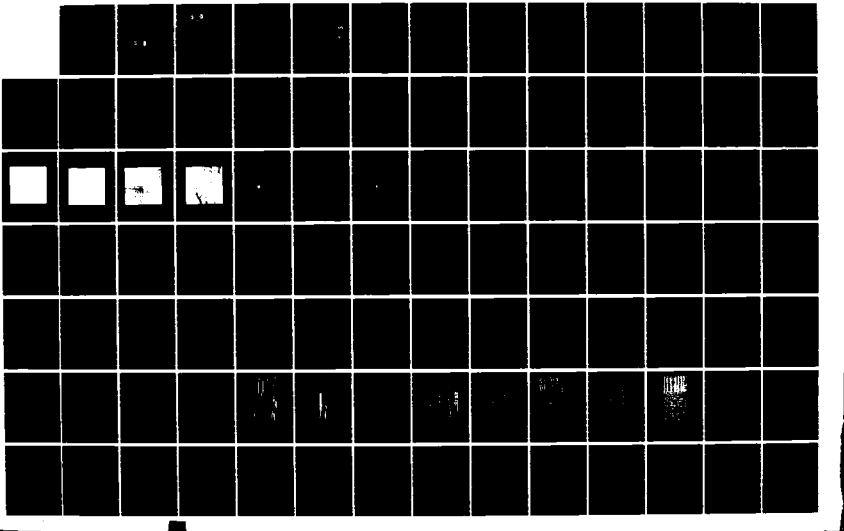

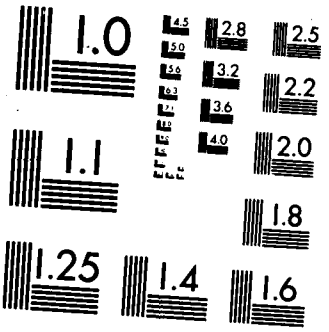

AFOSR-TR- 86-0941

unclassified
SECURITY CLASSIFICATION OF THIS PAGE

ADA173255

## REPORT DOCUMENTATION PAGE



| | |
|---|---|
| 1a. REPORT SECURITY CLASSIFICATION: unclassified | 1b. RESTRICTIVE MARKINGS |
| 2a. SECURITY CLASSIFICATION AUTHORITY | 3. DISTRIBUTION/AVAILABILITY OF REPORT: Approved for public release, distribution unlimited |
| 2b. DECLASSIFICATION/DOWNGRADING SCHEDULE | |
| 4. PERFORMING ORGANIZATION REPORT NUMBER(S) | 5. MONITORING ORGANIZATION REPORT NUMBER(S): AFOSR-TR- 86-0941 |
| 6a. NAME OF PERFORMING ORGANIZATION: Mechanical Engineering, Texas A&M University; 6b. OFFICE SYMBOL (If applicable) | 7a. NAME OF MONITORING ORGANIZATION: AFOSR/NA |
| 6c. ADDRESS (City, State and ZIP Code): College Station, Texas 77843 | 7b. ADDRESS (City, State and ZIP Code): Building 410, Bolling AFB, DC 20332-6448 |
| 8a. NAME OF FUNDING/SPONSORING ORGANIZATION: AFOSR; 8b. OFFICE SYMBOL (If applicable): NA | 9. PROCUREMENT INSTRUMENT IDENTIFICATION NUMBER: Grant No. AFOSR-84-0064 |
| 8c. ADDRESS (City, State and ZIP Code): Building 410, Bolling AFB, DC 20332-6448 | 10. SOURCE OF FUNDING NOS. — PROGRAM ELEMENT NO.: 61102F; PROJECT NO.: 2302; TASK NO.: B2; WORK UNIT NO.: |
| 11. TITLE (Include Security Classification): Delamination Fracture in Graphite/Epoxy Materials | |
| 12. PERSONAL AUTHOR(S): Walter L. Bradley | |
| 13a. TYPE OF REPORT: Annual; 13b. TIME COVERED: FROM 4/1/85 TO 3/31/86 | 14. DATE OF REPORT (Yr., Mo., Day): June, 1986; 15. PAGE COUNT: 179 |
| 16. SUPPLEMENTARY NOTATION | |
| 17. COSATI CODES — FIELD / GROUP / SUB. GR. | 18. SUBJECT TERMS (Continue on reverse if necessary and identify by block number): Composites; Fracture of Composites; Mode II Fracture; Delamination; Mixed Mode Fracture |

19. ABSTRACT (Continue on reverse if necessary and identify by block number)

In-situ observations of delamination fracture in the scanning electron microscope have indicated that a well defined damage zone develops in advance of the crack tip. The size of this damage zone which consists of microcracks depends on both matrix ductility and mode of loading. Delamination fracture is often dominated by interfacial failure, indicating that tougher resins will not necessarily enhace delamination fracture toughnesses unless the interface is also proportionately tougher. Strain field mapping based on an experimentally measured displacement fields and finite element analysis based on orthotropic linear elastic constitutive properties of the material are consistent with the observed damage zone size and shape determined through the in-situ fracture observations.

Delamination fracture toughness has been observed to increase monotonically with increasing mode II component of loading in brittle systems, with $G_{IIc} / G_{Ic} = 3$ for brittle systems. The delamination fracture toughness of composites with very ductile matrices is relatively insensitive to the loading mode. Micromechanistic interpretations for these observations have been made based on direct observations of fracture in the SEM.

| | |
|---|---|
| 20. DISTRIBUTION/AVAILABILITY OF ABSTRACT: UNCLASSIFIED/UNLIMITED ☒ SAME AS RPT. ☐ DTIC USERS ☐ | 21. ABSTRACT SECURITY CLASSIFICATION: unclassified |
| 22a. NAME OF RESPONSIBLE INDIVIDUAL: Dr. Anthony Amos | 22b. TELEPHONE NUMBER (Include Area Code): (202) 767-4937; 22c. OFFICE SYMBOL: NA |

DD FORM 1473, 83 APR — EDITION OF 1 JAN 73 IS OBSOLETE.



SECURITY CLASSIFICATION OF THIS PAGE

19 (Continuation)

A J-integral approach for mode I delamination of a split laminate specimen has been developed. Experimental work to confirm the approach is under way .

## TABLE OF CONTENTS

## 1.0 SUMMARY

In-situ observations of delamination fracture in the scanning electron microscope have indicated that a well defined damage zone develops in advance of the crack tip. The size of this damage zone which consists of microcracks depends on both matrix ductility and mode of loading. Delamination fracture is often dominated by interfacial failure, indicating that tougher resins will not necessarily enhance delamination fracture toughnesses unless the interface is also proportionately tougher. Strain field mapping based on an experimentally measured displacement fields and finite element analysis based on orthotropic linear elastic constitutive properties of the material are consistent with the observed damage zone size and shape determined through the in-situ fracture observations.

Delamination fracture toughness has been observed to increase mononotically with increasing mode II component of loading in brittle systems, with $G_{IIc}/G_{Ic} = 3$ for brittle systems. The delamination fracture toughness of composites with very ductile matrices is relatively insensitive to the loading mode. Micromechanistic interpretations for these observations have been made based on direct observations of fracture in the SEM.

A J-integral approach for mode I delamination of a split laminate specimen has been developed. Experimental work to confirm the approach is under way.

## 2.0 OBJECTIVES

The objectives of the research program proposed herein are:

2.1 to better define the deformation and fracture physics of delamination fracture in graphite/epoxy composite materials so that realistic micromechanics models of matrix dominated fracture can be developed; and

2.2 to develop and refine reliable experimental and analytical techniques to measure mode I, mode II and mixed mode delamination fracture of both unidirectional and multidirectional composite laminates to provide meaningful design parameters and benchmarks against which predictions of the various micromechanics models may be tested.

## 3.0 SUMMARY WORK STATEMENT

The following areas of work have been performed to achieve the stated objectives:

3.1 in-situ fracture studies in a scanning electron microscope (SEM) to better define the deformation and fracture processes which accompany mode I and mode II delamination fracture and delamination under compressive buckling conditions;

3.2 utilization of a technique to determine the strain field around a crack tip in a composite using displacement fields measured on specimens loaded in the SEM;

3.3 further refine testing and analytical techniques for characterizing mode I, mode II, and mixed mode delamination fracture using split laminates and distinguishing between initiation and propagation (or resistance curve) behavior;

3.4 develop a simple mathematical model consistent with the observations made in 3.1 and 3.2 which is capable of predicting the results obtained in 3.3.

## 4.0 SUMMARY OF ACCOMPLISHMENTS BY AREAS STATED IN WORK STATEMENT

### 4.1 In-Situ Fracture Observations

A new fixture has been designed and constructed to allow mode II delamination fracture to be performed in the scanning electron microscope (SEM). The fixture is essentially a three point bend fixture which uses a standard end-notch flexure test specimen (ENF).

The mode II delamination fracture of a very ductile system (T6C145/F185 by Hexcel) and a very brittle system (AS4/3502 by Hercules) have been studied this year. The size and shape of the damage zone for mode II delamination are very different from that previously observed for mode I delamination, as seen in Figures 1 and 2. Note the scale in the y-direction is much finer than the scale in the x-direction. Thus, the actual damage zone for mode II loading is much more long and narrow than it appears in Figures 1 and 2. Figure 3 shows the appearance of the damage zone as observed during delamination fracture in the SEM for AS4/3502. The details of the formation of the "hackles" which are characteristic of mode II delamination fracture of composites with a brittle resin are seen. By contrast, Figure 4 shows a much thicker damage zone for the T6C145/F185. This system shows a much greater amount of shear deformation, some microcracking but very few large "hackles" formed. Figures 5 and 6 show the post-mortem fractography for these systems, with "hackles" being the dominant feature in the AS4/3502 and shear deformation being the dominant feature in the T6C145/F185.

The difference in the size and shape of the damage zone

comparing mode I delamination to mode II delamination (compare Figures 1 and 2) can be understood in part to be a result of the difference in the stress fields for the two loading conditions. Figures 7-10 indicate the results of a finite element analysis for the test coupons loaded in mode I and mode II conditions. While we incorporated linear (orthotropic) constitutive material properties into the finite element analysis code used, making the results somewhat approximate, the difference in the shape of the respective stress fields and the different rates of decay of the stress fields are very consistent with the observations of damage zone size and shape shown schematically in Figures 1 and 2.

The size of the damage zone for several different composite material systems loaded in mode I is summarized in Table I. These results compare the damage zone size and shape as a function of matrix ductility whereas Figures 1 and 2 compare mode I loading to mode II loading. A comparison of Figure 1 to Figure 2 and a careful study of the results in Table I and II indicate the effect of resin mechanical properties on damage zone size and shape. The neat resin fracture toughness as well as the delamination fracture toughness for each system are also indicated for these same systems in Table II.

**4.2 Crack Tip Strain Field Measurements**

The strain field mapping technique using stereo-imaging has been developed and utilized to measure the strain field around a crack tip for mode I and mode II loading of AS4/3502. Results are presented in Figures 11 and 12. The relatively high levels of strain indicated would appear to be in error. However, a careful examination of mode II delamination in Figures 3 and 4

indicates that indeed very large local strains are involved through the microcracking damage that precedes crack advance. The stereo-imaging technique treats the material around the crack tip as if it is a continuum. Thus, voiding or microcracking will give a much higher indication of local strain than the resin could deliver in the absence of cracking or cavitation.

An alternative approach to mapping the strain field around a crack tip is currently being developed that is less tedious and more accurate than the current stereo-imaging technique being used. This technique will use a fine grid of points burnt onto the surface using a laser. The two dimensional grip will have points at five micron intervals. A photograph of the crack tip region prior to and after loading will allow a direct measurement of the displacement field, from which the strain field can be calculated.

**4.3 Fracture Mechanics Characterization of Materials**

Work in this area may be divided into two areas. First, we have continued to utilize already established techniques to characterize mode I and mode II delamination fracture toughness of materials where the test coupon geometry allows the determination of load-displacement curves which are essentially linear. Some of our results are summarized in Tables I and II.

Mixed mode I/mode II delamination studies have been made on several composite materials systems. These studies have been made using asymmetrically loaded split laminate specimens. The results indicate a monotonic increase in the total energy release rate with increasing mode II loading. This increase is greatest

for more brittle systems. The greater the observed increase in total energy release rate with increasing mode II loading, the more pronounced the observed hackle formation on the fracture surface. Composite materials with relatively ductile matrices do not form a very hackled surface, even for pure mode II loading, and they have a $G_{IIc}/G_{Ic}$ that is not very different from unity. Further details of this work are summarized in a paper entitled "Correlations Between Micromechanical Failure Processes and the Delamination Fracture Toughness of Graphite/Epoxy Systems" in Appendix I.

Mode I delamination of multiaxial layup specimens has been studied, with delamination as a function of layup stiffness for 0/0 ply angle at the delamination interface and for constant laminate stiffness but variable angle of plies across the delamination interface. The results so far indicate that the mismatch angle of the plies across the delamination interface does not significantly effect the delamination energy release rate for T6C145/F155. This resin is sufficiently viscous during processing that fiber nesting does not occur in the unidirectional specimens. A different result might be obtained on a system where fiber nesting does occur for unidirectional laminates. On the other hand, a significant variation in the energy release rate for delamination was observed for various layups of the panel which gave different stiffnesses, the angle between the plies at the delaminating interface being held constant. It has been determined that this variation in calculated energy release rate results from varying degrees of damage in the far field in the arms of the split laminate.

Reanalysis of the energy absorbed per unit area of crack extension using a J-integral approach (to be discussed later in this report) indicated the more reasonable result that the energy absorbed per unit area of crack extension did not vary with laminate stiffness. The apparent increase in such energy was the result of varying degrees of far field damage in the various plies with different ply stiffness.

A second area of activity has been the development of new experimental and analytical techniques to assist in the fracture toughness characterization of materials. Our work in this area has been in three different directions.

**4.3.1** J-Integral Analysis for Split Laminate Coupons

In conjunction with Dr. Richard Schapery, we have been working to develop a general J-integral approach to the characterization of delamination fracture toughness for mode I loading. While unidirectional laminates of 16-24 ply thickness tested for mode I delamination fracture toughness can be analyzed using linear analysis, testing of quasi-isotropic specimens has demonstrated that a nonlinear analysis is needed. The nonlinearity in this case is not just geometric (such as has previously been analyzed by Devitt, Schapery and Bradley). It is a result of significant permanent damage in the far field (i.e., in the cantilevered arms of the split laminate). The analysis and preliminary experimental results are summarized in the paper in Appendix I entitled "Delamination Analysis of Composites with Distributed Damage Using a J-Integral".

**4.3.2** Mode II Delamination Fracture Toughness Measurements

A method for measuring $G_{IIc}$ by bending a split laminate has previously been developed at Texas A&M University. More recently, Street and Russell have developed an alternative test to measure $G_{IIc}$ called the end notch flexure test (ENF) which utilizes a three point bend test. We have made measurements of $G_{IIc}$ using our end load split laminate test and the end notched flexure test (ENF) to see how the results compare. The two test geometries are shown in Figure 13 with the results compared in Table III. It should be noted that the results from the two different tests are very consistent. It should also be emphasized that both tests suffer from permanent far field deformation (indicated by the load-displacement curve not returning to the origin when the specimen is unloaded) due to shear when a relatively ductile material such as T6C145/F185 is studied. Thus, the measurement of mode II toughness $G_{IIc}$ determined using the area method should be considered upper bound values for the T6C145/F185 system. These results have indicated the need to develop a J-integral analysis for the mode II test as well. This will be done in the coming contract year.

4.3.3 Fracture Toughness Measurements of Tougher Neat Resins

The use of tougher neat resins in composites has increased the need to develop a technique similar to ASTM-E813 for measuring the fracture toughness of neat resin constituients of various composite materials. Current practice has been to introduce cracks using razor blades and then use a linear elastic analysis. We have found that different values of $J_{1c}$ are obtained if one introduces a fatigue precrack and properly analyzes the load-displacement using a J analysis. For example,

the widely published value of $G_{1C}$ for Hexcel F185 is 5-6KJ/$m^2$. We measured a $J_{1c}$ of 8.1KJ/$m^2$. Further efforts are planned in this coming year using polycarbonate as a model system to develop the technique and also study the effect of strain-rate on the measured $J_{1c}$ values.

**4.4 Micromechanics Modeling**

A simple micromechanics model has been developed to try to predict the delamination fracture toughness from the neat resin toughness. This model considers the size of the damage zone in the neat resin compared to the size of the damage zone in the composite and also considers the effect of the fibers which act as rigid filler in the deformation/damage zone. The details are presented in the paper in Appendix I entitled "A Comparison of the Crack Tip Damage Zone for Fracture of Hexcel F185 Neat Resin and T6C145/F185 Composite". The simple model overestimates the actual mode I delamination fracture toughness. This may be due to the lower strain to failure present in the composite at the crack tip due to constraint and/or interfacial failure. The details of this work are summarized in a paper in Appendix I entitled "The Relationship Between Resin Ductility and Composite Delamination Fracture Toughness". Strain field mapping of both the neat resin and the composite in this coming year should provide some clarification of the reason for the discrepency. We will also be utilizing a more detailed micromechanics model developed by Dr. Don Adams to try to improve our predictive capability. We should also be able to improve the micromechanics model as we see where it significantly deviates from the measured

strain field around the crack tip.

**4.5 Fractography and Failure Analysis**

While not specifically called for in this research work statement, we have spent some time assisting Mr. Frank Fechek of the Air Force Wright Aeronautical Laboratories in developing a failure analysis methodology. Because we have been doing in-situ and post-mortem fractography to achieve our other objectives, it has been a simple extension of this work to apply it to failure analysis. The results of this effort are summarized in a paper in Appendix I entitled "The Meaning and Significance of Hackles in Composite Materials Failure Analysis".

**5.0 PUBLICATION RESULTING IN WHOLE OR IN PART FROM WORK SUPPORTED BY AFOSR** (Note all manuscripts are provided in Appendix I.)

5.1 "Micromechanisms of Fracture in Toughened Graphite-Epoxy Laminates", W.M. Jordan and W.L. Bradley, ASTM STP entitled **TOUGHENED COMPOSITES**, submitted, 4/85; accepted with revisions, 9/85.

5.2 "The Meaning and Significance of Hackles in Composite Materials Failure Analysis", W. Jordan, M. Hibbs, and W. Bradley, **Proceedings of International Conference: Post Failure Analysis Techniques for Fiber Reinforced Composites**, Dayton, Ohio, July, 1985.

5.3 "A Comparison of the Crack Tip Damage Zone for Fracture of Hexcel F185 Neat Resin and T6C145/F185" Composite", E.A. Chakachery and W.L. Bradley, submitted, September, 1985; accepted without any revision in March, 1986, for publication in **POLYMER**

**SCIENCE AND ENGINEERING.**

5.4 "Correlations Between Micromechanical Failure Processes and the Delamination Fracture Toughness of Graphite/Epoxy Systems", M.F. Hibbs and W.L. Bradley, submitted for publication in ASTM STP on Fractography (November, 1985, Nashville).

5.5 "The Relationship Between Resin Ductility and Composite Delamination Fracture Toughness", W. Bradley and W. Jordan, **Proceedings of International Symposium on Composite Materials and Structures**, submitted February, 1986; published, June, 1986.

5.6 "Delamination Analysis of Composites with Distributed Damage Using a J Integral", **Proceedings of International Symposium on Composite Materials and Structures**, submitted February, 1986; published, June, 1986.

5.7 "J-Integral Measurement of Fracture Toughness on Tough Resin Systems", *to be presented* and submitted for publication, ASTM Meeting on Nonlinear Fracture Mechanics, Knoxville, TN, October, 1986.

5.8 "Mode II Delamination Fracture Characterization of Composite Materials", to be submitted to **Journal of Composite Materials**, (August, 1986).

5.9 "Study of Possible Microcracking in Gold/Palladium Film Used to Prevent Charging in SEM", to be submitted to **Journal of Materials Science** (August, 1986).

**6.0 *PROFESSIONAL PERSONNEL ASSOCIATED WITH RESEARCH EFFORT***

6.1 William M. Jordan, Ph.D. awarded, December, 1985, dissertation title: "The Effects of Resin Toughness on the Delamination Fracture Behavior of Graphite/Epoxy Composites".

6.2 Carlos Corleto, M.S., awarded, June, 1986, thesis title:

"Mode II Delamination Fracture Toughness of Unidirectional Graphite/Epoxy Composites".

6.3 Mike Hibbs, Ph.D. candidate with expected graduation date of fall, 1986.

6.4 Robert Jones, Jr., new Ph.D. student on project.

**7.0 PRESENTATIONS**

7.1 "The Meaning and Significance of Hackles in Composite Materials Failure Analysis", International Conference: Post Failure Analysis Techniques for Fiber Reinforced Composites.

7.2 "A Comparison of the Crack Tip Damage Zone for Fracture of Hexcel F185 Neat Resin and T6C145/F185", invited paper presented at Symposium on Fracture in Polymers and Composites, sponsored by the American Chemical Society, Chicago, September, 1985.

7.3 "Correlations Between Micromechanical Failure Processes and the Delamination Fracture Toughness of Graphite/Epoxy Systems", presented at ASTM Symposium on Fractography and Fracture, Nashville, November, 1985.

7.4 "Direct Observations of Fracture in Composite Materials in the SEM", invited presentation at Gordon Research Conference on Composite Materials, Santa Barbara, California, January, 1986.

7.5 "The Relationship Between Resin Ductility and Composite Delamination Fracture Toughness", invited presentation for International Symposium on Composite Materials and Structures, Beijing, China, June, 1986.

7.6 "Mode II Delamination Fracture Toughness Testing", workshop meeting for round robin on Delamination Toughness Testing, ASTM spring meeting, Charleston, May, 1986.

## 8.0 SUMMARY OF SIGNIFICANCE OF ACCOMPLISHMENTS

Our work this past year has given a new insight into the details of the fracture process that occurs during delamination. For mode I delamination, failure in many systems is controlled by interfacial failures. Thus, increasing the resin toughness without a commensurate increase in the interfacial properties will not give any net increase in the delamination toughness.

We have also come to understand why the delamination toughness for mode I versus mode II is relatively similar for a ductile matrix composite but very different (3X) for a brittle composite. The fact that the fracture process is preceded by the development of a significant damage zone whose size depends both on resin properties and mode of loading is also significant in guiding the development of meaningful micromechanics models.

# TABLES

## LIST OF TABLES

TABLE

Table I. Summary of mechanical properties of resin and composites.

| Resin | $\varepsilon_f$ (%) | Transverse $\varepsilon_f$ for composites | UTS (MPa) | G' (GPa) | G" (GPa) | Tan $\sigma$ delta | $G_{Ic}$ ($J/m^2$) | $G_{Ic}$ ($J/m^2$) | $G_{IIc}$ ($J/m^2$) |
|---|---|---|---|---|---|---|---|---|---|
| 3502 | 0.3 | 0.050 | | | | | 70 | 139 | 570 |
| F155NR | 1.96 | 0.699 | 56.5 | 1.80 | 0.0180 | 0.0103 | | 335 | 1660 |
| F155 | 3.10 | 0.580 | 68.6 | 1.70 | 0.0400 | 0.0223 | 730 | 520 | 1270 |
| F185NR | 3.24 | 0.538 | 72.9 | 1.80 | 0.0329 | 0.0180 | 460 | 455 | 1050 |
| F185 | 8.87 | 8.580 | 46.4 | 1.40 | 0.0490 | 0.0350 | 8000 | 2205 | 2440 |

Table II. Deformation/Damage zone sizes for composites; determined from in-situ fracture observations for mode I delamination fracture.

| Composite System | Fiber Density (vol.%) | Size of Damage Zone ahead of crack ($\mu m$) | Size of Damage Zone above/below crack ($\mu m$) | $G_{1c}$ ($J/m^2$) |
|---|---|---|---|---|
| AS4/3502 | 76.4 | 20 | 5 | 190 |
| F155 NR | | 20 | 7 | 335 |
| T6T145/F155 | 59.6 | 30 | 20 | 1015 |
| T6T145/F155 | 70.5 | 20 | 10 | 615 |
| T6T145/F155 | 68.8 | 20 | 10 | 520 |
| F185 NR | | 75 | 35 | 455 |
| F185 | | 200 | 50 | 2205 |

Table III. Mode II Delamination Fracture Toughness of AS4/3502 and T6C145/F185

| | $G_{IIc}$ ($J/m^2$) | | | | |
|---|---|---|---|---|---|
| | ENF Test | | | ELS Test | |
| Material | Linear Beam Theory | Compliance Curve | Area Method | Linear Beam Theory | Area Method |
| AS4/3502 | 543 | 648 | 613 | 595 | 543 |
| T6C145/F185 | * | * | 2398 | * | 2260 @ |

* No calculation of $G_{IIc}$ is possible due to significant nonlinearity in load/deflection curves (permanent deformation). If one uses linear portion of curves to measure compliance and Pmax for crack extension, ignoring nonlinear behavior near Pmax, $G_{IIc}$ lower bound values of 1225 $J/m^2$ may be calculated.

@ Upper bound values because of permanent deformation observed in load/deflection record.

# FIGURES

## LIST OF FIGURES

Fig.

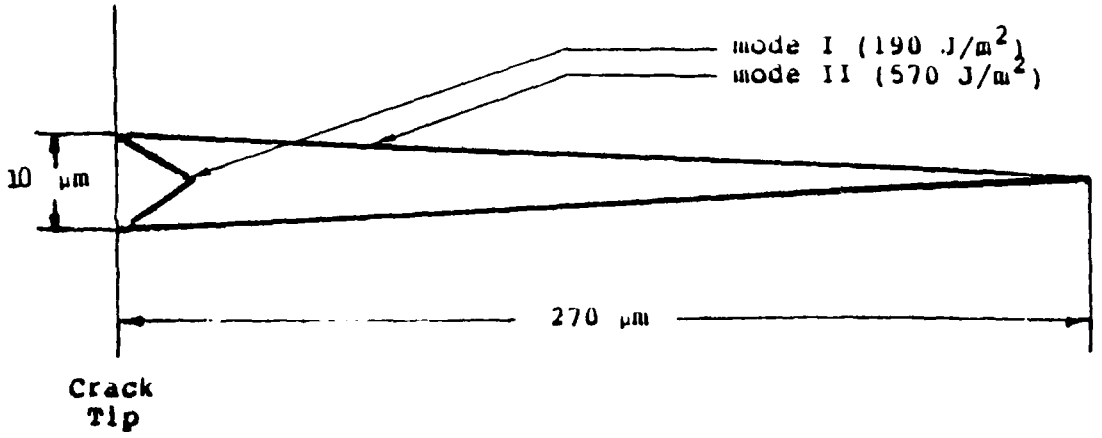


1. Damage zone size ahead of crack tip for mode I and mode II fracture of AS4/3502 graphite/epoxy composite.

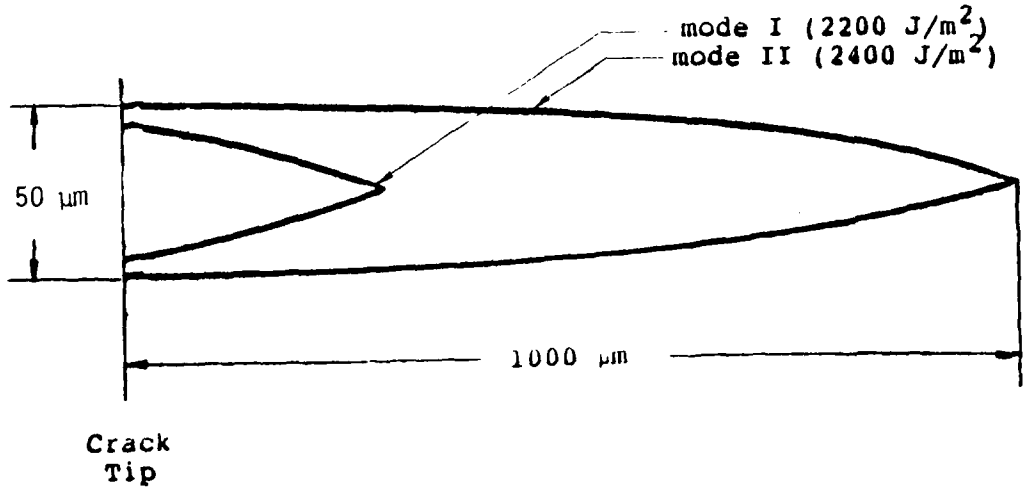


2. Damage zone size ahead of crack tip for mode I and mode II fracture of T6C145/F185 graphite/epoxy composite.

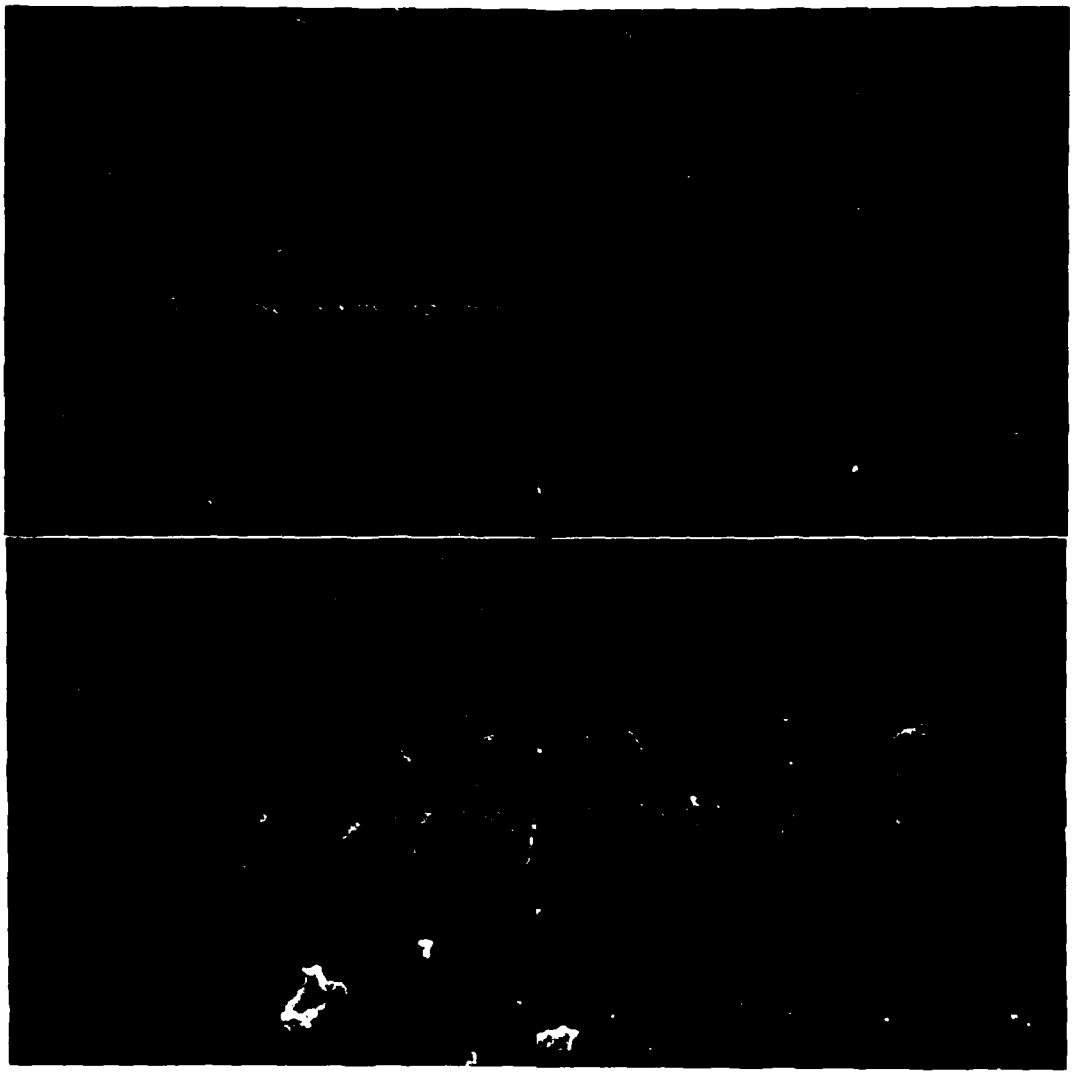

3. Damage zone and concurrent hackle formation process of AS4/3502 graphite/epoxy composite under mode II delamination fracture. (a) 1000x, (b) 4000x, (c) 3000x, (d) 3000x.

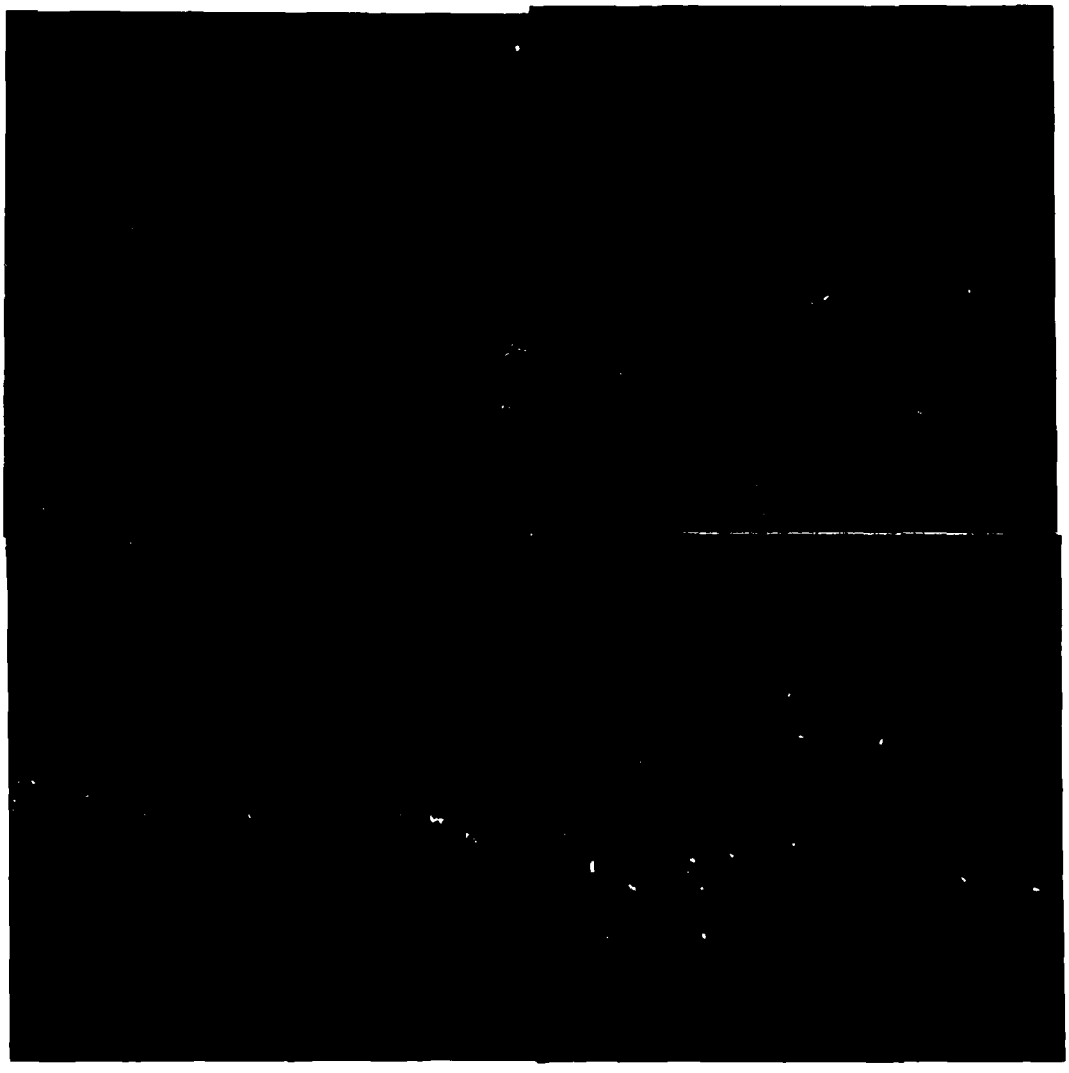

4. Damage zone and crack formation processes of T6C145/F185 graphite/epoxy composite under mode II delamination fracture. (a) 1000x, (b) 1000x, (c) 1500x, (d) 3000.

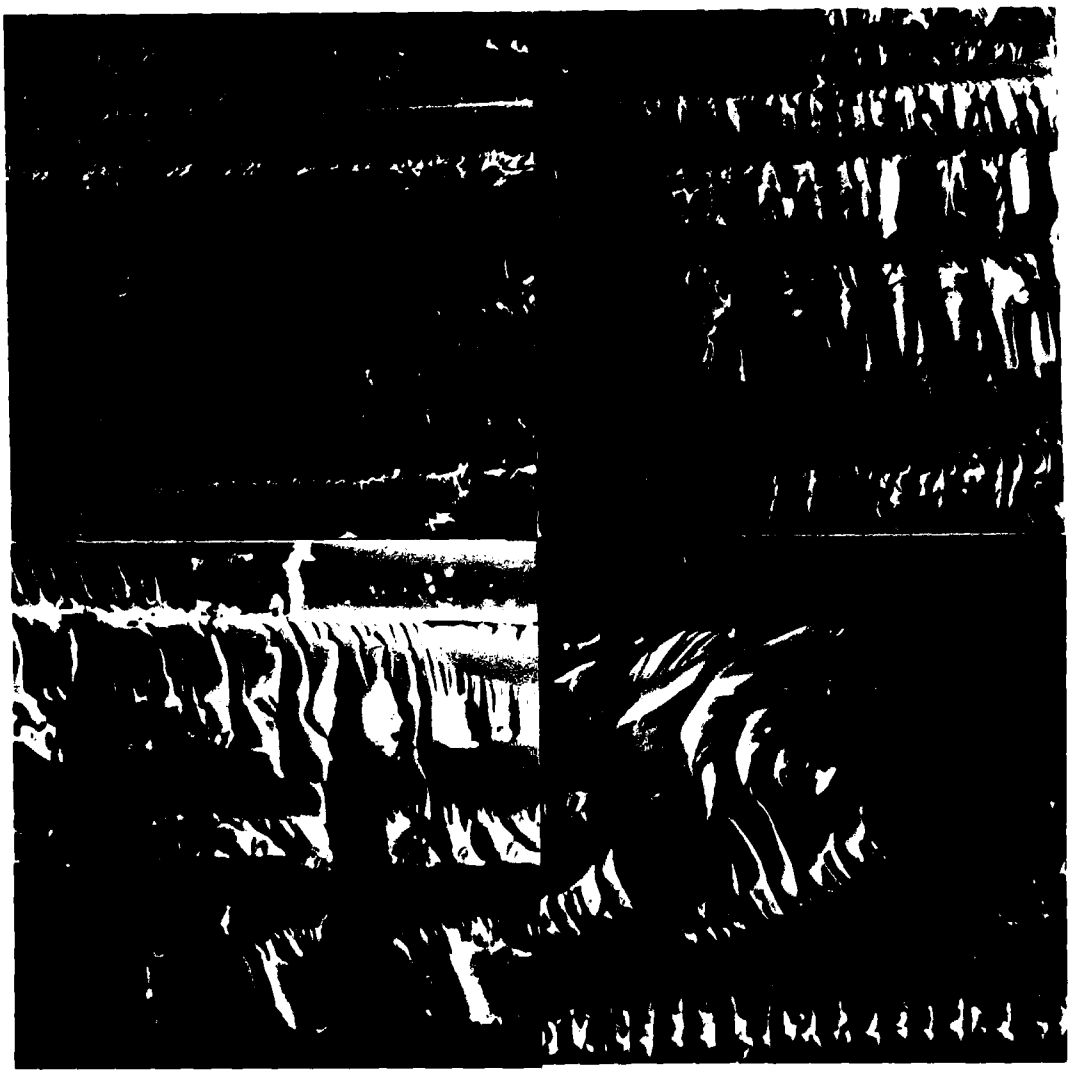

5. Post-mortem fractography of AS4/3502 delaminated under mode II fracture. Hackle formation is the major feature observed. (a) 1000x, (b)2000x, (c)2000x, (d) 1000x.

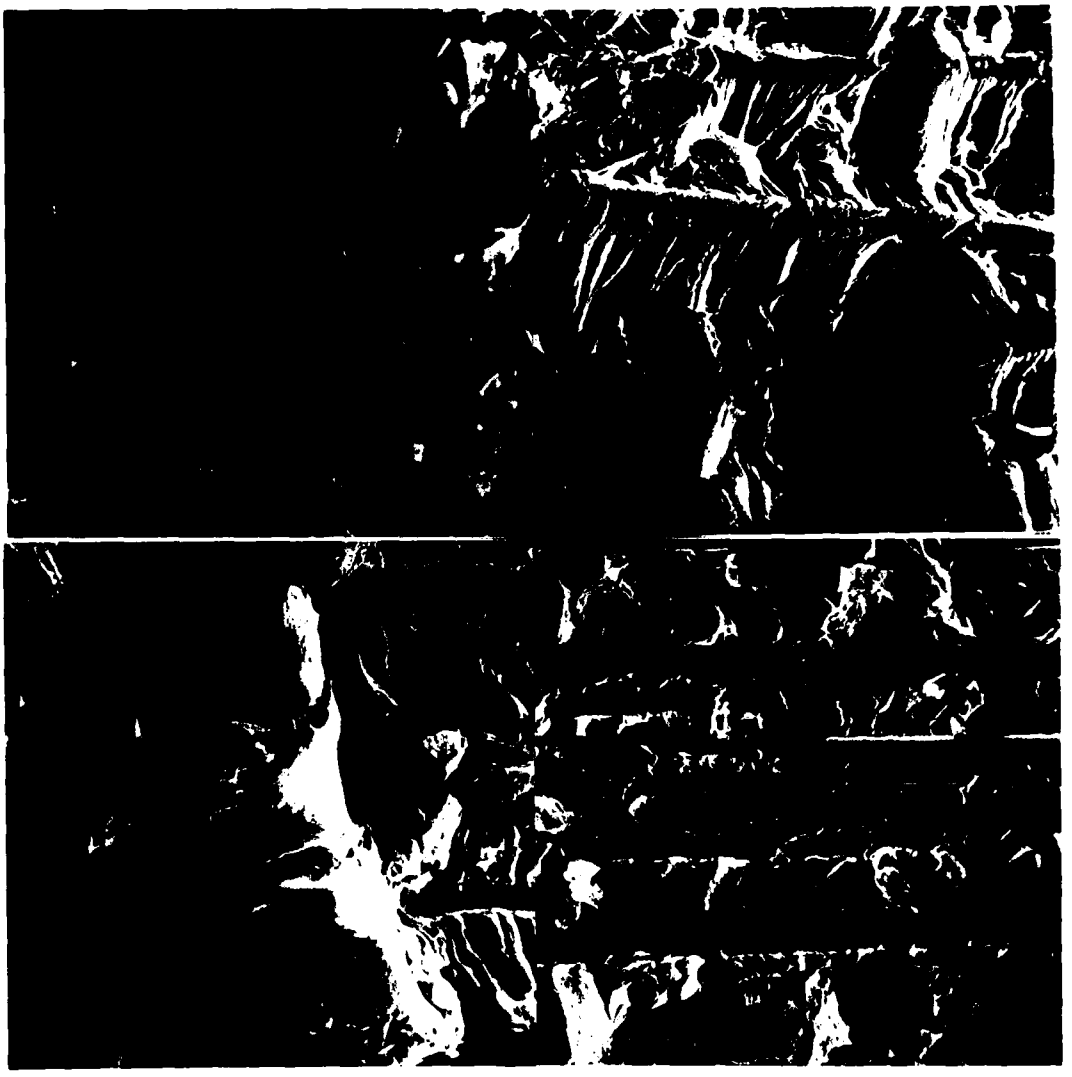

6. Post-mortem fractography of T6C145/F185 delaminated under mode II fracture. Shear deformation is dominant feature observed. 1000x (all).

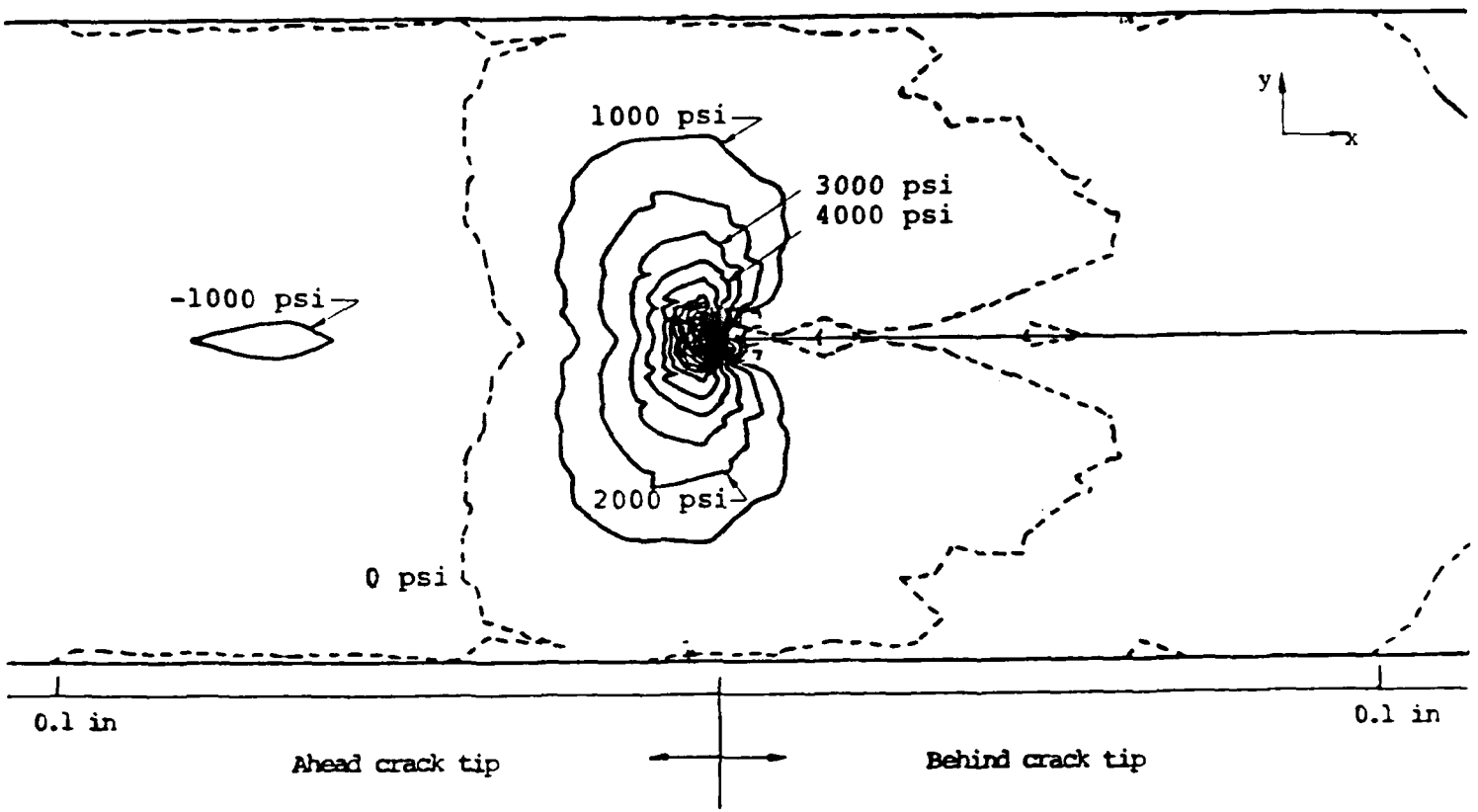


7. $\sigma_y$ stress contour plot of split laminate beam tested under mode I conditions.

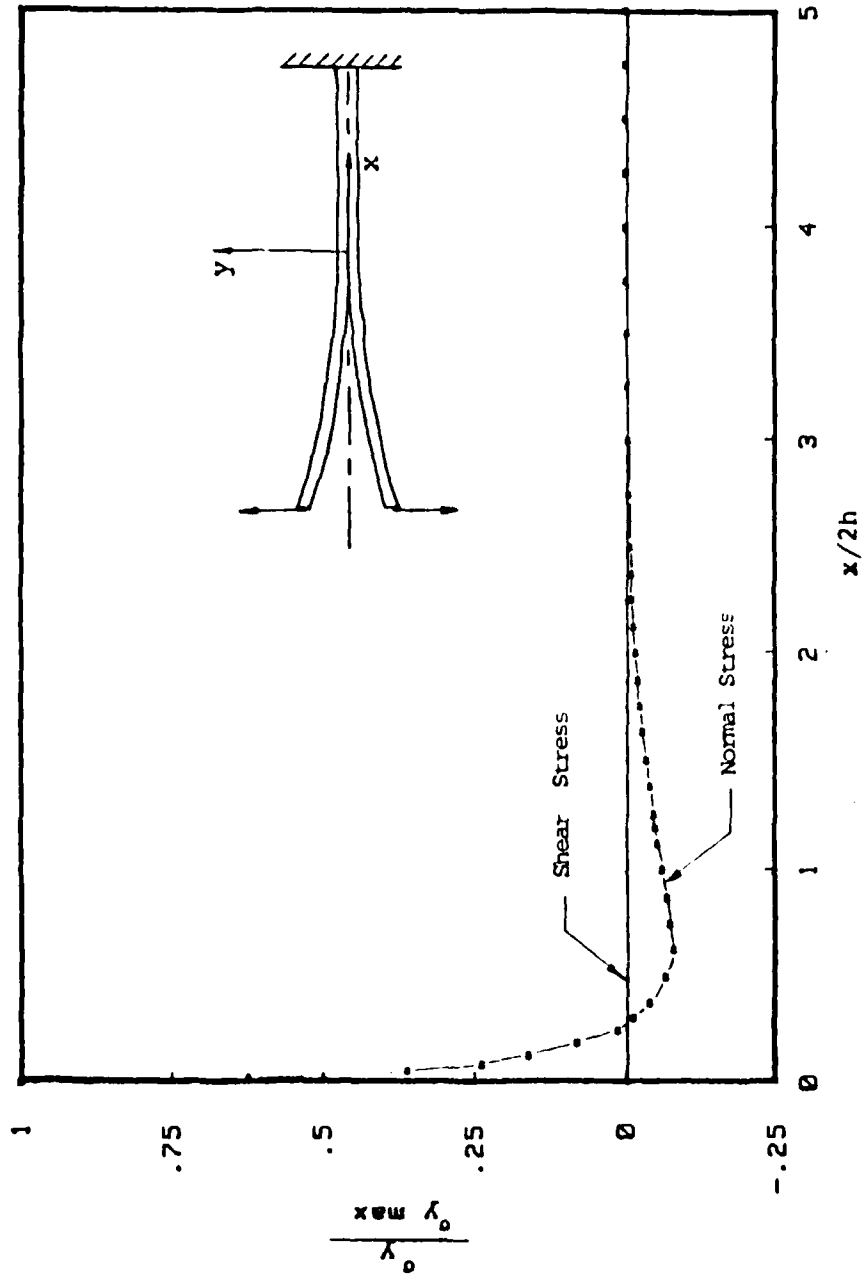


8. Stress field ahead of crack tip of split laminate beam tested under mode I conditions.

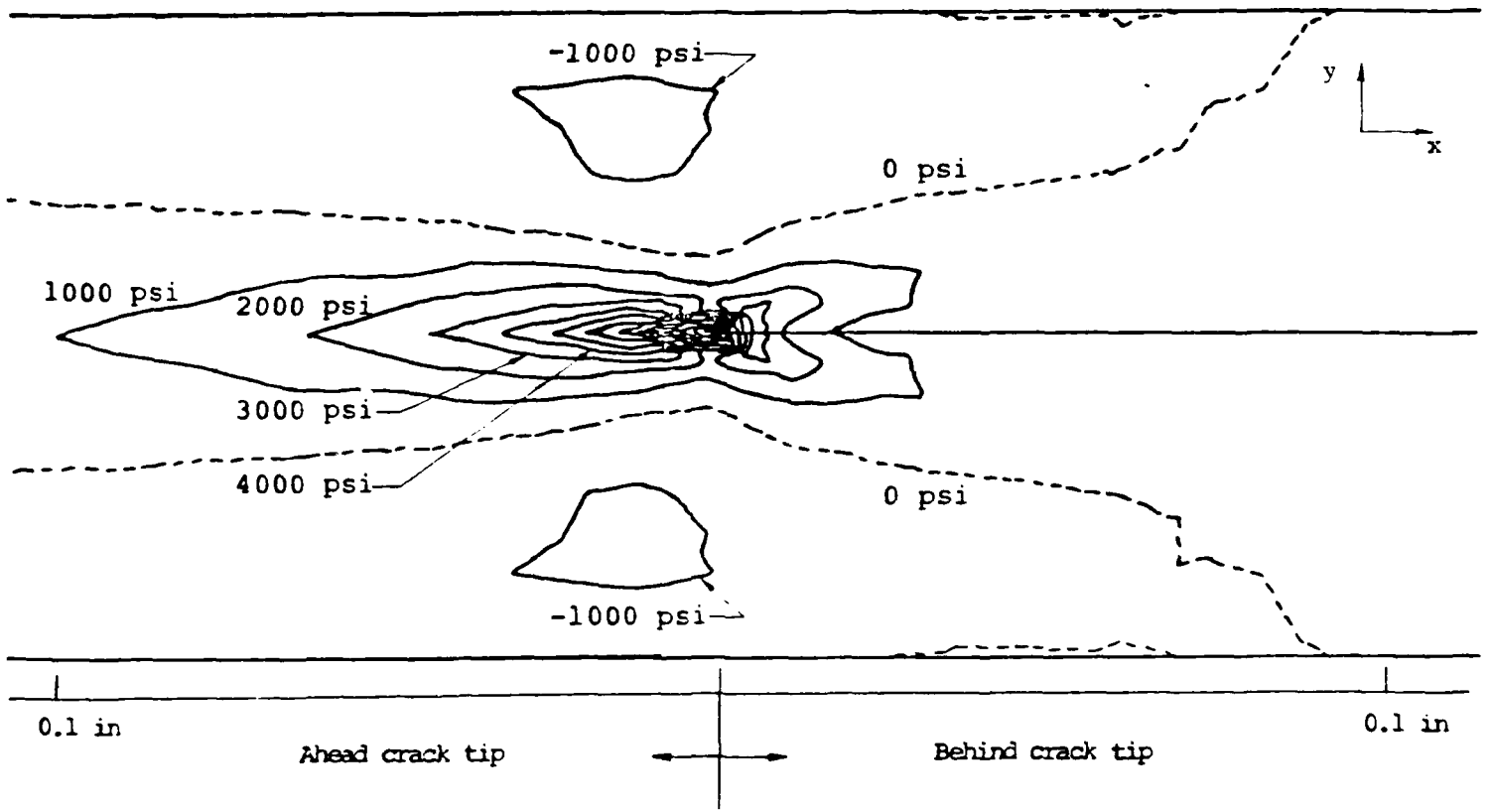


9. $\tau_{xy}$ stress contour plot of split laminate beam tested under mode II conditions.

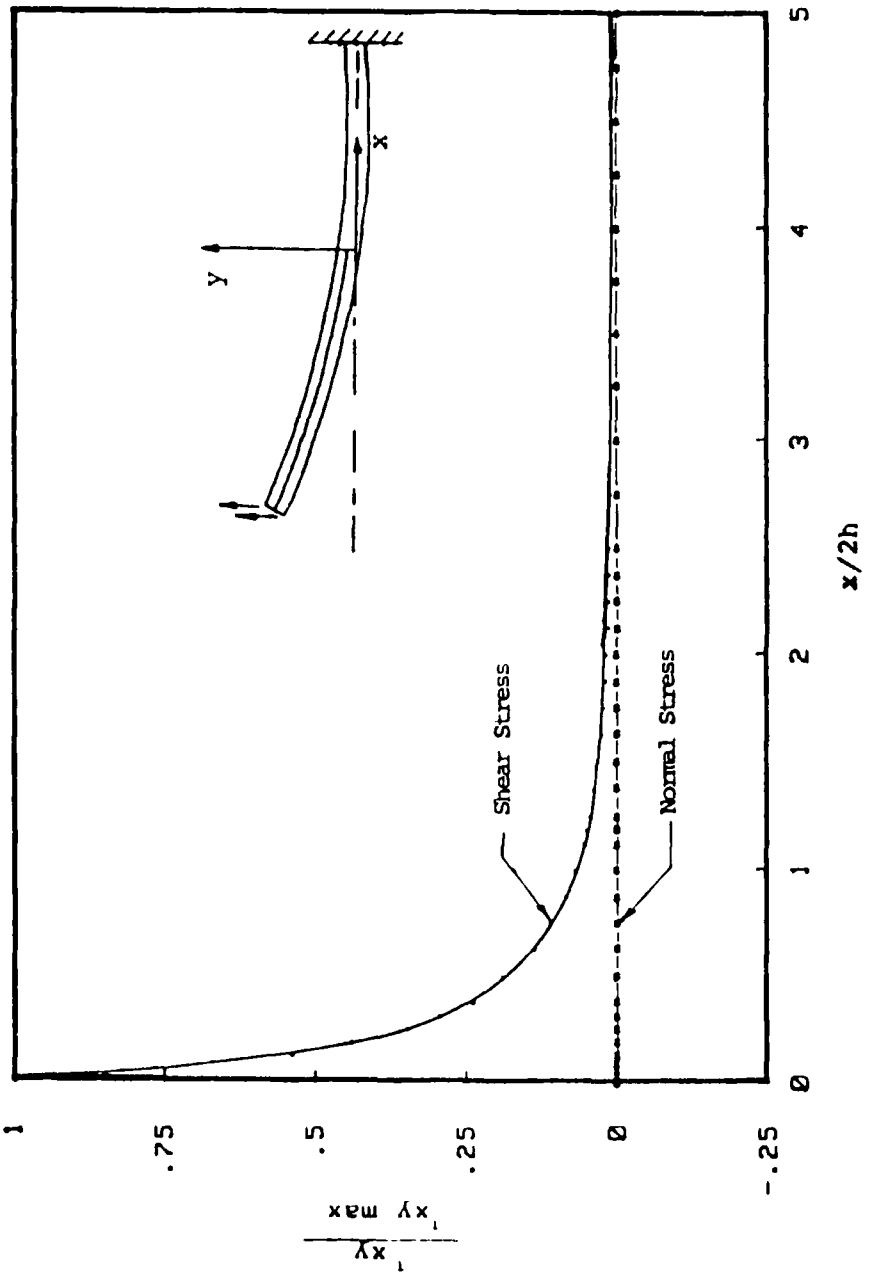


10. Stress field ahead of crack tip of split laminate beam tested under mode II conditions.

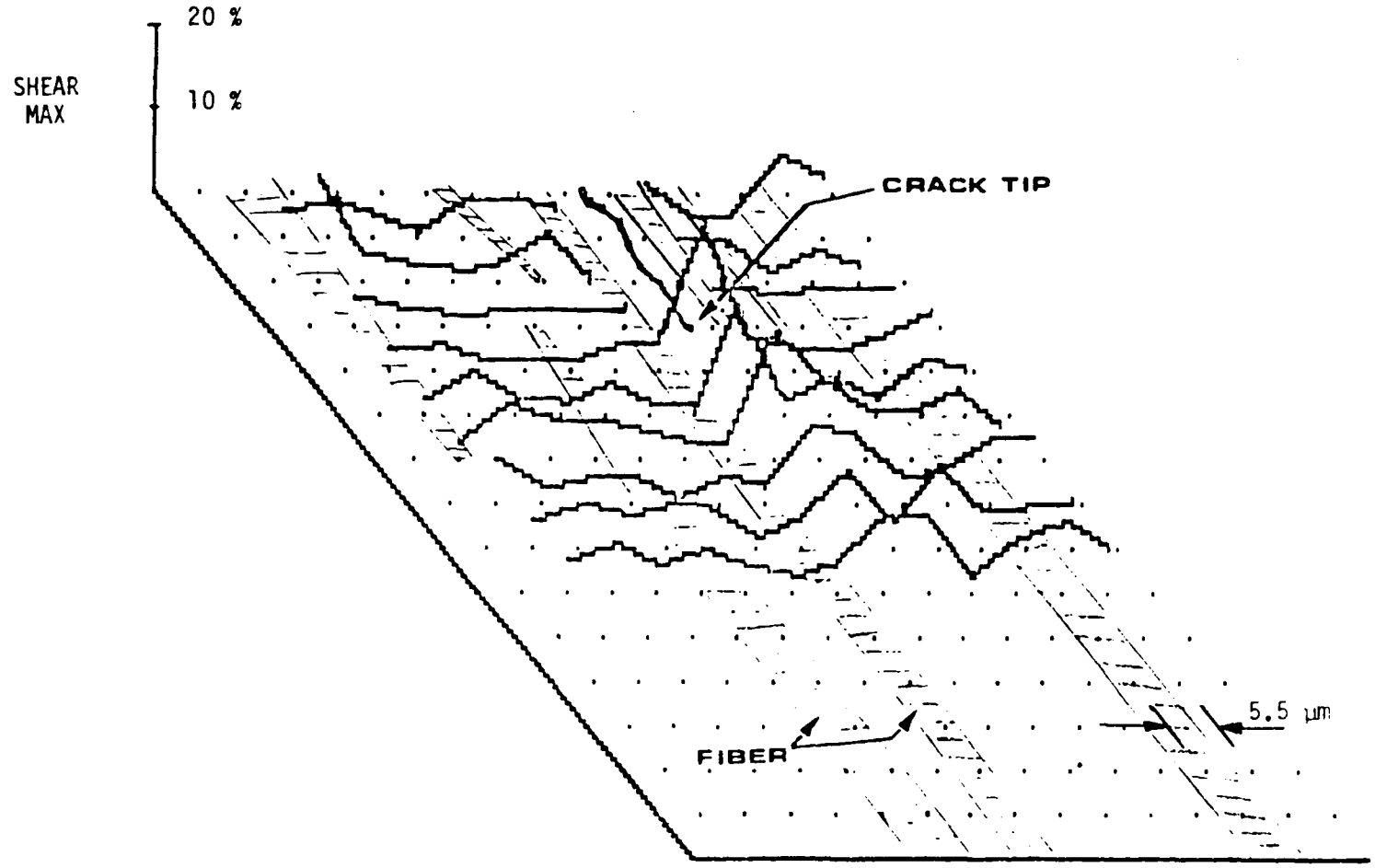


11. Three dimensional strain field map in the region of the mode I delamination crack tip for AS4/Dow P7 graphite/epoxy composite. The strain is seen to be confined in the resin region between the fibers (shaded areas). The maximum strain occurs at the crack tip and decreases rapidly ahead of the crack tip.

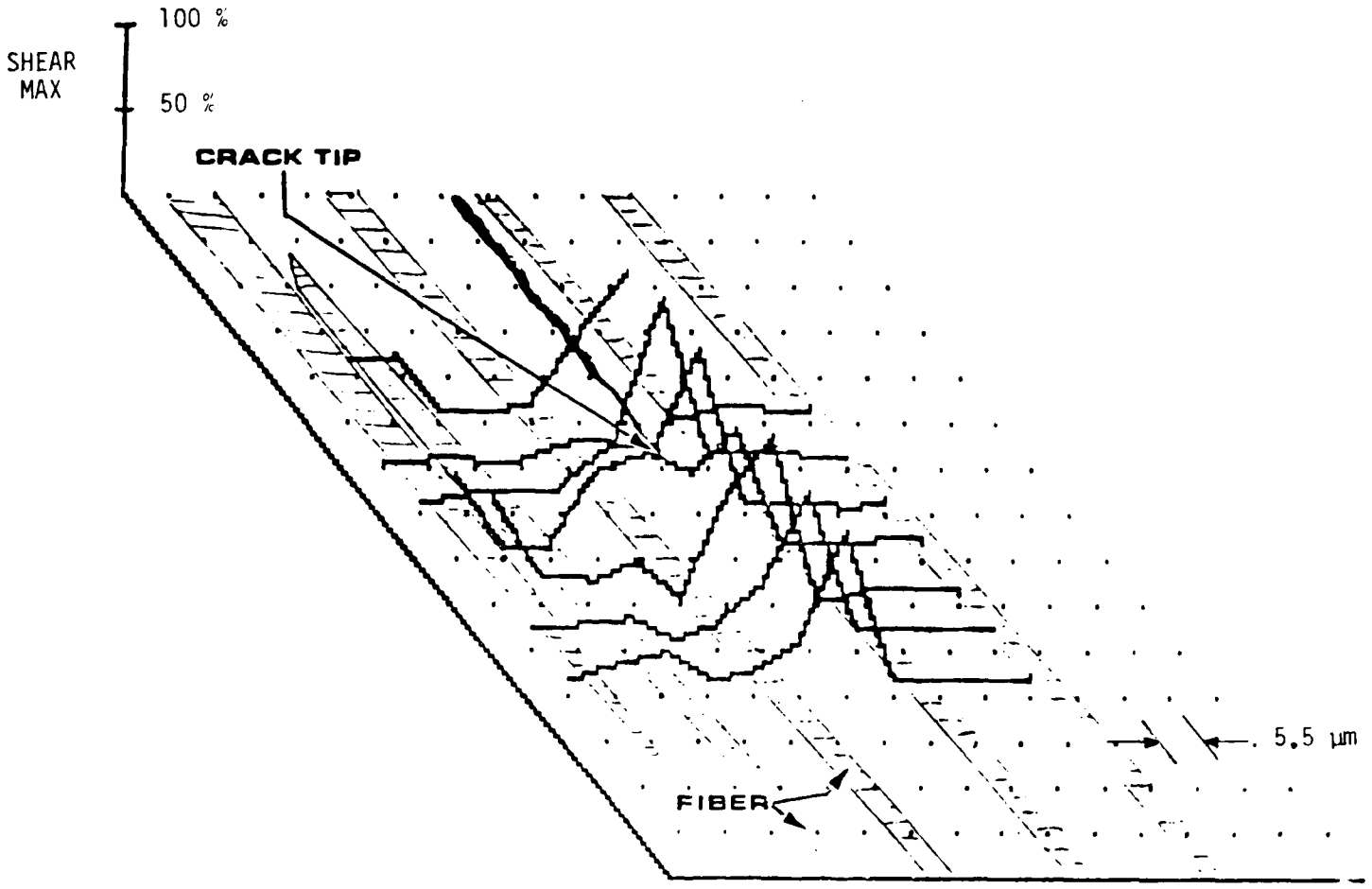


12. Three dimensional strain field map in the region of the mode II delamination crack tip of AS4/3501-6 graphite/epoxy composite. The strain is seen to be confined in the resin region between the fibers (shaded areas). The maximum strain occurs at the crack tip and remains fairly constant in the remaining field of view ahead of crack tip.

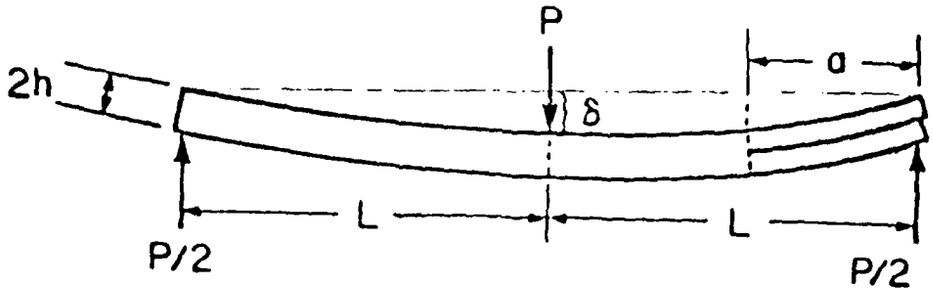


ENF Test

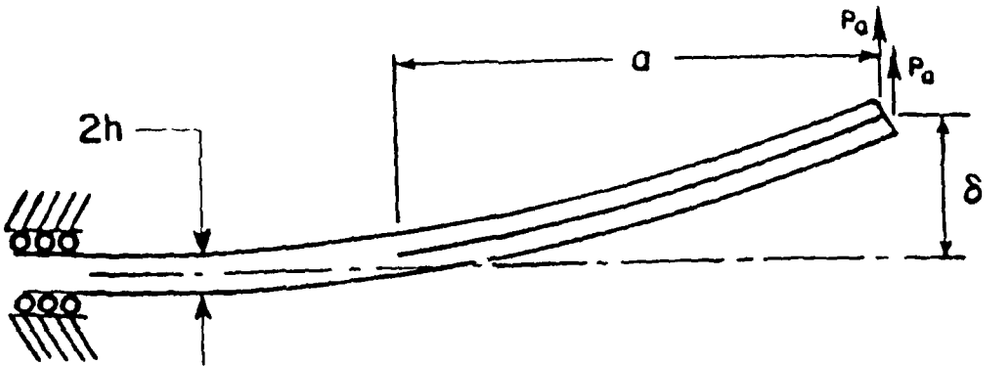


ELS Test

13. End-notched flexure (ENF) test and end-loaded split laminate (ELS) test configurations.

# APPENDIX

# MICROMECHANISMS OF FRACTURE IN TOUGHENED GRAPHITE-EPOXY LAMINATES

W. M. Jordan and W. L. Bradley
Mechanical Engineering Department
Texas A&M University
College Station, Texas 77843

presented at
ASTM Symposium
on
Toughened Composites
Houston, Texas
March 13-15, 1985

This work performed at Texas A&M University was supported by the Air Force Office of Scientific Research with Major David Glasgow as project monitor.

**ABSTRACT**

The combination of low crosslink density and elastomer additions has been seen to give the most potent toughening for neat resins. A relatively small increment of the additional neat resin fracture toughening above $800J/m^2$ is actually reflected in the delamination fracture toughness of a composite. Mode II delamination toughness of brittle systems may be as much as three times the mode I delamination fracture toughness while a ductile system may have a mode II delamination fracture toughness that is similar the the mode I value. The energy aborbed per unit area of crack extension for delamination seems to be independent of ply orientation if proper accounting of the near and far field energy dissipation is made.

**KEY WORDS:** composite materials, delamination, mode I, mode II, mixed mode, toughened epoxy

LIST OF SYMBOLS

B specimen

E elastic modulus in the fiber direction

$G_{Ic}$ critical energy release rate for stable crack growth for mode I loading

$G_{IIc}$ critical energy release rate for stable crack growth for mode II loading

$G_{Tot,c}$ total critical energy release rate for mixed mode loading

I moment of inertia for cracked portion of split laminate

$L_c$ crack length in split laminate

$P_s$ asymmetric load component $(P_u + P_L)/2$ (see Fig. 1)

$P_a$ symmetric load component $(P_u - P_L)/2$ (see Fig. 1)

$P_u$ load applied to upper half of split laminate (See Fig. 1)

$P_L$ load applied to lower half of split laminate (See Fig. 1)

$\Delta_s$ total opening displacement (see Fig. 1)

LIST OF FIGURES

9b. Post-mortem fractography of F155 composite delaminated in 43% Mode II conditions. (Bottom surface of fractured specimen). Note leaf like artifacts are oriented in opposite direction to those on the top surface (center, at 1500x).

10. Post-mortem fractography of HX205 composite delaminated in 43% Mode II conditions (bottom, 300x).

11a. Post-mortem fractography of AS4/3502 composite delaminated in Mode II conditions. Zipper like artifacts appear to be formed by coalescence of series of signodial shaped microcracks (top, 1500x).

11b. Post-mortem fractography of F155 composite delaminated in Mode II conditions. Note extensive resin deformation (center, at 1000x).

11c. Post-mortem fractography of HX205 composite delaminated in Mode II conditions. Note extensive resin deformation (bottom, at 1000x).

## INTRODUCTION

Graphite/epoxy composite materials are very attractive for a number of aerospace applications because of their high strength and stiffness to weight ratios. Furthermore, the ability to tailor the stiffness and thermal expansion coefficients by the appropriate layup of the material gives them great appeal. The first generation of graphite/epoxy composites were developed to maximize stiffness and glass transition temperature, $T_g$, by utilizing were found to delaminate rather easily when out of plane stresses were applied.

Subsequently, attempts have been made to improve the composite toughness by improving the toughness of the resin systems. This has had somewhat disappointing results in that a large increase in resin toughness has not been found to give a proportionate increase in composite toughness. Scott and Phillips (1) found that a tenfold increase in resin toughness increased composite toughness by a factor two. Similar results on different systems were found by Bascom et al. (2,3), Vanderkley (4) and Bradley and Cohen (5,6).

In this paper we will consider the question of whether some types of resin toughening mechanism are more effective than others in enhancing delamination toughness. In particular toughening by reductions in crosslink density and elastomer additions will be considered. The efficacy of the toughening mechanisms for both mode I, mode II and mixed mode loading will be considered.

## EXPERIMENTAL PROCEDURES AND ANALYSIS

Materials

Four graphite epoxy composite systems have been studied in this research effort. Hercules AS4/3502 composite which utilizes a highly crosslinked, and therefore, relatively brittle, resin system was chosen to be compared with three tougher systems; namely, Hexcel T6T145/F155, T6T145/F185 and T6T145/HX205. The Hexcel F155 resin has a lower crosslink density [280 atomic mass units between crosslinks(7)] than the Hercules 3502 resin [a.m.u. between crosslinks not available]. The Hexcel F185 and HX205 resins have even lower crosslink densities [430 a.m.u. between crosslinks(7)]. Thus, the three Hexcel resins differ from the Hercules 3502 resin in that they have lower crosslink densities, with the associated lower $T_g$ values and higher resin ductility.

A second difference between the Hexcel F155 and the Hexcel F185 resins and the Hercules 3502 resin is that the two Hexcel resins have elastomeric material added to enhance their respective toughnesses. Approximately 6% carboxy-terminated butadiene acrylonitride (CTBN) is included in the F155 resin. This CTBN rubber precipitates as a second phase with a diameter which varies from 0.1 micron to 1.0 micron (2,3). The F185 resin includes both a 6% addition of the CTBN rubber which precipitates and approximately 8% of prereacted rubber which has been mechanically blended into the resin (2,3). These prereacted rubber particles have a bimodal distribution of diameters with peaks at 2 microns and 8 microns. The Hexcel HX205 has had no elastomer additions. Whatever toughness it manifests is a result

of its relatively low crosslink density, which is the same as the Hexcel F185 resin, as previously noted.

Unidirectional, 24 ply thick panels of the AS4/3502 and the T6T145/F155 were laid up using prepreg from the respective manufacturers and then cured in an autoclave/press at Texas A&M University. Additional panels of T6T145/F185 containing some plus and minus 45° plies were prepared to study the effect of ply orientation across the delaminating plane on the delamination fracture toughness. Unidirectional, 24 ply thick panels of T6T145/F185 and T6T145/HX205 were prepared at NASA Langley for this study.

All panels contained a 0.025 mm thick strip of teflon laid to a depth of 3cm from one edge of the panel between the center two plies to provide a crack starter. Since the teflon strip introduces a relatively blunt notched "crack", a natural crack extension of at least 3 cm was made prior to the measurement of any critical energy release rates. Thus, the $G_c$ values reported in this study are for crack growth rather than crack initiation.

Split laminate specimens 2.5cm wide by 30cm in length were cut from the composite panels (fibers running the length of the specimens for the unidirectional panels) for macroscopic testing while much smaller specimens (3 cm long by 0.6 cm wide) were cut to be fractured in the scanning electron microscope.

Castings of neat resin were provided by Hexcel for the F155, F185 and HX205 systems. Rectangular specimens 1.27cm wide by 0.318cm thick by 3.56cm long were machined from the neat resin castings to be tested on a dynamic mechanical spectrometer manufacturered by Rheometrics, Inc. Standard tensile specimens

were also machined from the neat resin castings, as were compact tension specimens for fracture toughness testing. The compact tension specimens were a standard 1T size according to ASTM-E399, but with a thickness of approximately 0.5cm, which was the thickness of the castings.

Mechanical Properties Testing

Delamination Fracture Toughness Tests--Delamination fracture toughness tests were run at ambient temperature (24C) in opening mode (mode I), shear mode (mode II) and mixed mode conditions on split laminate test specimens using an MTS materials testing system operated in stroke control at 0.0085cm/s. Load and displacement were continuously measured, while the crack length was measured visually at the surface at discrete intervals (about once every 1cm of crack extension). Unload compliance measurements were made at intervals of about 2-3cm.

Mixed mode and mode II tests were also performed using split laminate specimens. This was accomplished by asymmetrically loading the cracked end of the split laminate while restricting vertical displacement of the uncracked end, which was still free to translate horizontally, as seen in Figure 1. This procedure was first developed by Vanderkley (4) at Texas A&M University. The mixed mode loading can be analyzed by utilizing the superposition principle and noting that an asymmetrically loaded split laminate can be treated as the sum of pure bending and pure mode I loading, with the pure bending giving essentially a pure mode II state of stress (see Figure 1). When the specimen is loaded as shown in Figure 1 with the uncracked end and the upper

arm of the split laminate held stationary and the lower arm of the split laminate displaced (through actuater displacement), the percentage of mode II loading will vary continuously throughout the test from pure mode I to a mode II energy release rate that is approximate 40% of the total energy release rate.

Two special cases of the loading configuration seen in Figure 1 may be noted. First, if the upper arm of the cracked end of the split laminate is unconstrainted ($P_u$=0), then the specimen will experience a constant fraction of mode II loading throughout the test, which gives a mode II energy release rate that is 43% of the total energy release rate. Second, if both upper and lower arms of the split laminate are pulled down with equal force using the actuater ($P_u = -P_L$), then a pure mode II loading condition results. This loading arrangement is, in effect, one half of a three point bend test, and thus, is very similar to the end notch flexural test developed by Russell and Street (8).

For the mode II tests, a 0.79mm teflon spacer was placed between the crack faces of the split laminate specimen to minimize any frictional effects which might occur by the rubbing of the two surfaces together. This spacer would constitute a superimposed mode I loading, but because the spacer was very thin, the mode I energy release rate it produces is trivially small. A scanning electron microscopy examination of the fractured surfaces after mode II testing gave no indication of rubbing between the two fractured surfaces.

Neat Resin Fracture Toughness Tests--Fracture toughness tests were run on several of the neat resins where $G_{1c}$ values

were either unavailable or were regarded with some suspicion (literature values on F185 used linear elastic fracture mechanics, which is questionable for such a ductile system). The procedures specified in either ASTM-E399 or ASTM-E813 were followed, with a single specimen, multiple compliance approach used for the ASTM-E813 on the Hexcel F185 system. Fatigue precracking was used to introduce cracks in the compact tension specimens.

Rheometrics Tests--Rheometric tests were run on neat resin specimens. These specimens were subjected to dynamics torsional cycling over a wide range of temperatures which bracketed the glass transition temperature, $T_g$. The loss and storage modulus were recorded as a function of temperature. The glass transition temperature was assumed to correspond to the temperature where the loss modulus value was a maximum.

Tensile Tests--Tensile tests were conducted on the neat resin systems according to ASTM D638. Strain was measured using strain gages which were mounted on the front and back face of each specimen and were capable of measuring strain of up to 10%. Complete stress-strain behavior was determined for each specimen from which tensile strength, yield strength and elongation were noted.

## Analysis of Delamination Fracture Toughness Tests

Mode I Critical Energy Release Rate Analysis, $G_{Ic}$, For Delamination Fracture--Generally the term critical energy release rate is used to refer to initial crack extension from some preexisting flaw or fatigue precrack. In this work it is used to

refer to the work required per unit area of new crack surface created for stable crack propagation, rather than for initiation. The mode I critical energy release rate was calculated using linear beam theory as described by Vanderkley(4) where

$$G_{Ic} = [P_s L_c]^2/3EI \quad (1)$$

where $P_s$ is the symmetric loading ($[P_u+P_L]/2$, see Figure 1), $L_c$ is the crack length, B is the specimen width and EI is the flexural stiffness of the arms of the cracked portion of the specimen.

The flexural stiffness was calculated from measured values of load, $P_s$, displacement $\Delta_s$, and crack length $L_c$ using a relationship also derived from linear beam theory; namely,

$$EI = 2P_s L_c^3/3\Delta_s \quad (2)$$

A value for EI was calculated at each of the approximately 20 points per specimen where crack length was measured. An average value of EI for the specimen was then determined and used in Equation 1 to calculate $G_{1c}$ values, also at approximately 20 points for each specimen. Three split laminate specimens of each composite were tested in mode I with the reported $G_{Ic}$ values being the average of approximately sixty calculated values.

The results from all mode I tests were also analyzed using the unload compliance measurements analyzed using the method suggested by Wilkins et al., with the calculated values of $G_{1c}$ typically falling within 3% of the values calculated using linear beam theory (i.e., Equations 1 and 2). The only mode I tests for which it was not possible to use the linear beam theory analysis (or the Wilkins analysis) were the T6T145/F155 specimens containing all plus and minus 45° plies. Because of the lower

compliance, a significant degree of geometric nonlinearity was noted in the load-displacement records for these specimens. Furthermore some far field damage in the split laminate arms was evident in view of the fact that the load-displacement record did not return to the origin on unloading. As a result, the nonlinear beam theory analysis first developed by Devitt et al. (10) was used to analyze these results. However, this approach is only good for nonlinear elastic behavior. A J-integral analysis is currently being developed to use in analyzing these results which include not only geometric nonlinearities but also nonlinear viscoelastic behavior of the resin.

Mixed Mode and Mode II Critical Energy Release Rate Analysis, $G_{IIc}$, For Delamination Fracture--For mode II delamination fracture toughness analysis, the following relationship for mode II critical energy release rate was derived by Vanderkley (4), again assuming linear beam theory and superposition (see Figure 1):

$$G_{IIc} = 3[P_a L_c]^2/4BEI \qquad (3)$$

where $P_a$ is the asymmetric load $(P_U-P_L)/2$ and the other terms are as previously defined.

For all pure mode II tests, the load-displacement records were found to be significantly nonlinear. Calculation of $G_{IIc}$ values using Equation 3 based on linear beam theory gave artifically high values of $G_{IIc}$ in comparison to the results of Russell and Street (8) on similar material. A critical energy release rate calculation for split laminate specimens based on nonlinear elastic beam theory has previously been published for

mode I loading (10) but not for mode II loading. Thus, we chose to use the area method approximation, whereby the area under a load-displacement record for loading, crack advance from $L_1$ to $L_2$, and unloading is determined and assumed to be equal to the work required to increase the crack area by $B[L_2-L_1]$, where B is the specimen width. This method assumes all of the work represented by the area bounded by the load, crack advance, unload-displacement curve goes into crack advance. Any far field energy dissipation would erroneously be lumped into the energy absorbed per unit area of crack extension relationship. Thus, the calculated values of $G_{IIc}$ using this approach may be considered upper bound estimates. Nevertheless, our results for $G_{IIc}$ using the area method were in reasonable agreement with Russell and Street's results (8) (which implies far field damage is minimal for the unidirectional, split laminate specimens studied in this work) and were much smaller than the values one would obtain by naively using linear beam theory on the obviously nonlinear load-displacement records obtained on the mode II specimens.

Mixed Mode Critical Energy Release Rate Analysis, $G_{Tot,c}$ For Delamination Fracture--Most of the load-displacement records for the mixed mode delamination tests were quite linear so that $G_{Ic}$ and $G_{IIc}$ could be calculated using Equations (1) and (3) with $G_{Tot,c}$ calculated as the sum of $G_{Ic}$ and $G_{IIc}$. Where this was not the case, no analysis was attempted since neither superposition nor linear beam theory would be appropriate.

### Real Time Observations of Delamination Fracture In Scanning Electron Microscope

Real time observation of fracture in the scanning electron microscope (SEM) is a relatively new technology. Theocaris and Stassinakis (11) have fractured composite specimens loaded in tension in the SEM while Beaumont (12) has fractured composite and polymeric systems using torisonal loading in the SEM. In this study small split laminate specimens were fractured in a JEOL 35 scanning electron microscope specially equipped with a loading stage. Delamination is obtained by pushing a delaminating specimen over a blunt stationary wedge. A blunt wedge was used so that crack growth would result from pushing apart the two crack surfaces in essentially mode I loading, without any direct pressure applied at the crack tip by the wedge. The wedge tip remained well away from the crack tip so that mode I conditions would dominate at the crack tip. The fracture process was recorded on video tape and standard sheet film. A post-mortem fractographic examination was made of the fractured macroscopic split laminate specimens and the miniture split laminate specimens fract

## EXPERIMENTAL RESULTS

### Results from Mechanical Properties Tests

The results of the various mechanical properties tests are summarized in Tables 1-4. The glass transition temperature results are presented in Table 1, where the 3502 is seen to have the highest $T_g$, F185 has the lowest and HX205 and F185 have an identical value of $T_g$. The three more ductile systems, HX205, F185 and F155 all have $T_g$ values well below the relatively

brittle 3502. The tensile tests results are summarized in Table 2. No as-cast 3502 resin was obtained. Thus, a tensile test was not run on this resin. The F155 and the HX205 have nearly identical tensile properties, which is not surprising since they have the same $T_g$. The F185 resin is much more soft and ductile, than the F155 or the HX205, as expected. Though tensile properties were not obtained for the 3502 resin, it would be expected to be somewhat stronger with a smaller elongation to failure than the other three resins.

The neat resin fracture toughness values, $G_{Ic}$, are summarized in Table 3 and correlate nicely with the $T_g$ results and the tensile test results presented in Tables 1 and 2. The different values of mode I and mode II delamination fracture toughness noted in Table 3 for T6T145/F155 are for two different batches of material purchased approximately one year apart. The ratio of composite delamination toughness, $G_{Ic}$, to neat resin fracture toughness, $G_{Ic}$, is seen to decrease as the resin toughness increases, as previously noted by Bradley and Cohen (6) and Hunston (15). A second important trend to note from Table 3 is that the mode II delamination toughness is always higher than the mode I delamination toughness, with a ratio of mode II delamination toughness to mode I delamination toughness of approximately 3X for the brittle system decreasing to a value just barely larger than 1.0X for the most ductile system.

The effect of fiber orientation across the plane of delamination on delamination fracture toughness, $G_{Ic}$, is seen in Table 4. For a specimen with plus or minus $45^{\circ}$ plies across the interface that is debonding but with a stiffness similar to a

unidirectional composite, the delamination critical energy release rate was found to be very similar to the results for unidirectional laminates ($600J/m^2$ compared to $520J/m^2$). Chai(16) has previously noted a similar result; namely, that ply orientation across the plane of delamination does not significantly effect the delamination fracture toughness for laminates with similar stiffness. The much larger value for $G_{Ic}$ indicated for the second multi-axial layup is a result of far field damage due to nonlinear viscoelastic behavior by the resin. As will be seen presently, the resin carries a significant load in the axial direction for a composite laminate with all $+-45^{o}$ plies. This significant resin loading not only in the crack tip region but at other locations removed from the crack tip will cause the resin to undergo nonlinear viscoelastic deformation. This energy dissipation in the far field should not be counted in the crack tip energy dissipation per unit area of crack extension. The use of a J-integral approach allows one to properly distinguish between the far field energy dissipation and the crack tip energy dissipation.

### Results From Real-Time Observations of Delamination Fracture in Scanning Electron Microscope

The observations of fracture in the SEM had as it purpose the determination of the details of the delamination fracture process for the various systems to gain a better understanding of how resin toughness can be translated into delamination fracture toughness. The damage zone size around the crack tip as well as the critical event (i.e., resin fracture, interfacial debond,

etc) can be determined from such observations.

In-situ fractography for the four composite systems are shown in Figures 2-5. The damage zone as evidenced by fine microcracking is seen to be very small for the AS4/3502 and the critical fracture event is usually interfacial debonding (see Figure 2). In Figure 2, the cracking appears to be through the resin, but is in fact along a fiber just beneath the surface, as indicated by the charging (light colored region) adjacent to the fracture plane. Crack advance in the AS4/3502 was usually discontinuous. As the wedge was inserted further into the specimen, crack advance would not occur continuously but in a burst of interfacial debonding which resulted in significant crack advance. This unstable mode of crack growth suggests that the interfacial bonding in this system is quite heterogeneous. Crack arrest probably occurs at some locally better bonded region. The energy release rate must be increased to initiate crack growth. However, once the locally better interfacial bonding is overcome, crack advance occurs until the energy release rate decreases (which it does for crack extension under displacement controlled loading) to a value lower than the local resistance, $G_{1c}$, which is probably at the next region of better interfacial bonding.

A much more extensive damage zone is seen around the crack tip for T6T145/F155 (see Figure 3). The microcracked zone is much larger in extent than for the AS4/3502 and has a much greater density of microcracks. Inspite of this fact, a significant amount of crack extension occurred by interfacial failure. It did not appear that the interfacial failure in the

T6T145/F155 was always due to debonding. Rather it sometimes appeared that the microcrack density was greater adjacent to fibers, and therefore, made coalescence more likely in that region. Thus, it was rather exception to see a bare fiber in the post-mortem fractography of the T6T145/F155 while bare fibers were quite common in the AS4/3502.

The in-situ fractography for the T6T145/HX205 is presented in Figure 4 where the damage zone is again seen to be characterized by significant microcracking. The extent of the damage zone is somewhat greater than for the T6T145/F155, but the density of microcracking is much less. Failure seemed to proceed in the interfacial area between resin and fiber, not by debonding but by coalescence of microcracks which seemed to exist in greater number in the interfacial region in the T6T145/HX205.

Finally, the damage zone around the crack tip in the T6T145/F185 is seen in Figure 5 to be both large in extent and high in density of microcracks. Again, the failure is still frequently near the interface, but due to a higher density of microcracks in this region rather than debonding. Very few regions of bare fiber are noted in the post-mortem fractography.

The in-situ fracture behavior of the T6T145/F155 composite with off angle plies is seen in Figure 6. Because the fibers are at an angle of $45^{\circ}$ to the length of the specimen, mode I loading of the split laminate gives significant loading of the resin along the length of the specimen as well as in the mode I opening direction. Thus, while microcracking similar to that observed in the specimens made from a unidirectional laminate is still

evident, the orientation is different and voiding at the resin/fiber interface is noted. In fact coalescence of these voids seems to play a significant role in the delamination fracture process in a split laminate with a large number of off axis plies.

Typical damage zone sizes around the crack tip of the various composites tested have been quantified and are summarized in Table 5.

### Results of Post-Mortem Fractographic Examination of Fractured Surface of Delaminated Specimens

The post-mortem fractographic examination included specimens fractured for mode I, mode II and mixed mode loading conditions. The results for the AS4/3502 consistently indicated bare fibers (except possible sizing) and interfacial debonding, whereas the three ductile systems gave only occasional indication of fiber debonding. Post-mortem fractographic results for T6T145/F155 and T6T145/HX205 are seen in Figures 7 and 8. The duplex appearance to the fracture surface in the T6T145/F155 appears to be the result of a variable thickness of the resin rich region between plies. Only a few bare fibers are noted.

Figures 9-11 present highlights of the results from the post-mortem fractographic examination of the specimens fractured in mode II and mixed mode. At the time this work was done, our stage was not yet adapted for mode II testing in the SEM. Thus, the post-mortem fractographic results on the mode II and the mixed mode delamination fractures constitute all of the fractographic information obtained for these loading conditions. The distinctive features on the fractured surface of the three

more ductile composite systems loaded with a significant percentage of mode II loading are leaf like artifacts whose orientation relative to the delamination plane increase monotonically with increasing percentage of mode II loading. The more brittle AS4/3502 had a very regular array of what appear to be sigmodial shaped microcracks which have coalesced to give macrocrack advance.

**DISCUSSION**

The significant results to be discussed in this section are as follows:

(1) the efficacy of rubber particle additions and lower crosslink density in enhancing neat resin fracture toughness;

(2) the efficacy of rubber particle additions and lower crosslink density in enhancing composite delamination fracture toughness;

(3) the change in fracture toughness with increasing fraction of mode II shear loading; and

(4) the effect of ply orientation and laminate stiffness on delamination fracture toughness.

These macroscopic fracture toughness results will be discussed in light of the in-situ and post-mortem fractographic observations.

Neat Resin Fracture Toughness

The neat resin toughness was found to correlate with $T_g$ and with elongation in a tensile test for the four systems studied. It is interesting to note that the F155 and the HX205 had quite similar tensile properties and $T_g$, though they were toughened somewhat differently; i.e., HX205 relied entirely on decreasing

the crosslink density while the F155 used a combination of reduction in crosslink density (compared to epoxy like 3502) and rubber particle additions. The F155 had a better fracture toughness for both neat resin and composite delamination. Materials with similar tensile elongations may have significantly different fracture toughnesses since fracture toughness depends on the ductility under a triaxial rather than a uniaxial states of stress. Since rubber particle additions can relieve this triaxial state of tension by voiding, the same elongation in a tensile test may correlate with a higher fracture toughness for rubber particle toughened resins.

The beneficial effect of rubber particle additions is particularly evident in the F185, whose neat resin toughness is 18X that of the HX205 even though their tensile ductilities differ by only a factor of 3X. The elastomer additions while giving some enhancement to elongation give a dramatic increase to the fracture toughness. Yee and Pearson (17) have noted that a resin needs to have some intrinsic capacity to deform in response to shear stress if it is to be benefited by rubber particle additions, which principally increase the shear stress in the crack tip region by relaxing constraint. Again, the very large fracture toughness of the F185 compared to the other systems suggests a strong synergistic effect between lowering the crosslink density, which increases the freedom to deform in response to shear stress and rubber particle additions, which allow larger shear stresses to be developed at the tip of a crack.

Translation of Neat Resin Toughness into Delamination Toughness

There appear to be at least two reasons why tougher resin systems give a much smaller fraction of their neat resin fracture toughness in delamination toughness. First, a tougher resin has a deformation zone that is much more extensive than the resin rich region between plies. In the composite, the fibers act like rigid filler in this deformation zone, which reduces load redistribution away from the crack tip, allowing the critical strain or critical stress condition for local failure to be achieved more easily. For resins where the deformation/damage zone ahead of the crack tip is on a scale less than or equal to the height of the resin rich region between plies, one might expect the neat resin toughness and the delamination toughness to be similar if interfacial failures do not dominate the delamination fracture behavior. Only in the case of the F185 is there extensive damage outside of the resin rich region between plies, and only in this system is there a dramatic difference in the neat resin fracture toughness and the composite delamination fracture toughness.

A second way the fibers may prevent delamination fracture toughness from achieving neat resin fracture toughness is that they allow heterogeneous nucleation sites for fracture. For mode I loading, all four of the composite systems studied had failure primarily in the interfacial region. Even where fiber bonding is good, the interfacial region seems to have a greater density of microcracks (or deformation), which leads to premature failure of the composite prior to extraction of the full toughness from the

resin system.

Mode II Delamination Fracture Toughness

The more brittle the system, the greater is the ratio of $G_{IIc}$ to $G_{Ic}$. This is the generalization from this work and other unpublished work at Texas A&M University. The increase in total energy release rate for increasing mode II in brittle systems can be understood to be the result of a whole series of sigmodial shaped cracks forming as brittle microcracks , impeded in their growth on their respective principle normal stress plane by the presence of the fibers. This both increases the area of fracture surface created and constitutes a more torturous path for crack propagation, each of which would require greater energy dissipation per unit area of crack extension.

Where the fracture is more ductile, the energy dissipation does not seem to be such a sensitive function of the imposed state of stress. Thus, ductile systems give similar values for $G_{Ic}$ and $G_{IIc}$.

The Effect of Off Angle Plies

The in-situ fractography seen in Figure 6 clearly indicates that significant resin deformation is occurring along the axis of the specimen. This specimen with all $+-45^{o}$ plies would certainly experience significant resin loading in the direction of the specimen axis due to bending stresses. While similar stresses would also be experienced by a unidirectional laminate specimen, the fibers would carry essentially all of the loading in the axial direction. It is this additional deformation, not only in the crack tip region, but presumably all along the specimen that

is the far field damage previously mentioned as being responsible for giving an artifically high value for $G_{Ic}$ of 1400J/m$^2$. It is worth noting that the specimen with +-45$^o$ plies at the interface where delamination is occurring but mainly unidirectional plies otherwise had a delamination fracture toughness similar to that for the unidirectional laminate. A J-integral analysis being developed at Texas A&M University has given approximately 600J/m$^2$ for $G_{Ic}$ for the laminate with all +-45$^o$ plies. If this proves to be a reliable result, then it suggests that the delamination fracture toughness in composite materials may be a material property independent of stacking sequence if the near and far field damage are properly separated.

**SUMMARY**

The combination of low crosslink density and elastomer additions has been seen to give the most potent toughening for neat resins. A relatively small increment of the additional neat resin fracture toughening above 800J/m$^2$ is actually reflected in the delamination fracture toughness of a composite. Mode II delamination toughness of brittle systems may be as much as three times the mode I delamination fracture toughness while a ductile system may have a mode II delamination fracture toughness that is similar the the mode I value. The energy aborbed per unit area of crack extension for delamination seems to be independent of ply orientation if proper accounting of the near and far field energy dissipation is made.

**ACKNOWLEDGEMENT**

The generous support of this work by the Air Force Office of Scientific Research (Major David Glasgow, project monitor) is acknowledged. Rich Moulton's (Hexcel Corporation) assistance in providing the materials studied is also recognized. The authors also acknowledge the technical support given by the Electron Microscopy Center of Texas A&M University.

REFERENCES

1. Scott, J.M., and Phillips, D.C., "Carbon Fibre Composites with Rubber Toughened Matrices", Journal of Materials Science, Vol. 10(1975), pp. 551-562.

2. Bascom, W.D., Bitner, J.L., Moulton, R.J., and Siebart, A.R. "The Interlaminar Frcture of Organic-Matrix, Woven Reinforcement Composites", Composites, January 1980,pp.9-18.

3. Bascom, W.D., Ting, R.Y., Moulton, R.J., Riew, C.K., and Siebert, A.R., "The Fracture of an Epoxy Polymer Containing Elastomeric Modifiers", Jounal of Materials Science, Vol. 16 (1981), pp. 2657-2664.

4. Vanderkley, P.S., "Mode I-Mode II Delamination Fracture Toughness of a Undirectional Graphite/Epoxy Composite", Master's Thesis, Texas A&M University, College Station, Texas, December 1981.

5. Cohen, R.N., "Effect of Resin Toughness on Fracture Behavior of Graphite/Expoxy Composites", Master's Thesis, Texas A&M University, College Station, Texas, December 1982.

6. Bradley, W.L., and Cohen, R.N., "Matrix Deformation and Fracture in Graphite Reinforced Epoxies", presented at ASTM Symposium on Delamination and Debonding of Materials, Pittsburg, Pa., November 8-10, 1983.

7. Moulton, R., Hexcel Corporation, Dublin, California, Personal Communication. Materials",

8. Russell, A.J., and Street, K.N., "Moisture and Temperature Effects on the Mixed-Mode Delamination Fracture of Undirectional Graphite/Epoxy," Delamination and Debonding of Materials, ASTM STP 876, S. Johnson, Ed., American Society for Testing and Materials, Philadelphia, 1985.

9.. Wilkins, D.J., Eisemann, J.R., Cumin, R.A., and Margolis, W.S., "Characterizing Delamination Growth in Graphite-Epoxy", in Damage in Composite Materials: Basic Mechanisms, Accumulation, Tolerance and Characterization, ASTM STP 775, American Society for Testing and Materials, 1982.

10. Devitt, D.F., Schapery, R.A., and Bradley, W.L., "A Method for Determining the Mode I Delamination Fracture Toughness of Elastic snf Biscoelastic Composite Materials", Journal of Composite Materials, Vol. 14, October 1980.

11. Theocaris, P.S. and Stassinakis, C.A., "Crack Propagation in Fibrous Composite Materials Studied by SEM", Journal of Composite Materials, Vol. 15(March 1981), pp.133-141.

12. Mao, T.H., Beaumont, P.W.R., and Nixon, W.C., "Direct Observations of Crack Propagation in Brittle Materials", Journal of Materials Science Letters, Vol. 2(1983).

13. Williams, D., "Mode I Transverse Cracking in an Epoxy and a Graphite Fiber Reinforced Epoxy", Master's Thesis, Texas A&M University, College Station, Texas, December 1981.

14. Product Bulletin, Hexcel Corporation, Dublin, California.

15. Hunston, D.A., "Composite Interlaminar Fracture: Effect of Matrix Fracture Energy," presented at ASTM Symposium on Toughened Composites, Houston, TX March, 1985.

16. Chai, H., "The Characterization of Mode I Delamination Failure in Non-Woven, Multi-Directional Laminates," Composites , Vol. 15,No. 4, October, 1984, pp 277-290.

17. Yee, A.F., and Pearson, R.A., "Toughening Mechanism in Elastomer-Modified Epoxy Resins--Part 1", NASA Contractor Report 3719, 1983.rimental work completed,

TABLE 1 Glass Transition Temperature of Resins

| Resin System | Glass Transition Temperature (°C) |
|---|---|
| 350Z | 191* |
| F155 | 118 |
| HX205 | 118 |
| F185 | 109 |

*Obtained from literature from Hercules.

TABLE 2 Resin Tensile Properties

| Resin System | Yield Strength (MPA) | Tensile Strength (MPA) | Elongation (%) |
|---|---|---|---|
| 3502 | -- | -- | -- |
| F155 | 58 | 69 | 3.10 |
| F185 | 38 | 46 | 8.87 |
| HX205 | 61 | 73 | 3.24 |

TABLE 3 Critical Energy Release Rates ($G_c$)
$J/m^2$

| Material | AS4/3502 | T6T145/F155 | T6T145/HX205 | T6T145/F185 |
|---|---|---|---|---|
| Mode I(neat resin) | 70(13) | 730(14) | 460 | 8100 |
| Mode I(composite) | 189 | 520/620 | 455 | 2205 |
| 20% Mode II | 264 | 525 | 796 | -- |
| 43% Mode II | -- | 548 | 789 | -- |
| Mode II | 570 | 1270/1800 | 1050 | 2440 |

TABLE 4 Effect of Fiber Orientation Upon Mode I $G_{1c}$

| Material | Layup | $G_{1c}$ |
|---|---|---|
| F155 | 0(24) | 520 |
| F155 | +45/-45/0(8)/-45/+45/ -45/+45/0(8)/+45/-45/ | 600 |
| F155 | +45(2)/-45(4)/+45(2)/ -45(2)/+45(4)/-45(2)/ | 1400 |

TABLE 5 Damage Zone Size and Corresponding Delamination Fracture Toughness

| Material | Size of Damaged Zone(Mm) | | $G_{1c}$ ($J/m^2$) |
|---|---|---|---|
| | Ahead of Crack Tip | Above or below delamination plane | |
| AS4/3502 | 20 | 5 | 189 |
| F155 | 20 | 10 | 520 |
| F155 +-45 | 50 | 10 | -- |
| HX205 | 75 | 35 | 455 |
| F185 | 200 | 35 | 2205 |

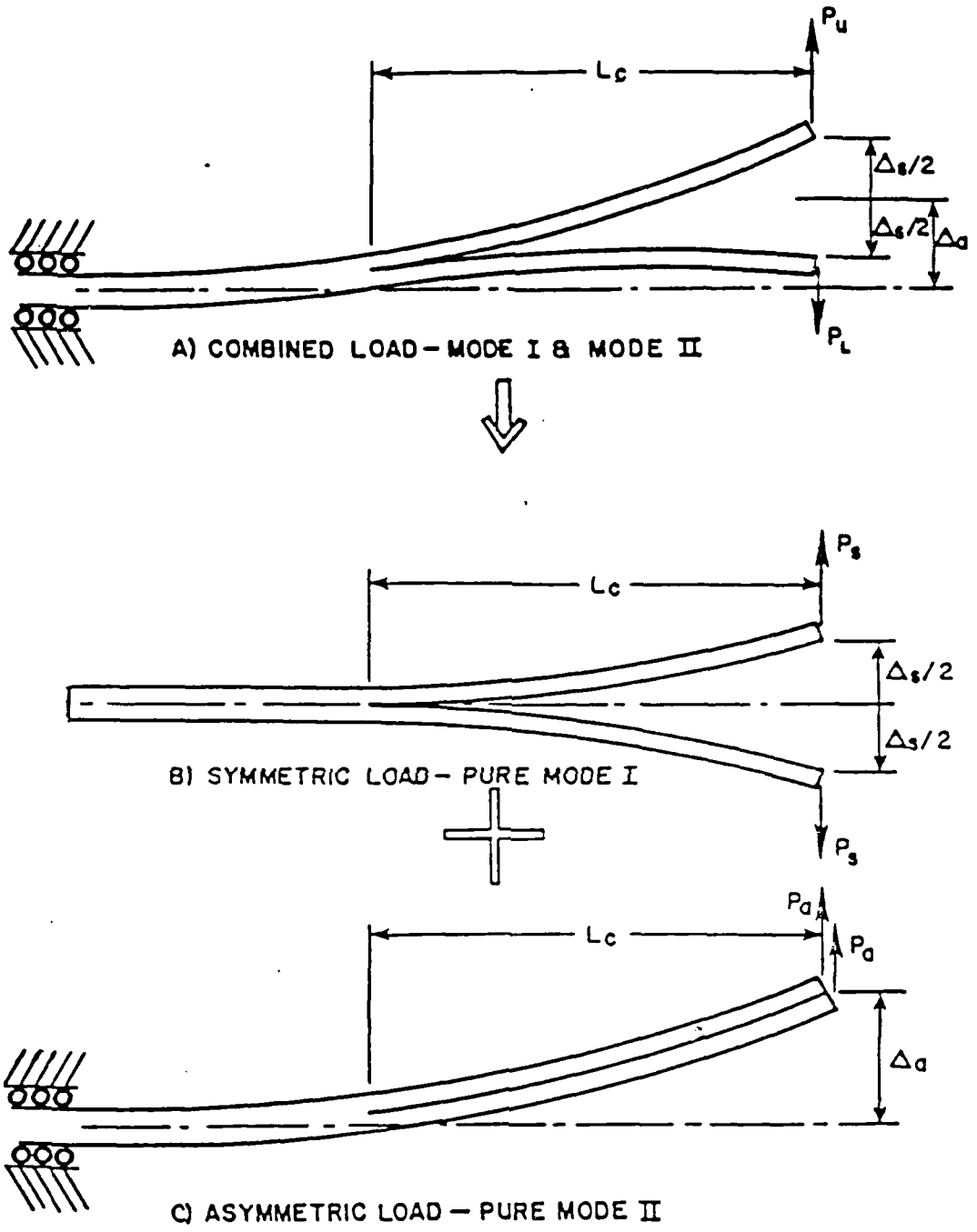


Figure 1. Schematic showing how asymmetric loading of split laminate can introduce a mixed mode I/mode II state of stress at the crack tip.

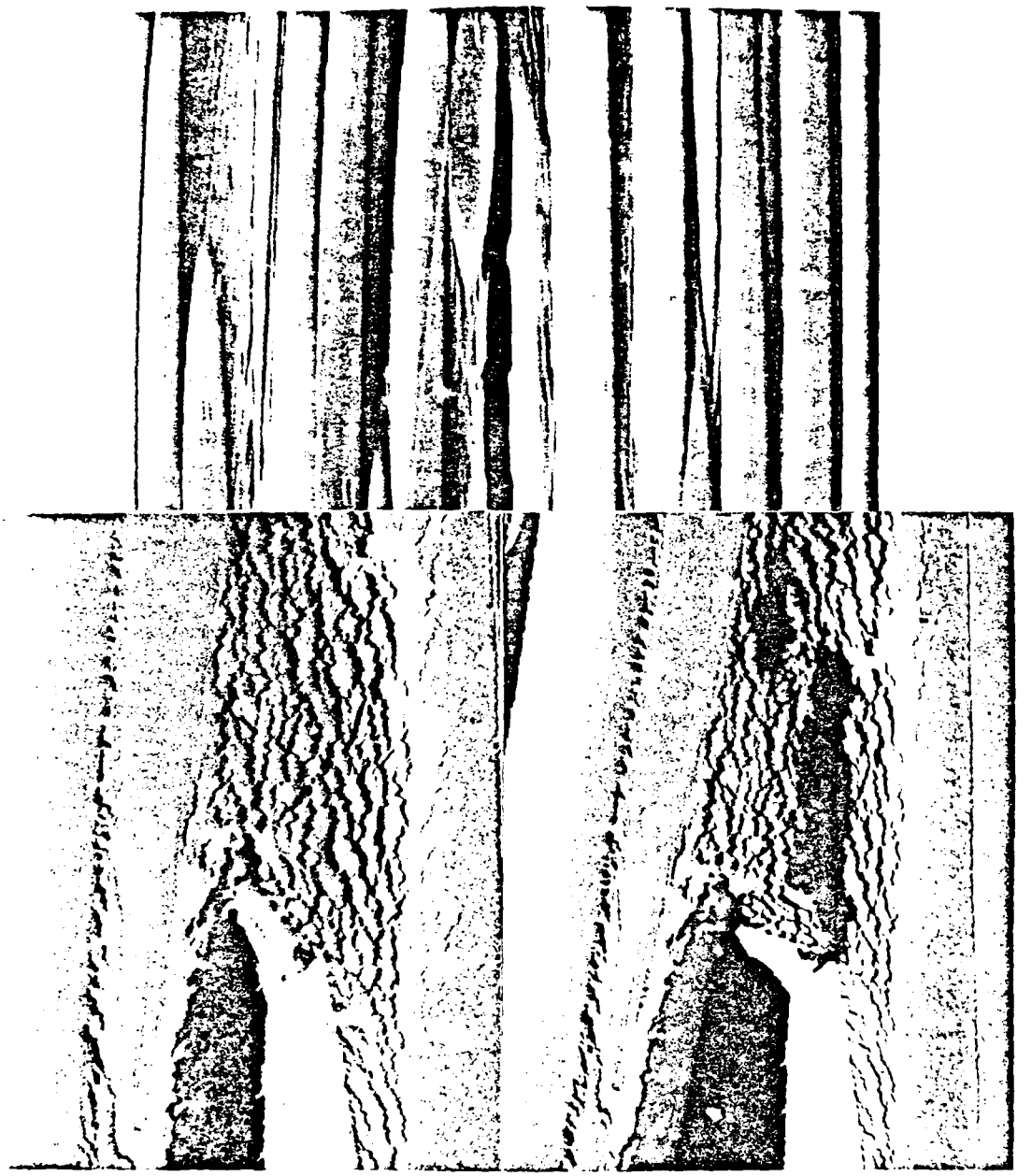

2. In-situ delamination of AS4/3502 showing debonding with very little resin damage (top, at 1000x).

3a. In-situ delamination of T60045/F155 showing extensive microcracking around the crack tip (left, at 3900 x).

3b. In situ delamination of T6T145/F155 showing coalescing of microcracks to form macroscopic crack growth (right, at 3000x).

3c. In situ-delamination of T6T145/F155 system. Debonding as well as microcracking is visible (1000x).

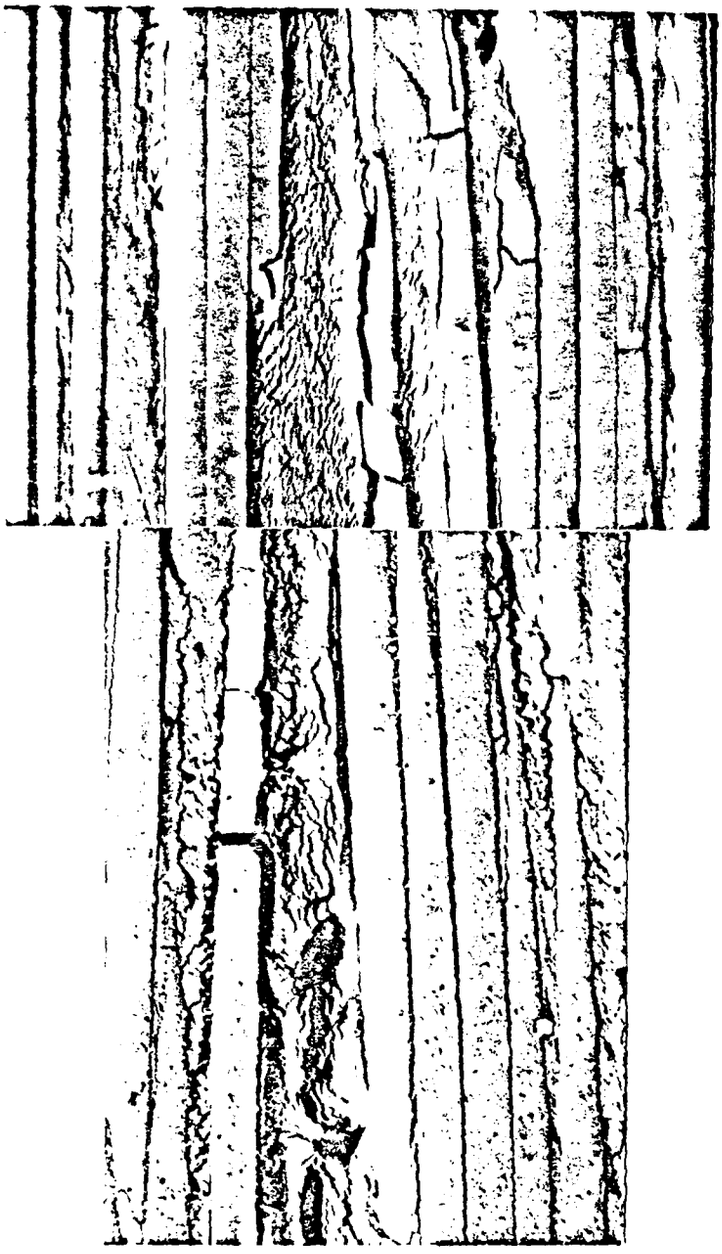

4a. In-situ delamination of HX205 system. Main crack grows is preceeded by developing af large microcrack zone ahead of the crack tip(top, at 800x).

4b. In-situ delamination of HX205 system. Extensive microcracking that coalesces into macroscopic crack growth (bottom, at 1000x).

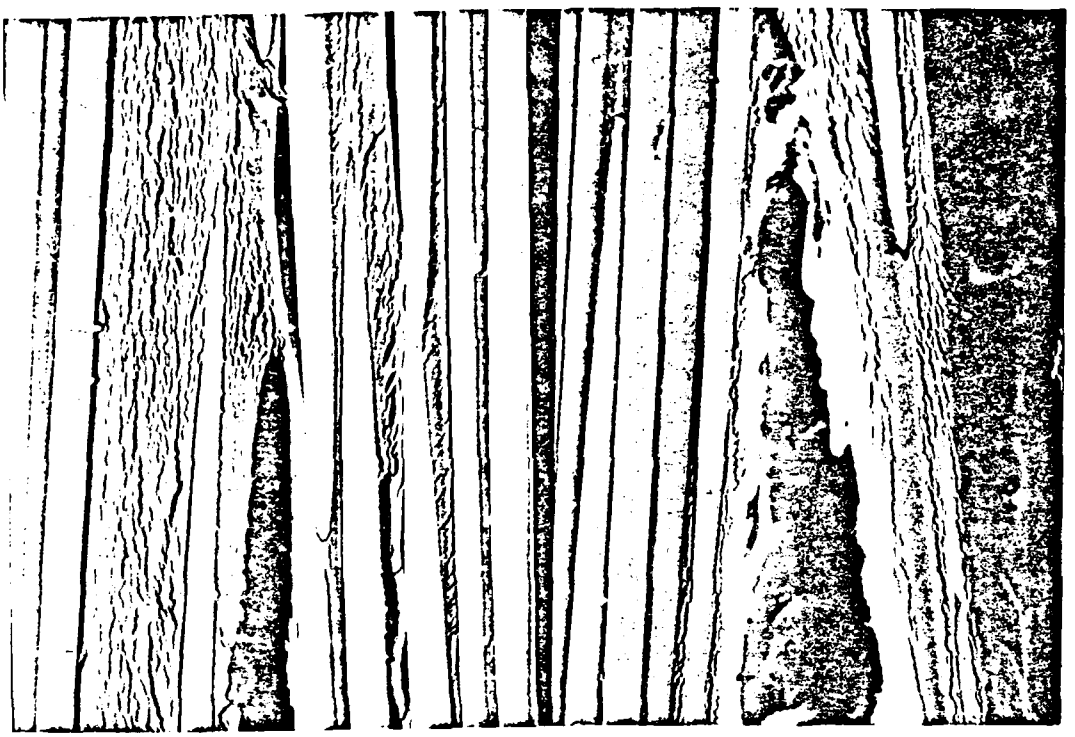

5a. In-situ delamination T6T145/F185 system. Large microcrack zone ahead of crack tip, with a significant extent above and below plane of crack (left, at 1000x).

5b. In-situ delamination of T6T145/F185 system. Resin tearing as well as microcracking is evident (right, at 1000x).

6a. In-situ delamination of T6T145/F155 system with fibers at +-45. (left, at 1000x).

6b. In-situ delamination of F155 system with fibers at +-45. Note microcracks that point back to macroscopic crack tip (right, at 1000x).

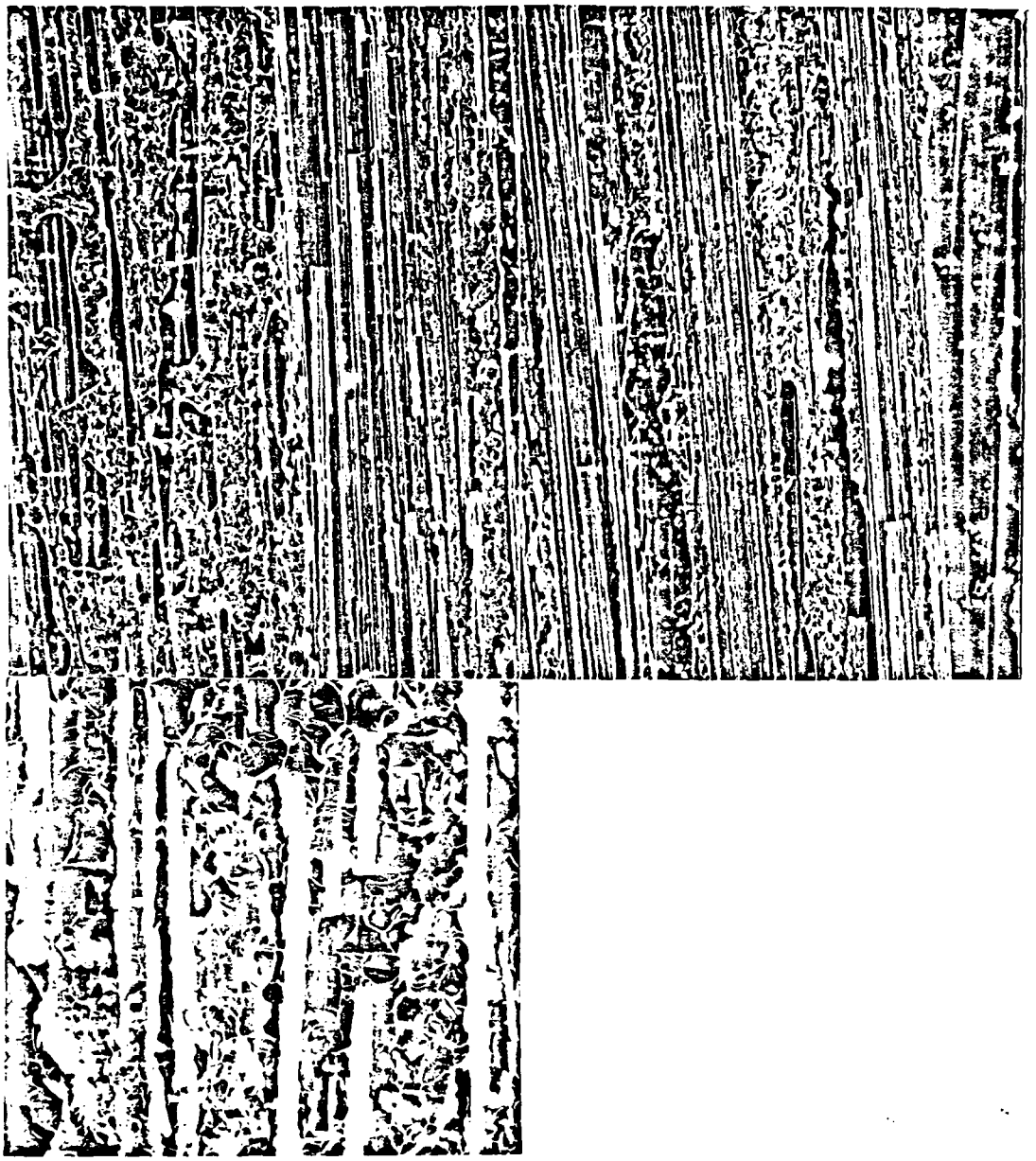

7a. Post-mortem fractography of F155 composite delaminated in Mode I conditions. (near center of specimen) (upper left, at 100x)

7b. Post-mortem fractography of F155 composite delaminated in Mode I conditions . (near edge of sample) (upper right, at 100x)

8a. Post-mortem fractography of HX205 composite delaminated in Mode I conditions. (lower left, at 300x)

9a. Post-mortem fractography of F155 composite delaminated in 43% Mode II conditions. (top surface of fractured specimen) (top, at 450x)

9b. Post-mortem fractography of F155 composite delaminated in 43% Mode II conditions. (Bottom surface of fractured specimen). Note leaf like artifacts are oriented in opposite direction to those on the top surface (center, at 1500x).

10. Post-mortem fractography of HX205 composite delaminated in 43% Mode II conditions (bottom, 300x).

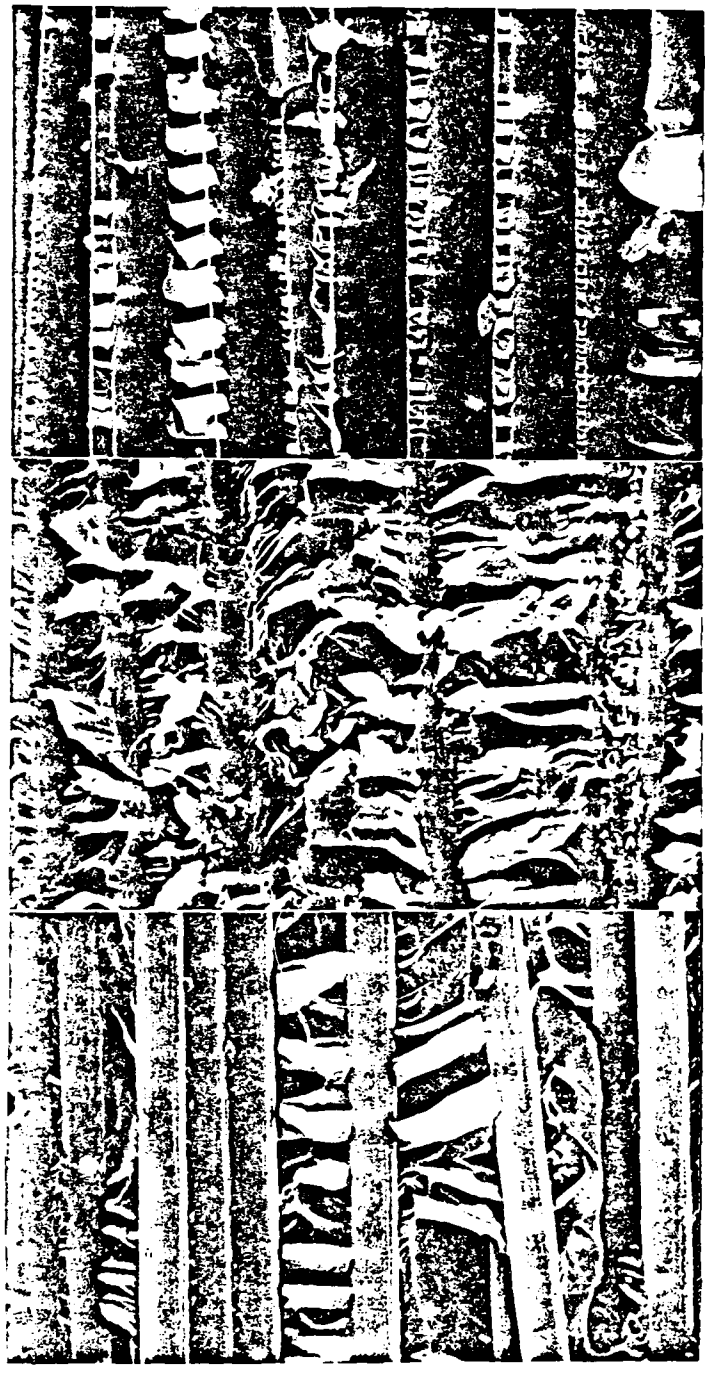

11a. Post-mortem fractography of AS4/3502 composite delaminated in Mode II conditions. Zipper like artifacts appear to be formed by coalescence of series of signodial shaped microcracks (top, 1500x).

11b. Post-mortem fractography of F155 composite delaminated in Mode II conditions. Note extensive resin deformation (center, at 1000x).

11c. Post-mortem fractography of HX205 composite delaminated in Mode II conditions. Note extensive resin deformation (bottom, at 1000x).

# A COMPARISON OF THE CRACK TIP DAMAGE ZONE FOR FRACTURE OF HEXCEL F185 NEAT RESIN AND T6T145/F185 COMPOSITE

E. A. Chakachery and W. L. Bradley

Texas A&M University

College Station, TX 77445

Presented at the ACS International Symposium

on Non-Linear Deformation, Fatigue and Fracture

of Polymeric Materials

ABSTRACT

A Comparison of the Crack Tip Damage Zone for Fracture of Hexcel F185 Neat Resin and T6T145/F185 Composite, E. A. Chakachery and W. L. Bradley, Texas A&M University, College Station, 77843. Hexcel F185 neat resin and T6T145/F185 graphite fibre reinforced composite were subjected to Mode I loading in the compact tension geometry (fibres parallel to the crack) and the energy per unit area of crack extension, $J_{Ic}$, determined to be 8100 and 1600 $J/m^2$ respectively. In-situ fracture studies in the SEM on a CT-type specimen of F185 showed extensive micorcracking in a damge zone ahead of the crack tip, which was similar to the microcracking observed in the whitened area ahead of the crack tip in the macroscopic CT specimens. A simple calculation using a rule of mixtures approach suggests that the diminished size of the damage zone and the presence of rigid fibres in the damage zone in the composite are not a sufficient explanation to account for the significantly lower toughness of the composite compared to the neat resin. From this it may be inferred that the strain to failure locally in the damage zone ahead of the crack in the composite may also be lower than that which can be tolerated in the neat resin. Evidence for this idea comes from the observation that microcrack coalescence seems to occur preferentially at the fibre/resin interface.

## INTRODUCTION

Delamination in graphite fibre reinforced resin composites is well known to limit the extensive use of these materials in some structural applications. Much effort has been directed in the past decade towards improving the delamination fracture toughness of graphite/epoxy composites (1-10). Since the delamination crack propagates through the interlaminar resin rich region, the emphasis has been on obtaining epoxy resins with improved fracture toughness. The addition of elastometric modifiers was shown (1-6) to dramatically increase the fracture toughness, $G_{Ic}$, of the matrix resin, but resulted only in a modest increase in the delamination fracture toughness of the composite (7,8). This was shown (8-10) to be primarily due to the reduced volume of resin deformation in the damage zone ahead of the delamination crack tip since the fibres act as rigid fillers in the ductile matrix. Evidence in support of this conclusion was obtained (9,10) from the observation that a decrease in the fibre volume fraction resulted in an increase in the delamination fracture toughness. The current investigation was undertaken to attempt to correlate the delamination fracture toughness of the composite with the fracture toughness of the neat resin. The determination of the fracture processes occurring in the vicinity of the crack tip in both the composite and the neat resin was a necessary first step. If these events are nominally the same, then there may be a relationship between neat resin toughness and delamination toughness.

To study the relationship between neat resin fracture toughness

and composite delamination fracture toughness, in-situ observations of each fracture process have been made in the scanning electron microscope. These observations have been correlated with macroscopic measurements of a composite made from this neat resin. A simple model has been proposed to relate the microscopic observations of the fracture processes to the observed macroscopic measurements of fracture toughness.

The resin system selected for this study was the F185 formulation commercially available from Hexcel Corp. It is a relatively ductile epoxy (9% elongation in a 2.5 cm gage section) with a reported fracture toughness of 6000 $J/m^2$ (7,11). The resin is primarily a diglycidyl ether of bisphenol A, (DGEBA), modified by the addition of 8.1 wt% of liquid CTBN (Hycar® 1300 x 13), a carboxyl terminated copolymer of butadiene and acrylonitrile. It is further toughened by the addition of 5.4 wt% of Hycar® 1472, a pre-reacted solid elastomer in a bimodal particle size distribution of nominally 2 μm and 8 μm diameters. The liquid CTBN undergoes partial phase separation into particles varying from 0.1 m to 10 m in size. The portion that does not phase separate out before gelation of the epoxy remains in solution in the epoxy matrix and has a plasticizing effect on the resin (3,4), thus lowering the yield strength of the epoxy matrix. The phase separated CTBN undergoes dilatation and rupture by cavitation (5,6) thus reducing the triaxial state of stress in the vicinity of the particle. This has the effect of locally increasing the shear stress and promoting deformation through the formation of shear bands (5,6).

## EXPERIMENTAL PROCEDURES

### Materials and Specimen Preparation

The F185 neat resin and the T6T/145/F185 graphite/epoxy composite used were both supplied by Hexcel Corporation. Plates, 1.25 cm, 0.5 cm, and 0.2 cm thick, of F185 were received as cast, and were machined according to ASTM E 813-81 to obtain standard 1T compact tension (CT) specimens, but with a thickness of 1.25 cm. The T6T145/F185 composite was obtained both as preimpregnated tape ( 25 cm wide) and as undirectional plates, 90 plies thick (A) and 24 plies thick (B). Compact tension specimens were machined from plate A such that the fibers and the laminate lay-up axis were transverse to the load line, with the direction of crack propagation parallel to the fibres. As with the F185 resin these were standard 1T compact tension specimens with a thickness of 1.25 cm. Plate B contained a teflon strip ( 2.5 cm wide, running perpendicular to the fibre direction ) between the twelfth and thirteenth plies. This created a region of debond which acted as an initial delamination crack. Two undirecitonal plates, sixteen plies (C) and twelve plies thick (D), were laid up from the preimpregnated tape with mid-plane teflon inserts (as in plate B), and cured according to the schedule described in the specification sheet supplied by Hexcel Corporation. Double cantilever beam (DCB) specimens (2.5 cm wide and 25 cm long) were machined from plates B and C such that the fibre direction was parallel to the specimen length. Tabs which allowed for free rotation were bonded to the DCB specimens at the end with the initial delamination crack.

Miniature DCB specimens of the composite (3.8 cm long and 0.7 cm wide) were cut from plate D and minature CT-type specimens of the neat resin (4 cm long, 2.8 cm wide and 0.2 cm thick) were also machined for in-situ studies. These were ground, polished (0.25 μm), cleaned ultrasonically and coated with a Au/Pd alloy (~150 A) prior to observation in the scanning electron microscope.

Specimen Testing

All macroscopic testing of DCB and CT specimens were performed on a Materials Test System (MTS) servo-hydraulic machine in displacement control under quasi-static loading conditions ($4 \times 10^{-5}$ to $7 \times 10^{-5}$ cm/sec) at room temperature. Load-displacement records were obtained directly from the MTS strip chart recorder and were also digitized simultaneously via a Hewlett-Packard HP 3497A Data Acquisition Unit and stored through a HP 9816 desk-top computer. All CT specimens were machined with a chevron notch and were pre-cracked in fatigue until the crack front was out of the chevron. Fatigue load limits were determined as per ASTM E 399-81 for the composite and ASTM 813-81 for the F185 resin. Post-mortem fractography was performed on a JEOL JSM-25 scanning electron microscope. A JEOL JSM-35CF scanning electron microscope equipped with a JEOL 35-TS2 tensile stage was used for the fracture studies in-situ in the SEM. Photomicrograpnic stills and real-time videotapes were obtained of the fracture processes.

## RESULTS, ANALYSIS AND DISCUSSION

### Macroscopic Fracture Toughness Measurements

The load-displacement results for the delamination tests were analyzed using a relationship derived from linear beam theory by Devitt et al (12), namely,

$$G = \frac{P^2 L^2}{BEI} \qquad (1)$$

where P is the load, L is the crack length, B is the width, E is the tensile modulus and I is the rotational moment of inertia for each half of the split laminate. The ratio of load line displacement to crack length remained well below the limit of 0.6 for linear beam theory to be applicable (12). The crack length was measured visually at the surface at approximately fifteen discrete points and the loads and displacements recorded at these same points. Critical energy release rates could then be calculated for each point. The calculated $G_{Ic}$ values remained essentially constant for various crack lengths. An average of the calculated values after the transient was found to be 1900 $J/m^2$ .

The 1T compact tension specimens of F185 was tested in displacement control with multiple, partial unloading to allow determination of the crack extension by the compliance method. The load-displacement record was quite nonlinear (Fig. 1), necessitating a J-integral analysis according to ASTM E813-81. A well defined J-R curve was obtained from which a $J_{Ic}$ value of 8100 $J/m^2$ was determined.

This is considerably higher than the value of 6000 J/m$^2$ reported by the manufacturer (11). This difference may be due to our use of fatigue precracking rather than razor notching or due to our use of a nonlinear rather than linear analysis. If we use the linear elastic analysis in ASTM E399-81,we obtain a $K_Q$ value of 2700 J/m$^2$ from the 5% secant offset value of $P_Q$. However, Pmax is much greater than 1.1 $P_Q$, and the specimen thickness is less than that required by ASTM-E399 for $K_Q$ to be equal to $K_{Ic}$. Thus, the linear elastic analysis is invalid for our specimen size. If we use Pmax and the actual crack length at Pmax in a LEFM calculation, we obtain a "$K_{Ic}$" which has an equivalent $G_{Ic}$ of 6300 J/m$^2$ which is similar to the 6000 J/m$^2$ obtained by Bascom (2) using a similar approach. We believe that the value of 8100 J/m$^2$ obtained in this work using fatigue precracked specimens and a J-integral analysis is a more meaningful measure of the fracture toughness of the F185 resin.

A J-integral approach was also used to analyze the data obtained in the CT specimens of the composite. The $J_{Ic}$ for transverse crack growth thus obtained was 1600 J/m$^2$ which compares very well with recent results by Bascom (13). The macroscopic test may be summarized as follows: the neat resin fracture toughness was 8100 J/m$^2$ whereas the delamination and transverse cracking in the composite gave toughness values of 1900 J/m$^2$ and 1600 J/m$^2$ respectively. Thus, crack growth in the composite parallel to the fibre direction is much easier than crack growth in the neat resin.

In-Situ and Post Mortem Fracture Observations in SEM

Fracture studies conducted in the scanning electron microscope on

the F185 neat resin indicate that the zone ahead of the crack tip undergoes extensive microcracking (Fig. 2). There has been some recent controversy as to whether these are actually microcracks in the resin or microcracks in the 150A thick gold-palladium coating applied to the specimens to minimize charging. To try to verify that these are actual microcracks in the material, we have recently polished two sides of an AS4/3501-6 graphite/epoxy composite, coated one side with a 150A thick layer of gold-palladium in the usual way, delaminated the specimen in the SEM, removed the specimen with the wedge in tact to avoid viscoelastic recovery and closure of the microcracks, and then coated the other side with gold-palladium in the usual way, and then examined it in the SEM with the wedge still in tact. The results of this exercise are presented in Figures 3(a) and 3(b). The microcrack morphology on the side coated and then deformed is essentially indistinguishable from the microcrack morphology seen on the side deformed and then coated. Thus, we believe that the Au/Pd coating is not responsible for the microcracking seen on the surface of our specimens.

The microcracked region ahead of the crack tip of the F185 neat resin (Fig. 2) extends 60-70 μm above and below the crack tip and is shaped somewhat like a kidney bean. Crack propagation under fixed grip conditions occurred in a discontinuous manner via a time-dependent coalescing of the microcracks ahead of a blunted crack tip. With each successive extension, crack advance of 120-150 μm was observed, resulting in a very sharp crack tip with relatively few microcracks ahead of it. The applied crack opening displacement was

then increased essentially instantaneously, and with this increase, the microcrack density ahead of the crack tip would gradually increase with time, accompanied by crack tip blunting at the formerly sharp crack tip. Again, a critical density of microcracks (or crack tip strain) is reached and crack extension occurs by microcrack coalescence as before. Evidence of this process is seen in the post-mortem fractographic examination as relatively flat regions of crack extension, separated by the small lips which probably arise from crack tip blunting, preceding the next crack extension (Fig. 4). This appearance is typical over the whole fracture surface, indicating that the phenomena observed at the surface is typical of the bulk fracture behavior.

If crack extension does indeed occur by microcrack coalescence, then the relatively flat regions between lips seen in Figure 4(a) and (b) should be found on examination at higher magnification to be composed of many small facets with ledges between them. This is exactly what is observed at 10,000X magnification, as shown in Figure 4(c). It is worth noting that even at this very high magnification that the individual facets do not seem to have fractured by a brittle cleavage. The surface is relatively textured, with cavitation presumably at the rubber particle additions, which suggests that the microcracking is a result of heterogeneous nucleation and growth by processes which require some local deformation. Thus, the microcracking may be a result of heterogeneities in the resin which facilitate crack nucleation and growth.

If the microcracks were just a result of coating cracking, the explanation would still be much the same except that the microcracking

would correspond to some threshold level of resin strain with the microcrack coalescence corresponding to some critical strain to failure in the resin. Thus, though we believe that the microcracks are in the resin rather than in the coating, the inference concerning the size of the deformation/damage zone ahead of the crack tip can be made equally well in either case. It should also be noted that microcracking and deformation have the same beneficial effect of redistributing the load away from the crack tip and lowering the local stresses at the crack tip. Thus, from a physical point of view, either process enhances toughness.

In-situ delamination studies on T6T145/F185 composite show that the resin microcracks quite extensively in the vicinity of the crack tip. The microcracking extends from the interlaminar region and into the ply about 50 μm above and below the crack (Fig. 5). Here, as in the resin, the crack propagates by microcrack coalescence and in the same discontinuous manner. At each stage, however, the crack tip blunting is apparently less than in the F185 resin and the discontinuous extension varies from 40-100 μm. The coalescence of microcracks occurs predominantly at the fibre resin interface. Thus it appears that the presence of the fibres prevents the development of the full resin toughness from being realized due to premature microcrack coalesence at the fibre resin interface.

The presence of the rigid fibres also restricts the height above and below the delamination plane over which deformation and microcracking occurs ( 100 μm in the composite, compared to 130 μm in the resin). However, the region of microcracking ahead of the crack

tip is actually increased from 25 μm in the resin to about 50 μm in the composite.

The fracture surface of the delaminated specimens showed evidence of cavitation, voiding and microcracking(Fig. 6). The resin region of the composite delamination fracture surface shows more coarse cavitation than in the neat F185 resin fracture surface, where voids were relatively fine and more homogeneously dispersed. Furthermore, the voids seem to be more dense in the resin adjacent to the fibres (Fig. 6(a),(b). The fibre resin interface probably provides heterogeneous nucleation sites for precipitation of the CTBN and facilitates the growth of larger particles. Microcrack coalescence at the fibre resin interface results in the highly scalloped features noticeable in Figure 6(b).

A Model to Predict Delamination Toughness from Neat Resin Toughness

A first order estimate of the delamination fracture toughness may be obtained by assuming that the delamination fracture process is essentially the same as the fracture process in the neat resin, except that the fibres act as a rigid filler, reducing the volume of resin available to deform in the crack tip region. It has previously been suggested by Bradley and Cohen (8) that the energy dissipation per unit area of crack extension may be calculated by picturing a small tensile specimen ahead of the crack tip which is slowly stretched as the crack tip approaches and finally breaks as the crack tip passses(Fig. 7). The energy absorbed per unit area of crack extension would be calculated for such a model by summing the energy abosrbed per unit volume of material over the volume of the hypothetical

tensile specimen. Such a summation may be written mathematically as follows:

$$G_{Ic} = \int_{-h}^{h} \int_{0}^{\varepsilon_{ij}} \sigma_{ij} \, d\varepsilon_{ij} \, dy \qquad (2)$$

where $G$ is the fracture toughness of the material

$2h$ is the height of the hypothetical tensile bar

$\sigma_{ij}$ is a component of the stress tensor

The addition of fibers to the neat resin can perturb the energy calculation in Equation 2 in several ways. First, the extent of the deformation zone might be changed (i.e., the height of our hypothetical tensile specimen), changing the value of h in Equation 2. Second, rigid filler would further reduce the effective gage length of material capable of deforming in our hypothetical tensile specimen. Third, fibre constraint and or debonding could change the local strain to fracture. These three factors could potentially account for the decrease in fracture toughness from 8100J/m$^2$ in the F185 resin to 1900J/m$^2$ in the composite delamination fracture toughness. The first two of these three factors can be quantified based on actual observations. If one assumes that microcracking begins for strains above a threshold strain, then the extent of the microcracked zone can be used to quantify the magnitude of the h in Equation 2.

A cross-section of the composite prepared metallographically to reveal the microstructure (Figure 8) may be used to determine the volume fraction of fibres in the hypothetical tensile specimen ahead of the crack tip. Since the volume fraction is quite nonuniform, the

microstructure was divided into three regions: the resin rich region between plies with a fibre volume fraction of 19%; the ply region with a volume fraction of fibres of 76% and a transition zone with a volume fraction of approximately 33%. The relative heights of these three regions are shown in the schematic in Figure 8, along with the height of the microcracked zone in the F185 resin. Using a simple rule of mixtures approach, and taking account of the smaller microcracked (and deformed) zone, one may estimate the delamination fracture toughness to be 4000J/$m^2$ as shown below:

$$G_{Ic} = \frac{J_{Ic}}{h_0} \left[ h_A (1-V^A_f) + h_B (1-V^B_f) + h_c (1-V^C_f) \right]$$

This calculation implicitly assumes that the local strain to fracture in the F185 resin and the composite are the same and that the stress distribution is also similar, at least on the average.

Since the measured value of delamination fracture toughness in this system is 1900 J/$m^2$ , the estimated value of 4000J/$m^2$ is seen to be quite excessive. It also strongly suggests what the in-situ fractograph has already indicated; namely, that preferential microcrack nucleation at the fibre/resin interface leads to premature failure, preventing the realization of 4000J/$m^2$ that might otherwise be possible. This suggests that more attention to the interphase region is required if a greater fraction of the intrinsic toughness of the neat resin is to be manifested in delamination fracture toughness of the fibre reinforced composite material.

## SUMMARY


1. The delamination fracture toughness of the T6T145/F185 composite is 1900 $J/m^2$ whereas the fracture toughness of the neat F185 resin is 8100 $J/m^2$.
2. Microcracking in the resin appears to be a significant deformation mode for load redistribution at the crack tip.
3. Crack progagation occurs in a discontinuous manner through microcrack coalescence ahead of the crack tip.
4. In the composite, the microcracking is coarser and coalescence seems to occur preferentially at the resin-fibre interface.
5. The height of the deformation zone, above and below the plane of crack propagation, is greater in the resin than in the composite.
6. Comparison of the relative heights of the damage zone yielded 4000 $J/m^2$ as a calculated delamination $G_{Ic}$ for the composite, which is an over-estimation by a factor of two.
7. It may be inferred that the strain to failure in the composite is lowered, probably due to premature microcrack coalescence at the resin fibre interface.


## ACKNOWLEDGEMENTS


The authors wish to acknowledge the generous financial support of both the National Aeronautics and Space Administration, Langley Research Center, (Dr. John Crews, Project Monitor) and the Air Force Office of Scientific Research (Major David Glasgow, Project Monitor). Special thanks are due Laurie Veeder for her careful macroscopic testing.

REFERENCES

1. C.K. Riew, E.H. Rowe, and A.R. Siebert, "Toughness and Brittleness of Plastics," R.D. Deanin and A.M. Crugnola, Eds., Adv. Chem. Ser. No. 154, Am. Chem. Soc., Washington, D.C., 1976, p. 326.

2. W.D. Bascom, R.Y. Ting, R.J. Moulton, C.K. Riew and A.R. Siebert, J. Maker. Sci., 16 , 2657 (1981).

3. L.T. Manzione and J.K. Gillham, J. Appl. Polym. Sci., 26 , 890 (1981).

4. L.T. Manzione and J.K. Gillham, J. Appl. Ploym. Sci., 26 , 907 (1981).

5. A.F. Yee and R.A. Pearson, "Toughening Mechanism in Elastomer - Modified Epoxy Resins - Part 1", NASA Contractor Report 3718, NASA Scientific and Technical Information Branch, Washington, D.C., (1983).

6. A.F. Yee and R.A. Pearson, "Toughening Mechanism in Elastomer - Modified Epoxy Resins - Part II", NASA Contractor Report 3852, NASA Scientific and Technical Information Branch, Washington, D.C., (1984).

7. W.D. Bascom, J.L. Bitner, R.J. Moulton and A.R. Siebert, Composites , ii, 9 (1980).

8. W.L. Bradley and R.N. Cohen, "Matrix Deformation and Fracture in Graphite Reinforced Epoxies", ASTM Symposium on "Delamination and Debonding in Materials", Pittsburgh, Nov. 1983.

9. W.L. Bradley and R.N. Cohen, "Delamination and Transverse Fracture in Graphite/Epoxy Materials", Fourth Internat. Conf. on Mech. Behavior of Mater., Stockholm, Sweden, August 1983.

10. W.M. Jordan, Ph.D Thesis, Interdisciplinary Engineering, Texas A&M University, College Station, TX, (1985).

11. Specification sheet for F185 resin from Hexcel Corporation.

12. D.F. Devitt, R.A. Schapery and W.L. Bradley, Composite Mater. 14 , 270 (1980).

AD-A173 255 DELAMINATION FRACTURE IN GRAPHITE/EPOXY MATERIALS(U) 2/2
TEXAS A AND M UNIV COLLEGE STATION DEPT OF MECHANICAL
ENGINEERING W L BRADLEY JUN 86 AFOSR-TR-86-0941
UNCLASSIFIED AFOSR-84-0064 F/G 11/4 NL

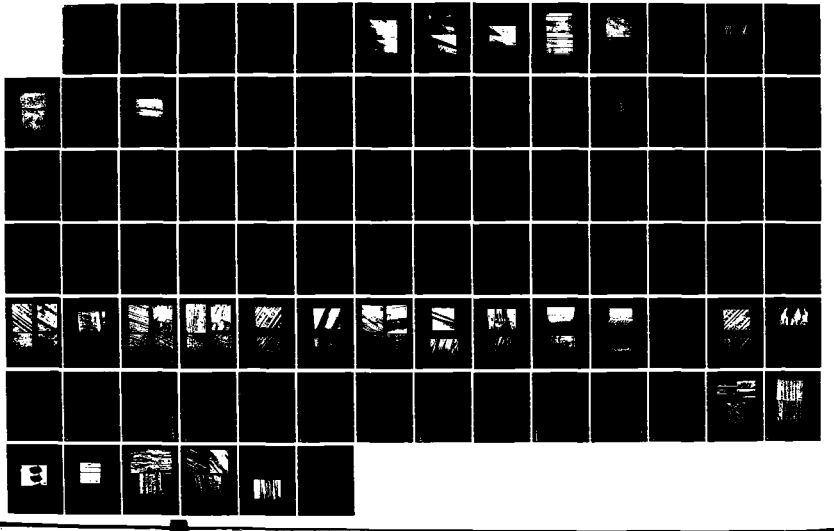

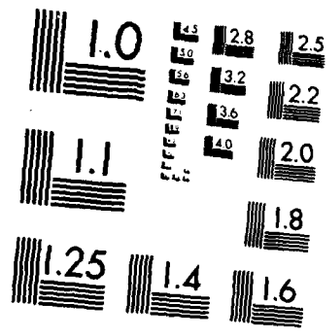

List of Nomenclature

| | |
|---|---|
| B | Width of double cantilever beam specimen |
| E | Elastic modulus in the fibre direction |
| $\varepsilon_{ij}$ | Failure strain for strain component |
| $G_{Ic}$ | Delamination fracture toughness under Mode I loading |
| h | Height of damage zone above the plane of crack propagation (2h = total height) |
| $h_0$ | Same as above for resin |
| $h_A, h_B, h_C$ | Same as above for the composite in regions of differing fibre volume fraction |
| I | Moment of inertia of one half of the DCB specimen |
| J | Resin fracture toughness under Mode I loading |
| L | Crack length (equivalent beam length for linear beam analysis) |
| $\sigma_{ij}$ | Component to stress tensor representing stress in hypothetical tensile bar (see Fig. 7) |
| P | Load applied to split laminate |

FIGURES

1. Load-displacement record for 1T compact tension specimen of F185 resin showing considerable non-linearity.

2. Microcracking ahead of the crack tip in F185 resin showing crack growth sequence under a constant applied displacement.
   (a) 1500x. Shape of the damage zone. Arrow markers correspond to regions similarly marked in Figure 2(e).

   (b) 3000x. Detail of crack tip. Arrow markers here correspond to similarly marked regions in Figures 2(c) and 2(d).

   (c) 900x. Crack propagation through microcrack coalescence to form a very sharp narrow crack.

   (d) 5000x. Crack extension of about 22 m. New crack tip is very sharp.

   (e) 1000x. Blunting of new crack tip with development of damage zone ahead of the tip. Total crack growth in the sequence is about 140 m (compare with Figure 2(a)).

3. Microcracking ahead of the crack tip in AS4/3502 at 3000x.
   (a) coated prior to loading
   (b) coated after loading

4. Fracture surface of F185 resin. Crack growth is from left to right.

   (a) 330x. Away from the free surface. Arrows indicate a lip formed by crack tip blunting after a growth sequence.

   (b) 330x. Just adjacent to the free surface.

   (c) 10,000x. Detail of a relatively flat region in (a). cavitation due to phase separated CTBN. Facets separated by ledges probably correspond to microcrack coalescence.

5. 1000x. In situ delamination of T6T145/F185 composite showing microcracking in the damage zone ahead of the crack tip. Note microcracking is more dense adjacent to the fibres. Preferential microcrack coalescence near the resin fibre interface where the micorcracks are inclined to the primary crack.

6. Fracture surface of T6T145/F185 composite.
   (a) 3000x. Higher density of cavitation adjacent to fibres.

   (b) 4500x. Scalloped appearance of resin between fibres from coalescence of inclined microcracks near resin-fibre interface.
   (c) 10,000x. Voiding adjacent to solid pre-reacted rubber

particles. Comparison with Figure 3 (c) shows that the cavitation due to phase separated CTBN is much coarser here than in the neat F185 resin.

7. Schematic of hypothetical tensile bar ahead of the crack tip with the strain distribution accross it.
8. 600x. Cross section of T6T145/F185 showing interlaminar resin rich region.

9. Schematic showing relative height of damage zone in F185 resin and T6T145/F185 composite.

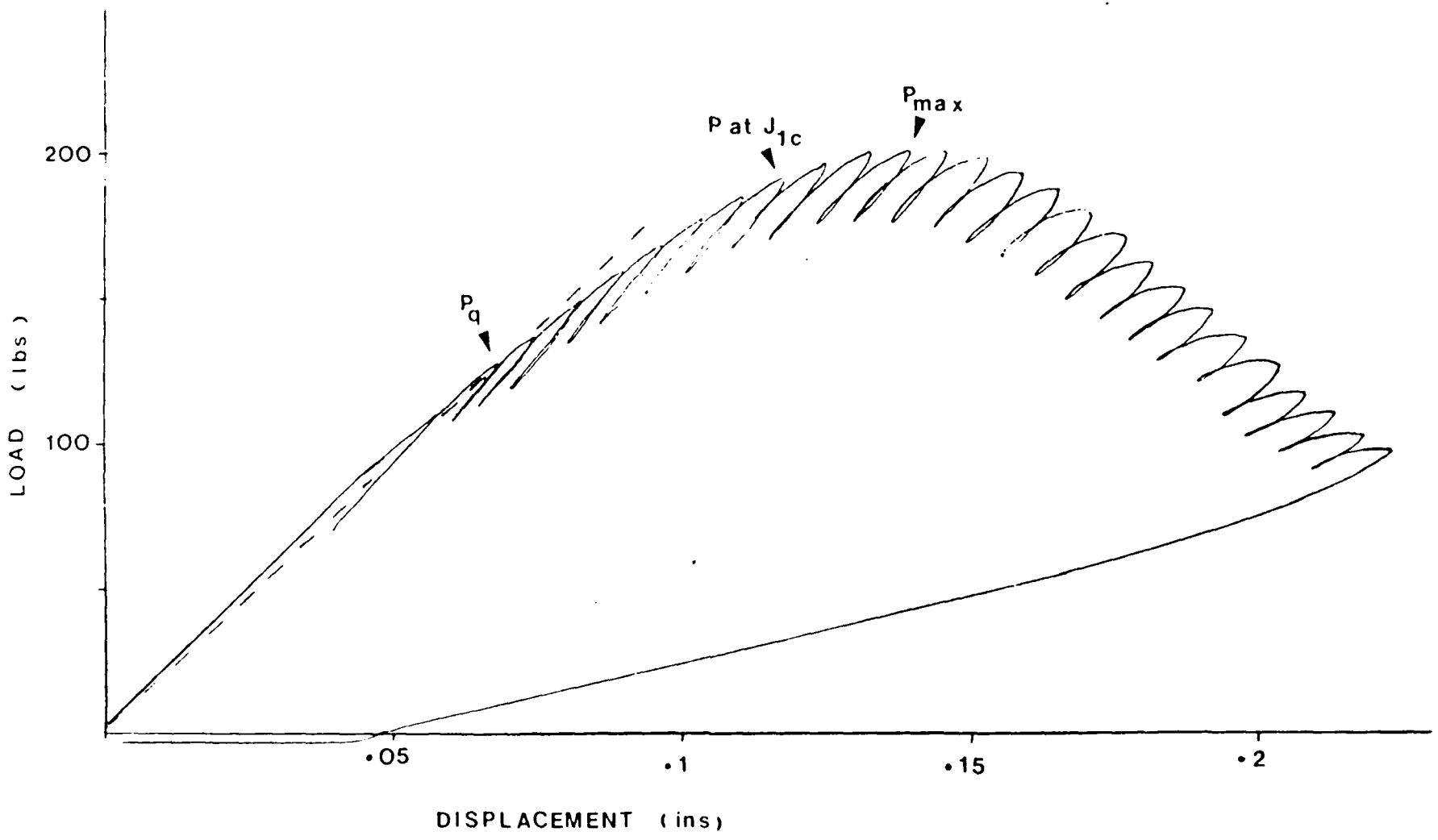
200
100
LOAD (lbs)
$P_q$
P at $J_{1c}$
$P_{max}$
.05
.1
.15
.2
DISPLACEMENT (ins)

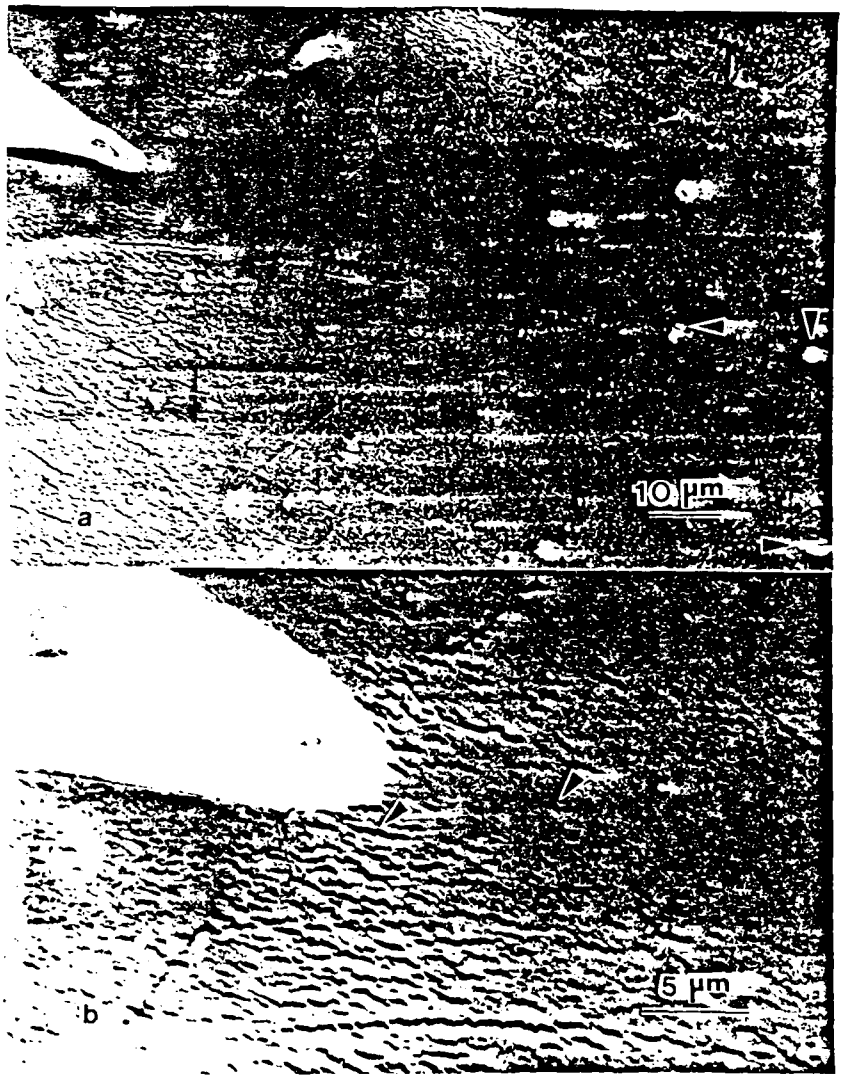
10 μm
a
5 μm
b

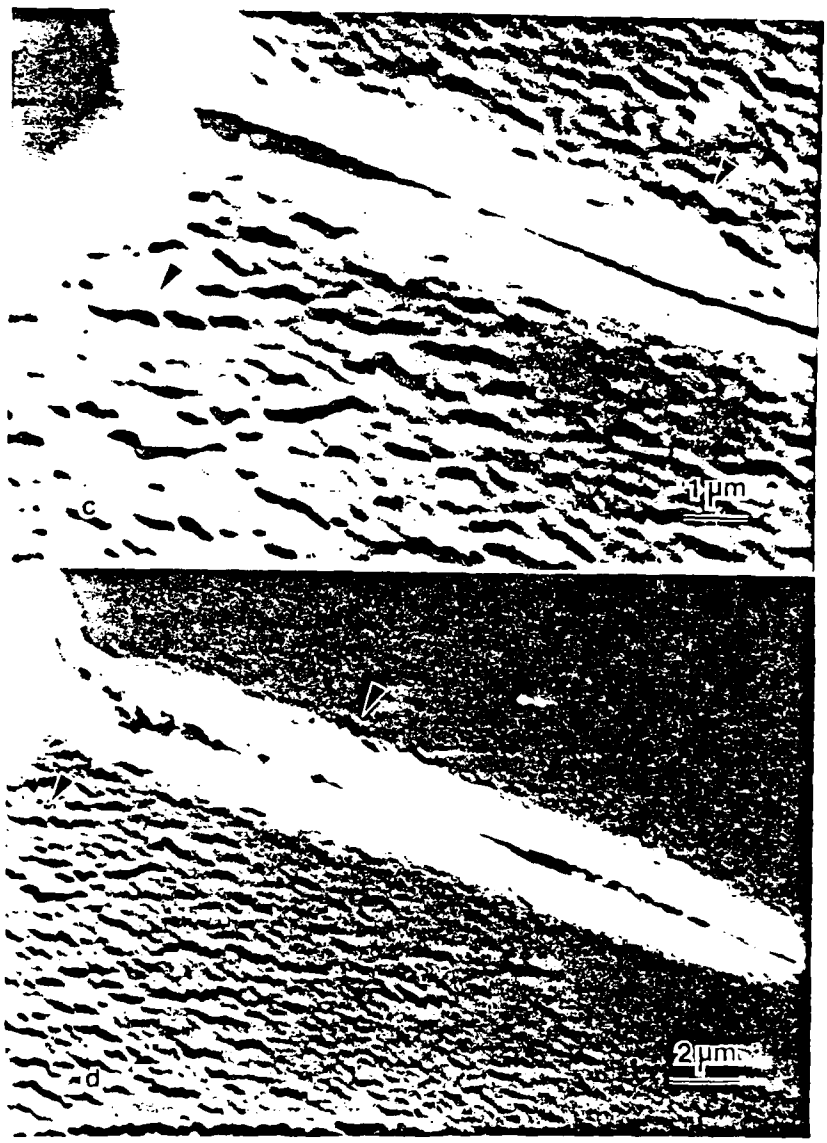
c
1 μm
d
2 μm

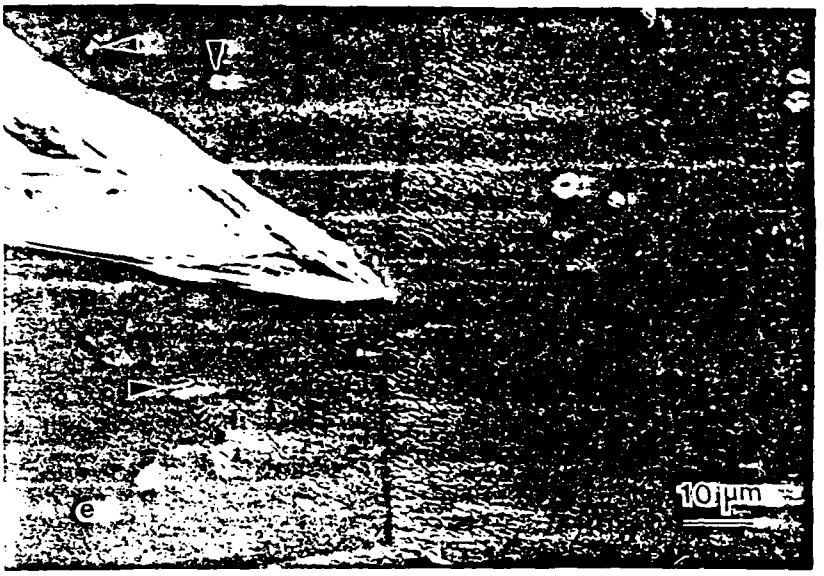
e
10 µm


a
30 µm
b

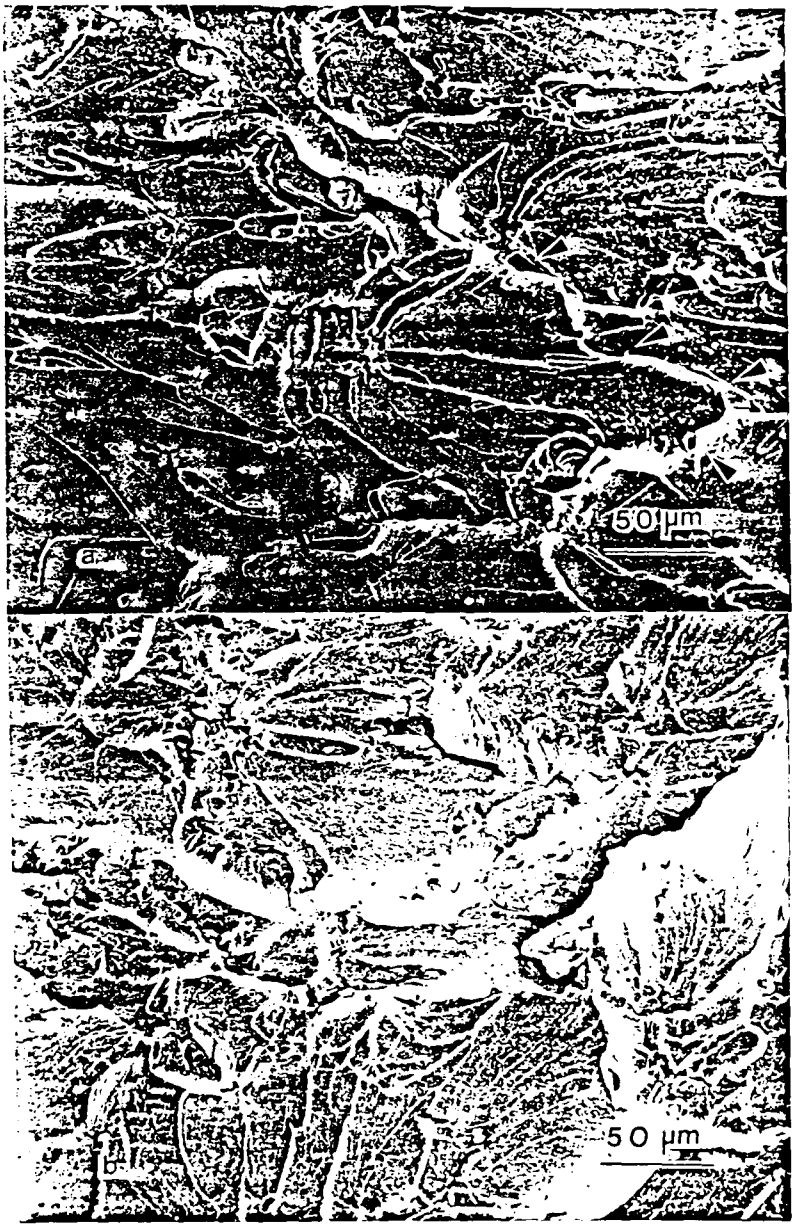
a
50 µm
b
50 µm

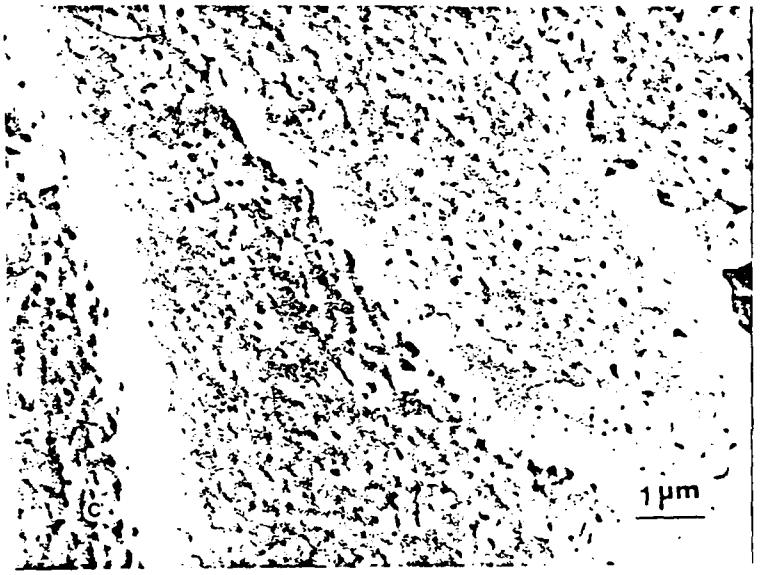
1 µm

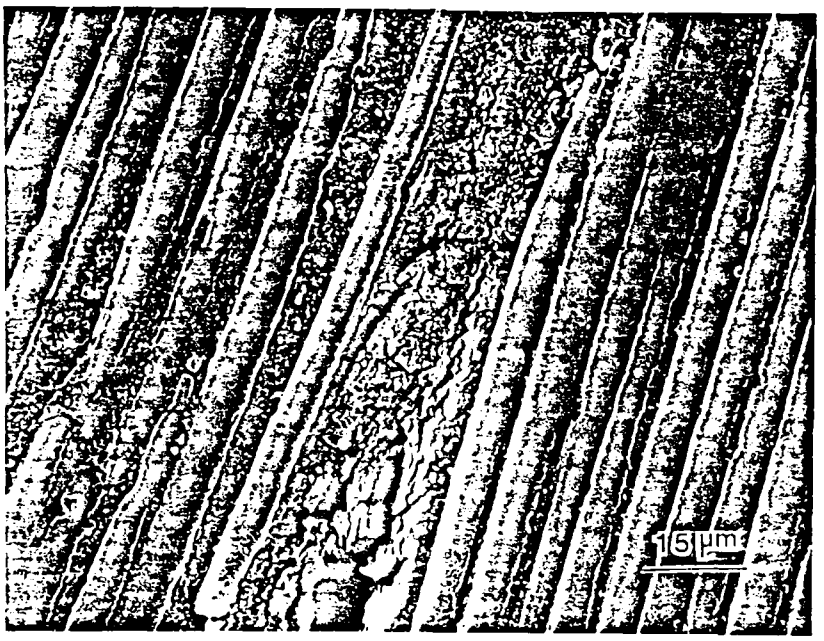
16 µm

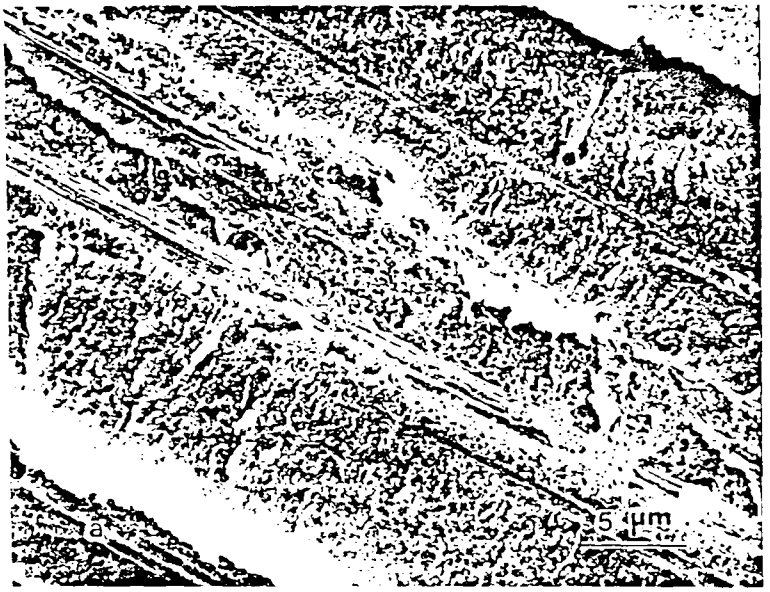
a
5 µm

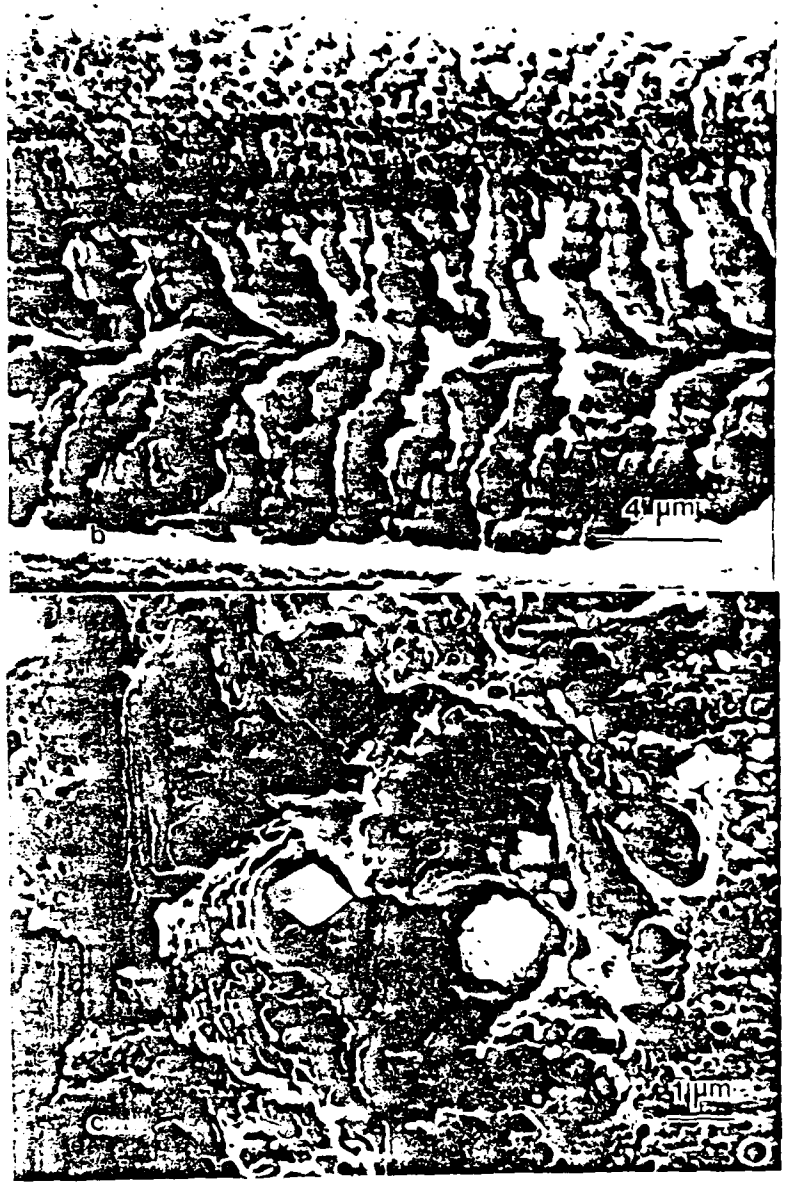
4 µm
b
1 µm
c

$$G_{Ic} = \int_{-h}^{h} \int_{0}^{\varepsilon_{ij}} \sigma_{ij} \, d\varepsilon_{ij} \, dy$$

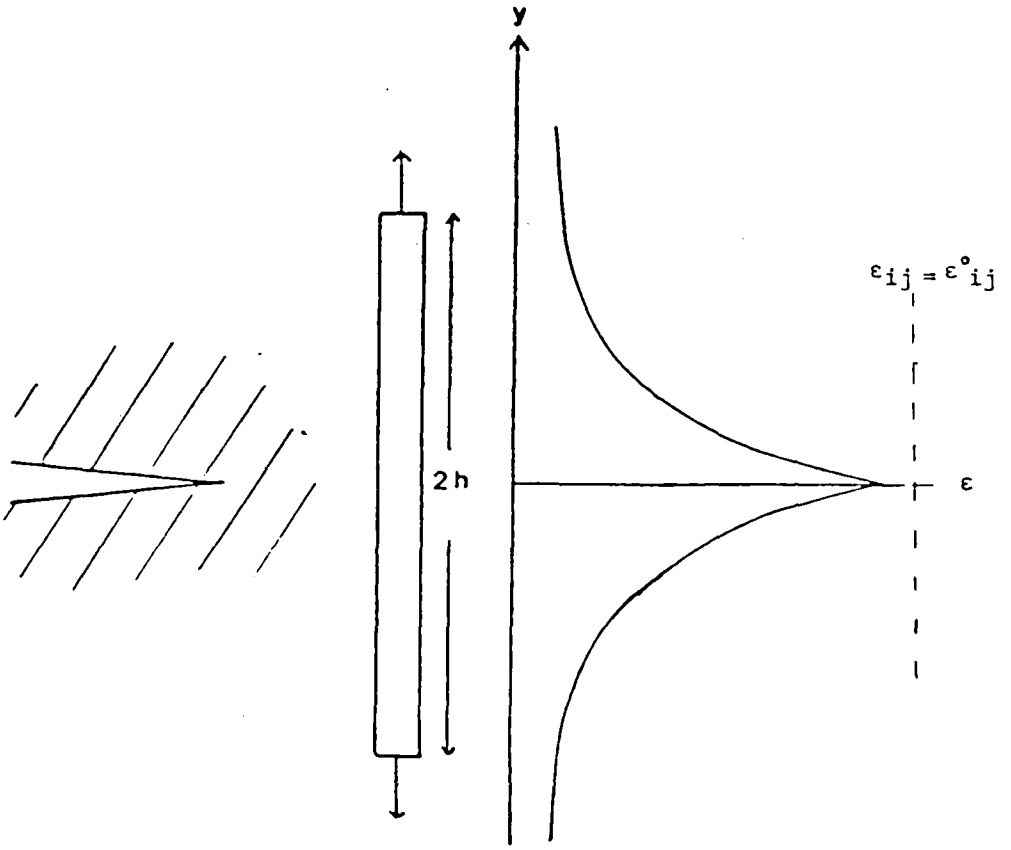

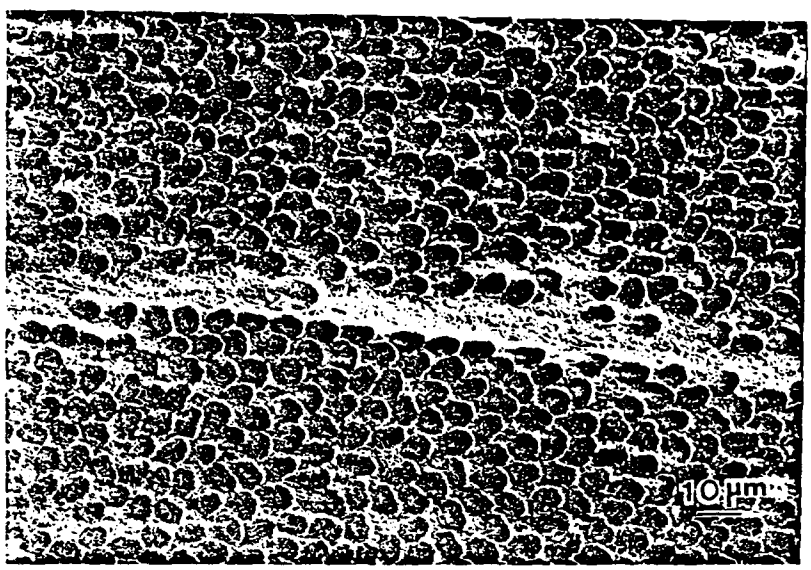
10μm

$$G_{Ic} \int_{-h}^{h} \int_{0}^{\varepsilon_{ij}} \sigma_{ij} \, d\varepsilon_{ij} \, dy$$

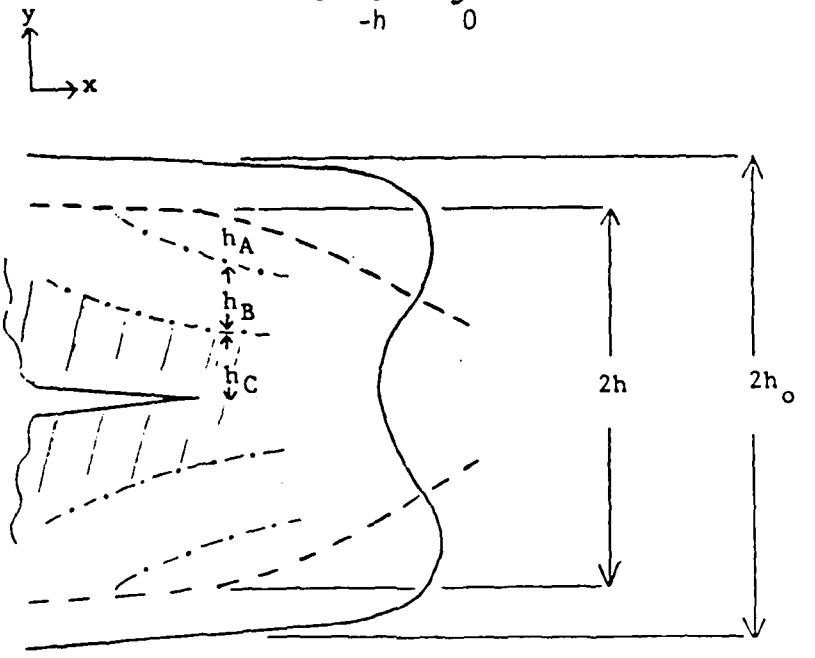


| | | | |
|---|---|---|---|
| ——— | resin | $2h_o$ | 130 μm |
| – – – – | composite | 2h | 100 μm |

# "The Relationship of Resin Ductility and Composite Delamination"

by

Walter Bradley and William Jordan

Texas A&M University

College station, Texas 77843

present to

International Symposium on Composite Materials and Structures

Beijing, China

June 1986

## INTRODUCTION

The first generation of high performance graphite/epoxy composite materials were made with resins developed to maximize stiffness and glass transition. However, composites made from these resins have been found to be susceptible to delamination fracture which adversely effects compressive strength (especially post impact compressive strength) and fatigue resistance. Thus, there has been an effort in recent years to develop new resin systems that would have enhanced resistance to delamination with a minimum penalty in stiffness and glass transition. As work has proceeded in this area, it has become apparent that large increases in resin toughness result in proportionately much smaller increases in composite delamination toughness[1]. Furthermore, the relationship between resin toughness and mode II delamination fracture toughness has only recently began to be studied. The purpose of this investigation has been to better define the relationship between increasing resin toughness and the resultant delamination toughness for both Mode I and Mode II loading.

## EXPERIMENTAL PROGRAM

Five resin systems have been selected for study in this program: (1) Hercules 3502 (highly crosslinked epoxy); (2) Hexcel F155 (moderate crosslink density-epoxy equivalent weight of 280-with 6% rubber particle additions); (3) Hexcel F155 without the rubber particle additions; (4) Hexcel F185 (low crosslink density-epoxy equivalent weight of 410-with 14% second phase rubber particles); and (5) Hexcel F185 without rubber particles. Note the two main variables in the resins systems selected for this study are crosslink density and rubber particle additions. The rubber particle additions relax triaxial tensile stresses at the crack tip by cavitation, allowing a larger shear stress to develop at the crack tip. The lower crosslink density provides more degrees of freedom for shear deformation.

The neat resin mechanical properties which potentially might correlate with delamination fracture toughness include tensile strain to failure, loss modulus G" or tan delta, and neat resin critical energy release rate $G_{1c}$. These neat resin

properties have been measured for each of the resins along with the tensile strain to failure for transverse fracture of unidirectional laminates loaded perpendicular to the fiber direction. These results have been correlated with delamination fracture toughness measures made for pure mode I and pure mode II loading conditions of split laminates. The delamination fracture toughness measurements have been made on unidirectional laminates fabricated from prepreg containing graphite fibers and the respective resin systems. Standard symmetrically loaded split laminate testing has been used to measure $G_{1c}$ while asymmetrically loaded split laminates have been used to determine $G_{IIc}$ [2]. To measure $G_{IIc}$ using an asymmetrically loaded split laminate the uncracked end of the split laminate is supported while both arms of the split laminate are loaded equally in the same direction.

The neat resin fracture toughness was determined using compact tension specimens. The more ductile systems were fatigue precracked prior to testing. The more brittle systems were tested by introducing a crack with a razor blade. Values from the literature were used for F155 [3] and 3502 [4]. Because of the large degree of nonlinearity in the load-displacement record for the F185, a J-integral analysis was used for this specimen. The $J_{1c}$ value determined for the F185 was somewhat larger than previously reported results [5] which presumably used a linear elastic analysis.

Scanning electron microscopy has been used to determine the micromechanistic fracture physics of the delamination process. This has been done using a combination of direct, real-time observation of the fracture process in the scanning electron microscope and post-morten fractographic examination of specimens after failure. Careful sample preparation using standard metallurgical techniques is necessary if one is to see the details of the fracture process as it occurs. Metallographic polishing of the edge of the specimen where the fracture process is to be observed allows one to clearly see the graphite fibers and the matrix and to note the interaction of the fracture process with each of these microstructural constituents.

## EXPERIMENTAL RESULTS

The experimental results are summarized in Table I. Some of the results from Table I are also presented graphically in Figs. 1-3 to facilitate analysis. Figs. 1 and 2 show the expected monotonic increase in fracture toughness with strain to failure and tan delta. However, a sharp increase in the neat resin fracture toughness is noted at higher values of strain and tan delta without a commensurate increase in delamination fracture toughness for either mode I or mode II loading. This is also evidenced by a sharp break in the plot of delamination $G_{1c}$ and $G_{IIc}$ versus neat resin $G_{1c}$ in Fig. 3. Such a break has previously been noted by Hunston [1] with a qualitative prediction for such behavior suggested by Bradley and Cohen [6]. It is also interesting to note in Fig. 3 that the ratio of $G_{IIc}$ to $G_{1c}$ is approximately 3.0 for the less ductile resins (neat resin $G_{1c}$ less than 500J/m$^2$) but falls to a value only slightly

greater than 1.0 for the very ductile F185 resin system.

Post-mortem fractographic results are presented in Figure 4. A crack tip damage zone develops in each of the systems. The size of this damage zone, which consists of microcracking and fiber debonding, can be readily measured during in-situ observation of the fracture process. It has been suggested that the microcracking is principally in the gold-palladium film sputter coated onto the surface to minimize charging[7]. Recent results by the authors to be published elsewhere have clearly shown that this is not the case, though if it were, one could still interpret the microcracked zone as indicating the size of the zone ahead of the crack tip over which a critical threshold strain had been achieved. The size of the damage zone for mode I delamination fracture is summarized in Table 2 along with the corresponding delamination fracture toughness $G_{Ic}$. A good general correlation between delamination fracture toughness and damage zone size is noted except for F185 NR.

## DISCUSSION

The observed increases in mode I and mode II delamination fracture toughness with increasing neat resin strain to failure (or tan delta) is consistent with what one might intuitively expect. Two observations which need further explanation, however, are the large ratio of $G_{IIc}$ to $G_{Ic}$ for the less ductile resin systems and the poor incremental increase in mode I and mode II fracture toughness with increasing neat resin toughness above neat resin toughness of 1000 $J/m^2$.

The delamination fracture process for mode I loading of composite consists of crack growth through the resin rich region between plies with occasional interfacial debonding facilitating the fracture process. For mode II loading of a composite made with a brittle resin, the details of the fracture process are quite different. First, the fracture process becomes much more discontinuous. A series of brittle microcracks form ahead of the crack tip and macrocrack advance occurs by the coalescence of these microcracks. This considerable increases the fracture surface created during fracture and represents a much more torturous path of crack advance than is observed for mode I fracture (see Figs. 4). Thus, the material resistance to mode II fracture is much greater than the material resistance to mode I fracture for delamination of a composite made with a brittle epoxy. For a composite made with a ductile resin, the fracture process for mode I and mode II delamination fracture is very similar as can be seen in Fig. 4 where the fracture surfaces are seen to be quite similar in surface roughness. Thus, the mode II and mode I delamination energies are essentially the same.

The much reduced rate of increase in delamination fracture toughness per increment of increase in neat resin toughness (see Fig. 3 and note break in curve) for tougher resin systems is believed to be associated with the deformation/damage zone increasing to a size that is no longer contained in the resin rich region between plies. Thus, the energy dissipation and/or crack tip blunting that would otherwise take place is hampered by the presence of the fibers which act as rigid filler in the

deformation/damage zone. Considerable support for this idea is seen in the data in Table II for F155 with varying fiber volume fraction. The different fiber volume fractions were achieved by using two different prepregs and making a laminate with and a second laminate without bleeding during processing. The difference in fiber volume fraction has been determined by metallographic examination to be manifest in a doubling in the thickness of the resin rich region between plies. Thus, the deformation/damage zone can be much larger before the constraint of the adjacent fibers becomes important. Doubling the thickness of this resin rich region between plies in the F155 effectively doubled the mode I delamination fracture toughness. Chakachery and Bradley have recently shown that the low ratio of mode I delamination to mode I neat resin fracture in F185 can be explained by the deformation/damage zone extending several fiber diameters above and below the resin rich region between plies [8].

A second important consideration in the full utilization of intrinsic toughness of more ductile resins is that these systems requires a better interface so that the resin can be strained to failure before interfacial failure occurs. It is worth noting that the greatest degree of fiber bridging occurred in the F185 composite.

## CONCLUSIONS

The important conclusions of this work may be summarized as follows:

1. Increasing resin ductility increases delamination fracture toughness, but the rate of increases drops off sharply for resins with fracture toughness in excess of $1000 J/m^2$.

2. The fracture toughness for mode II delamination is much greater than for mode I delamination because the fracture process is significantly altered. For tougher resin systems, the fracture process for mode I and mode II delamination are more similar and the critical energy release rates are similar as well.

## ACKNOWLEDGMENTS

The support of this project by the Air Force Office of Scientific Research under the direction of Dr. Tony Amos is gratefully acknowledged.

## REFERENCES

1. Hunston, D., presented at the ASTM Symposium on Toughned Composites, Houston, Tx, March 13-15, 1985.
2. Vanderkley, P., Master's Thesis, Texas A&M University, Dec. 1982.
3. Hexcel S.A. Sales Bulletin.
4. Williams, D., Master's Thesis, Texas A&M University, Dec. 1981.
5. Bascom, et.al., Journal of Materials Science, Vol. 16, 1981.
6. Cohen, R. and Bradley, E., presented at ASTM Symposium on Delamination and Debonding of Materials, Pitts, PA. Nov. 1983.
7. Kinlock, A., et.al., Journal of Materials Science Letters, 4: 1276-1279, 1985.

8. Chakachery, E. and Bradley, W., to be published in Polymer Science & Engineering, 1986.

| Resin | $\epsilon_f$ (%) | transverse $\epsilon_f$ for composites | UTS (MPa) | G' (GPa) | G" (GPa) | tan δ delta | $G_{1c}$ (J/m²) | $G_{1c}$ (J/m²) | $G_{1c}$ (J/m²) |
|---|---|---|---|---|---|---|---|---|---|
| 3502 | .3 | .05 | | | | | 70 | 139 | 570 |
| F155NR | 1.96 | .699 | 56.5 | 1.80 | .0180 | .0103 | | 335 | 1660 |
| F155 | 3.10 | .580 | 68.6 | 1.70 | .0400 | .0223 | 730 | 520 | 1270 |
| F185NR | 3.24 | .538 | 72.9 | 1.80 | .0329 | .018 | 460 | 455 | 1050 |
| F185 | 8.87 | 8.58 | 46.4 | 1.40 | .0490 | .035 | 8000 | 2205 | 2440 |

Table I. Summary of mechanical properties determined for resin and composites.

| Composite System | Fiber Density (vol.%) | Size of Damage Zone ahead of crack (μm) | Size of Damage Zone above/below crack (μm) | $G_{1c}$ (J/m²) |
|---|---|---|---|---|
| AS4/3502 | 76.4 | 20 | 5 | 190 |
| F155 NR | | 20 | 7 | 135 |
| T6T145/F155 | 59.6 | 30 | 20 | 1015 |
| T6T145/F155 | 70.5 | 20 | 10 | 615 |
| T6T145/F155 | 68.8 | 20 | 10 | 520 |
| F185 NR | | 75 | 35 | 455 |
| F185 | | 200 | 35 | 2205 |

Table II Deformation/Damage zone sizes for composites; determined from in-situ fracture observations for mode I delamination fracture.

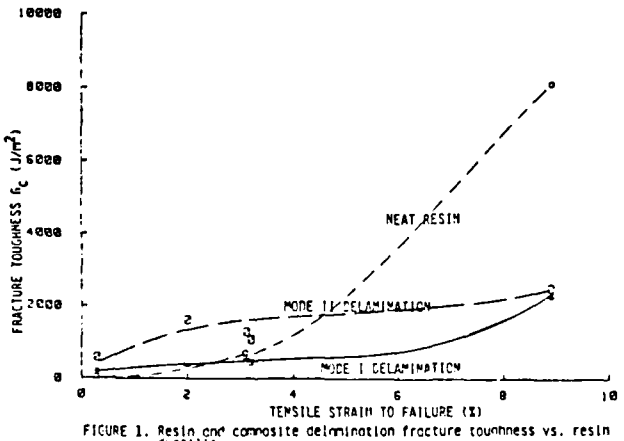


FIGURE 1. Resin and composite delamination fracture toughness vs. resin ductility.

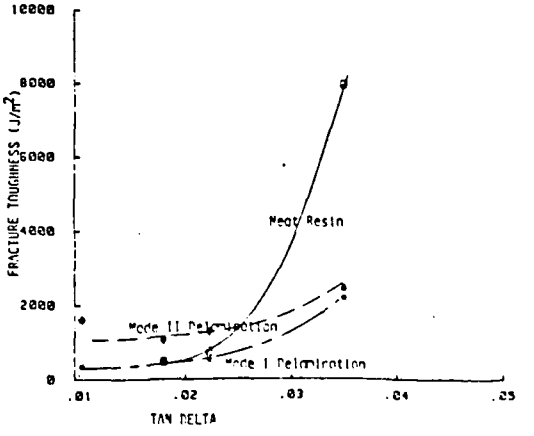


Figure 2. Fracture Toughness versus Tan Delta of Neat Resin

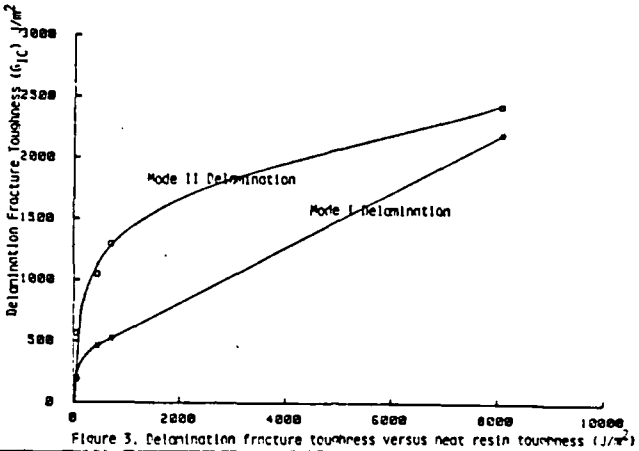


Figure 3. Delamination fracture toughness versus neat resin toughness ($J/m^2$)

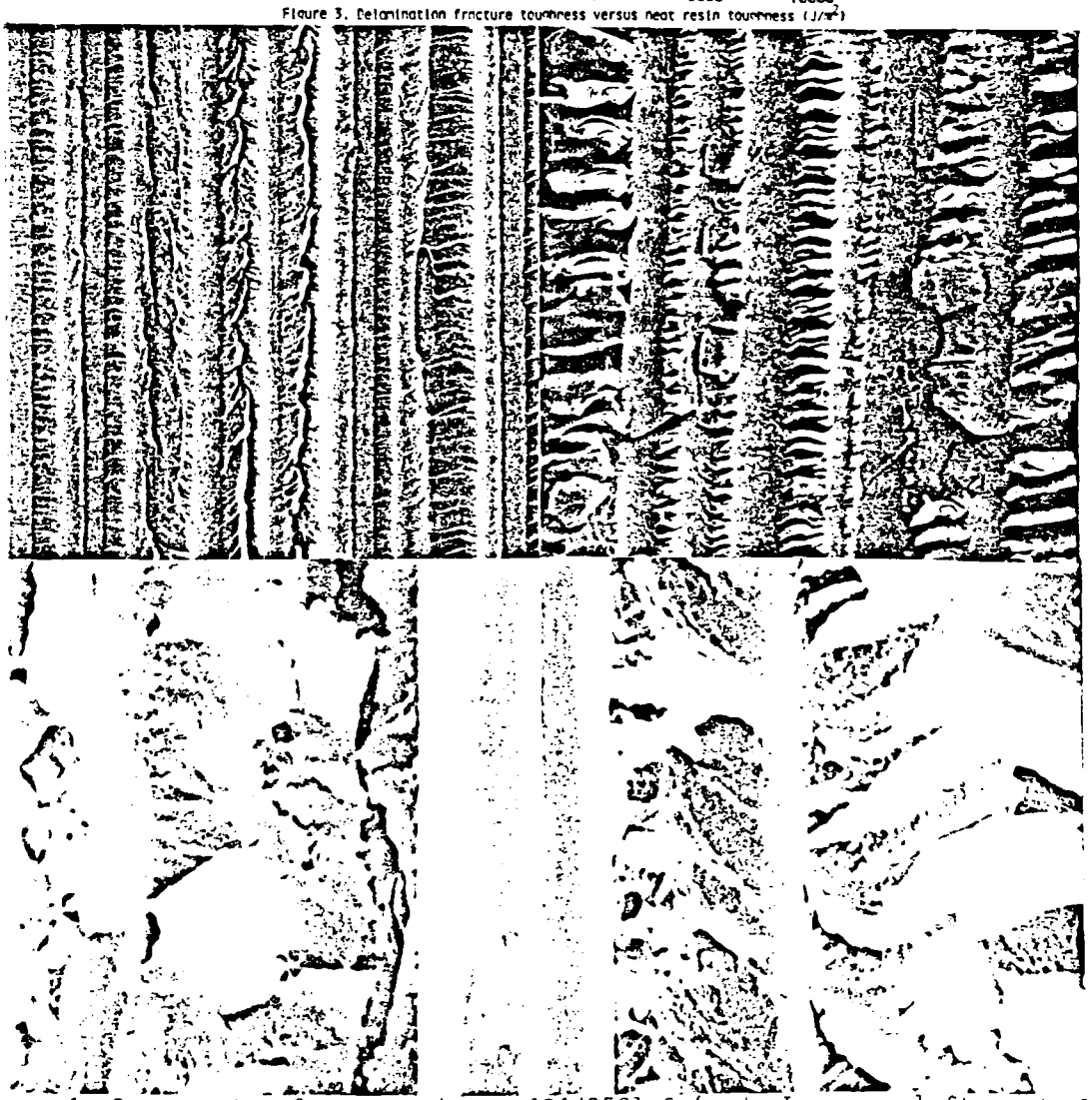

Figure 4. Post-mortem fractography on AS4/3501-6 (mode I, upper left; mode II, upper right) 1000X and T6T145/F185 (mode I, lower right; mode II, lower left) 3000X.

Texas A&M Report MM 5034-86-6
February 1986

# Delamination Analysis of Composites with Distributed Damage using a J integral*

R.A. Schapery
W.M. Jordan
D.P. Goetz

## ABSTRACT

The J integral theory for fracture analysis of materials with distributed damage is discussed and then specialized to a form that is useful for analyzing opening-mode delamination crack growth. Tests on double-cantilevered beam specimens of two different graphite/epoxy material systems and three different layups are described and then analyzed.

## 1. Introduction

Fiber-reinforced plastic laminates may sustain an appreciable amount of microcracking and other types of damage before global structural failure occurs. In order to characterize the resistance to delamination and to predict delamination when there is globally distributed damage such as microcracking, it may be necessary to account for the nonlinear inelastic behavior produced by this distributed damage. In this Section we briefly give some background on the J integral. The theory is then specialized in Section 2 to opening-mode delamination of double-cantilevered beams (DCB) and illustrated in Section 3 using experimental data from tests of two different graphite/epoxy laminates.

A two-dimensional version of the J integral was introduced by Rice [1], and was shown to be especially useful in nonlinear elastic fracture mechanics. Its primary usefulness comes from its path independence and its relationship to the crack tip stress field and work input to the crack tip. Numerous generalizations (including extension to three-dimensions and large strains) and applications have since appeared, such as discussed in a recent book by Kanninen and Popelar [2]. Except for steady-state conditions [3], the properties of the J integral are usually considered to depend on the existence of strain energy potential $W=W(e_{ij})$, where

$$s_{ij} = \partial W/\partial e_{ij} \tag{1}$$

in which $s_{ij}$ and $e_{ij}$ are components of the stress and strain tensors. Schapery extended the J integral to nonlinear viscoelastic materials [4] and further showed that important characteristics of the J integral carry over to other types of inelasticity, including that due to distributed

---

*Prepared for International Symposium on Composite Materials and Structures, Beijing, China, June 1986.

R.A.S. and D.P.G., Professor, Civil and Aerospace Engineering and Graduate Research Assistant, Mechanical Engineering, respectively, Texas A&M University, College Station, TX 77843. W.M.J., Assistant Professor, Mechanical Engineering, Louisiana Tech University, Ruston, Louisiana 71272.

microcracking and other types of damage [4,5]. These generalizations depend on the existence of a potential which is analogous to strain energy, Eq. (1), but which may be multivalued. Figure 1 illustrates such a potential for uniaxial stressing. The net work input to the sample at any time in the loading or unloading history is the so-called work-potential,

$$W \equiv \int_0^e s \, d \, e \tag{2}$$

In general, s and W are multivalued functions of e since they depend on whether s is the loading or on the unloading curve. Arguments for the existence of multivalued work potentials in three dimensions which satisfy Eq. (1) were given by Schapery [4,5].

Here we shall assume a work potential exists and use it in a J integral to analyze delamination fracture. For the materials and conditions studied experimentally viscoelastic effects were very small, and these effects are therefore neglected in the theory.

2. J Integral for the DCB Specimen

Figure 2 shows a DCB specimen. In the cases studied here, the beam is a laminate, and applied force F causes the crack to propagate in a plane parallel to the plane of lamination (which is perpendicular to the plane of the page). We assume a' is long enough for the legs to be in plane stress over a significant portion of their length.

The J integral for the DCB specimen is

$$J = \int_C [W dx_2 - (T_1 \frac{\partial u_1}{\partial x_1} + T_2 \frac{\partial u_2}{\partial x_1}) dL] \tag{3}$$

where W is the work-potential per unit volume, $T_1$ and $T_2$ are tractions along C, Fig. 3, and $u_1$ and $u_2$ are displacements; the indices indicate components in $x_1$ and $x_2$ directions. This equation is valid for large strains and rotations as long as we interpret $x_1$ and $x_2$ to be coordinates of the undeformed geometry. The integration is counterclockwise along the curve C in Fig. 3, which includes top and bottom beam surfaces and vertical segments. The right vertical segment is taken far enough from the crack tip that the material is unstressed, and thus gives no contribution. Assuming small strains and that the left segment is close enough to the crack tip that we can use small rotation beam theory (but far enough to the left of the tip for plane stress conditions to apply) yields,

$$J = \frac{2}{B} \int_0^M k(M') dM' - 2 \frac{F}{B} \frac{du_2}{dx_1} \tag{4}$$

where M and $du_2/dx_1$ are the moment and slope, respectively, at the left vertical segment; B is the beam width. Integrate $k = d^2u_2/dx^2$ to the tip (assuming plane stress) to obtain the slope, use $dM = Fdx_1$ and Eq. (4) reduces to

$$J = \frac{2}{B} \int_0^{M_a} k(M) \, dM \tag{5}$$

where $M_a$ is the crack tip moment; this is the same result derived by Rice [1] for a split beam under pure end moments $M_a$. It is seen that the result is independent of the location of the left integration segment and, in fact, is that in Eq. (4) when the segment is located at the crack tip (where $du_2/dx_1 = 0$). It should be mentioned, however, to obtain this path independence (i.e. derive Eq. (5) from (4)) it was necessary to assume if k(M) is multivalued (similar to the s-e curve in Fig. 1) that the unloading curve is the same for all left vertical segments used. This latter

condition will be met for all material (to the left of the current tip) which had experienced the same maximum moment when the crack tip passed by. Inasmuch as the experimental results discussed later indicate the maximum moment is constant (and recognizing that the moment decays with distance from the tip) this condition is met all of the way to the location of the initial crack tip. To the left of the initial tip the maximum moment is less than $M_a$ and one finds J depends on the location of the left segment. This path dependence in beam theory is fully consistent with that predicted from the exact J integral for a continuum with variable damage in the regions of unloading [4].

Strictly speaking one should consider the effect of the three-dimensional state of stress around the crack tip in developing the J integral for the DCB specimen. If indeed one does this starting with the theory in [4], one still arrives at Eq. (5) if the maximum amount of damage is essentially that defined by the beam theory and the slope is adequately predicted by plane stress theory. Weatherby [6] studied this problem using the finite element method for two dimensional deformation of a highly inelastic isotropic beam and found that Eq. (5) is an excellent approximation.

Finally, we observe that for a delamination propagating at a constant tip moment in a long laminate which is homogeneous in the $x_1$ direction in its initial state, the state of stress and strain in the neighborhood of the tip is constant in time if effects of shear force changes are neglected. This is a type of "self-similar" growth and therefore J is the work input to the crack tip [4] (per unit of new area projected onto the delamination plane).

3. Experimental Study of DCB Specimens

Materials and Test Procedure: Two commercially available graphite/epoxy composites were tested: T6T145/F155 (Hexcel Corporation) and AS4/3502 (Hercules, Incorporated). The epoxy in the former system is toughened with 6 vol. % rubber particles. Several layups were tested as reported by Jordan [7]. Here we report on four different layups with some of the data coming from [7], but most data are from more recent tests.

Prepreg was used to make plates which were cured in the Texas A&M University air-cavity press using the manufacturer's recommended temperature cycle. A thin 3.5 cm wide teflon strip was inserted in the midplane along one edge of each plate during the layup step in order to provide a 3.5 cm long starter crack in the beams cut from the plates; each beam was approximately 2.5 cm wide by 30 cm long. Those layups with off-axis fiber orientations are listed in Table 1. Besides these laminates, unidirectional beams with 0° fiber orientation (fibers parallel to the beam axis) for both systems were tested.

Table I
Laminates with Off-axis Fibers

| Laminate Designation | Material System | Layup (fiber orientations) | |
|---|---|---|---|
| A | T6T145/F155 | [±45/0(8)/∓45(2)/0(8)/±45] | (24 plies) |
| B | T6T145/F155 | [±45/∓45(2)/∓45(2)∓45(2)/±45] | (16 plies) |
| C | AS4/3502 | [±45/0(4)/∓45(2)/0(4)±45] | (16 plies) |

In all three cases, the delamination crack was in the middle plane of the beam, between a +45 and -45 ply. For A and C layups the beam legs

above and below the delamination are balanced and symmetric in the undamaged state. These designs were used to minimize twist and bending-stretching coupling to simplify specimen analysis in this exploratory investigation.

At least two samples of each laminate were delaminated in stroke control in a servohydraulic test machine. The test was stopped several times and the beam unloaded to measure the moment arm to the crack tip (loaded state) and length of the delamination (unloaded state), and to determine the force-displacement curve with loading and unloading for use in an energy-based data analysis method.

Additional tests were conducted on single cantilevered beams to obtain the moment-curvature relationship for use in the J integral analysis. These beams were made with fiber orientations corresponding to the layup above the middle surface in the beams used for delamination tests. Strain gages were mounted above and below the beam near the clamped end in order to determine the curvature k from the equation $k = \Delta e/t$ where $\Delta e$ is the difference in strain readings on the top and bottom surfaces and t is the beam thickness. The beam support at the clamped end was mounted on bearings to provide free axial movement. In these tests and the delamination tests, the external load was applied vertically through bearing-supported pins.

Discussion of Results: Figures 4 and 5 show the force-displacement diagram for two layups in Table 1. Figure 6 shows results from one of the cantilevered beam tests used to obtain the moment-curvature relationship; specimen type B exhibited the most hysteresis. The maximum moment is the crack-tip value determined from the delamination test. According to Eq. (5), J is the area to the left of the loading curve multiplied by 2/B. Table 2 summarizes the results. Two numbers are given in most cases, each coming from different specimens.

Table 2
Summary of Results on Fracture Toughness
(in $J/m^2$)

| Laminate Designation | $J_c$ (Eq. (5)) | $J_a$ (Eq. (5)) | $G_c$ (area) | $G_c$ (stiffness [8]) |
|---|---|---|---|---|
| A | 615/510 | - | 601/557 | 588 |
| B | 522 | - | 725/725 | 1333 |
| C | 538/525 | 389/380 | 440/434 | 383 (arrest value) |

The values in the column in Table 2 labeled $G_c$ (area) were obtained by determining the area between successive loading-crack growth-unloading curves (as in Figs 4 and 5). Assuming the specimens are linearly or nonlinearly elastic, this area divided by the new crack surface area is the $G_c$ value required for propagation. The last column is based on the method described by Devitt et al. [8]. It uses load-deflection-crack length data to obtain $G_c$; it is based on the assumptions of linear elastic behavior and no midplane strain, but it allows for large rotations. (The beam rotation at the load-point was as high as 40° in layup C; only for layup A was the geometric nonlinearity negligible.) It should be added that all three methods used to develop the values in Table 2 allow for geometric nonlinearities. Material nonlinearities and midplane strains (due here to nonlinearity) are not neglected in the methods used except for that in [8].

For the specimen type C, delamination occurred usually in distinct

steps, as illustrated in Fig. 5. When growth initiated there was a significant and sudden jump in crack length; the loads used in data analysis at each pair of initiation and arrest points are connected by dashed lines. The corresponding moments were used with moment-curvature results to predict $J_c$ (initiation) and $J_a$ (arrest) values. Specimen types A and B delaminated quite smoothly in most cases.

The moment at which propagation occurred was essentially constant for each specimen with the variation being no larger than ±5% from the average. Once or twice during the delamination test of most beams an exceptionally high or small moment was obtained, but these values were not used in calculating the averages in Table 2. (These unusual values did not necessarily occur at either the shortest or longest cracks.) The arrest moment in specimen type C exhibited scatter similar to that for initiation moments.

It is of interest to compare the fracture toughness values in Table 2 with those for the same systems but with all $0^\circ$ fiber angles. Jordan found that for the Hexcel system $G_c$ varied from 400 to 650 $J/m^2$ and for the Hercules system $G_c$ varied from 180 to 200 $J/m^2$. The former values are consistent with the $J_c$ values in Table 2 (specimen types A and B), whereas the latter values are less than one-half those reported in Table 2 (specimen type C). These low values are consistent with observation of fracture surface roughness, in that the surface of the $0^\circ$ fiber specimen was very smooth, whereas many microcracks running parallel to fibers could be seen on C type specimens.

The B specimens do not have any $0^\circ$ fibers, and therefore the effect of distributed damage in the legs should be the largest. It is believed the high $G_c$ values reported for this layup using the deflection-based methods, compared to $J_c$, reflect this fact. For example, the area method gives a $G_c$ which includes the work of both distributed damage and delamination.

## 4. Conclusions

A relatively simple expression, Eq. (5), was developed for determining the J integral. Only the work of bending was considered for the beam near the delamination tip; nowever, the analysis could be readily generalized to allow for shear and axial deformation work when appropriate. The preliminary assessment of the approach using double-cantilevered beam specimens is very encouraging. As predicted by the theory, it was found that the delamination propagated at essentially a constant crack-tip moment. Also, for one material system it yielded fracture toughness values which are essentially the same for three different layups. In contrast, the other deflection-based methods typically yielded higher toughness values when distributed damage was significant.

## Acknowledgements

This research was sponsored by the U.S. Air Force Office of Scientific Research, Office of Aerospace Research. The authors are grateful to Messrs. B.C. Harbert and R.E. Jones, Jr. for their help on portions of the experimental work.

## References

[1] Rice, J., "A Path Independent Integral and the Approximate Analysis of Strain Concentration by Notches and Cracks," J. Appl. Mech., Vol. 35, 1968, pp. 379-386.

[2] Kanninen, M.F., and Popelar, C.H., Advanced Fracture Mechanics, Oxford Univ. Press, New York, 1985.

[3] Budiansky, B., Hutchinson, J.W., and Lambropoulos, J.C., "Continuum Theory of Dilatant Transformation Toughening in Ceramics," Int. J. Solids Structures, Vol. 19, 1983, pp. 337-355.

[4] Schapery, R.A., "Correspondence Principles and a Generalized J Integral for Large Deformation and Fracture Analysis of Viscoelastic Media," Int. J. Fracture, Vol. 25, 1984, pp. 195-223.

[5] Schapery, R.A., "Deformation and Fracture Characterization of Inelastic Composite Materials Using Potentials," Texas A&M Report No. MM-5034-85-22, Dec. 1985.

[6] Weatherby, J.R,"Finite Element Analysis of Crack Growth in Inelastic Media", Ph.D. Dissertation, Mechanical Engineering Dept., Texas A&M Univ., May 1986.

[7] Jordan, W.M., "The Effect of Resin Toughness on the Delamination Fracture Behavior of Graphite/Epoxy Composites," Ph.D. Dissertation, Mechanical Engineering Dept., Texas A&M Univ., Dec. 1985.

[8] Devitt, D.F., Schapery, R.A., and Bradley, W.L., "A Method for Determining the Mode I Delamination Fracture Toughness of Elastic and Viscoelastic Composite Materials," J. Composite Materials, Vol. 14, 1980, pp. 270-285.

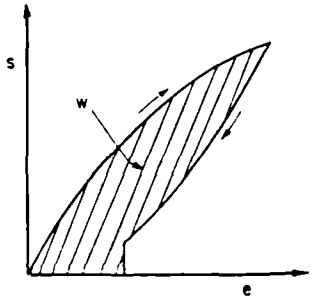


Figure 1. Uniaxial stress-strain curve for material with increasing damage during loading and constant damage during unloading.

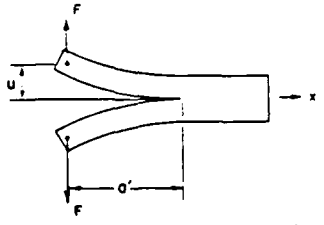


Figure 2. Double-cantilevered beam (DCB) for delamination fracture studies.

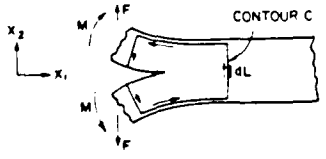


Figure 3. Contour used to evaluate J integral

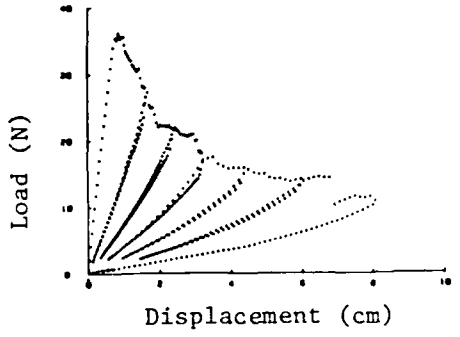


Figure 4. Load vs. displacement (2u) for type B specimen.

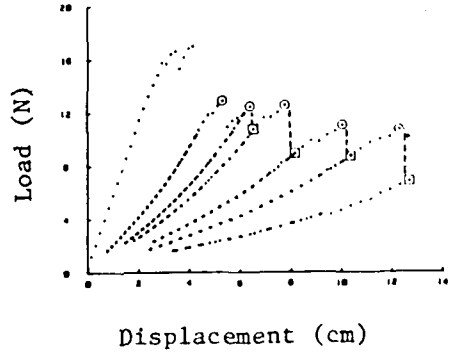


Figure 5. Load vs. displacement (2u) for type C specimen.

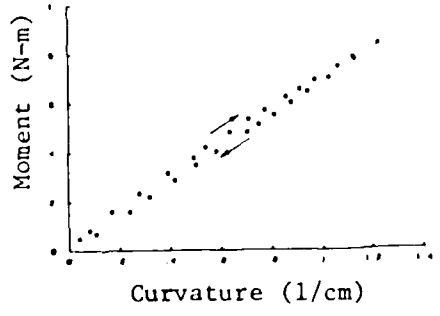


Figure 6. Moment-curvature for type B specimen

# Correlations Between Micromechanical Failure Processes and the Delamination Fracture Toughness of Graphite/Epoxy Composites"

by

Michael Hibbs and Walter Bradley

presented at

ASTM Symposium on
Fractography of Engineering Materials
Nashville, Tennessee
November, 1985

Title of Paper: Correlations Between Micromechanical Failure Processes and the Delamination Fracture Toughness of graphite/epoxy systems

Authors: Michael F. Hibbs and Walter L. Bradley
(Texas A&M University)

Key Words: Graphite/Epoxy Composites, Delamination, Fracture Toughness, Failure Analysis.

Abstract

A combination of macroscopic delamination fracture toughness, SEM real time fracture observations, and post-fracture morphology, were used to study the micromechanical processes of delamination failure in several graphite/epoxy systems.

Strain energy release rate GIc, GIIc and mixed mode G I&IIc were obtained from unidirectional double cantilever beam specimens. Comparisons of these energy release rates with the resulting fracture surface morphology are used to clarify the relative importance of the formation of hackles and the fiber matrix interface adhesion to delamination toughness under mode I, mode II, and mixed mode I & II loading conditions.

Real-time fracture observations of composite delamination in the scanning electron microscope revealed the micro-processes of microcrack formation and coalecsense. These observations coupled with GIc for the neat material, determined from compact tension specimens, provide insight on how resin toughness can be translated into composite delamination toughnes.

The implications of hackle formation and their importance in failure analysis of graphite/epoxy systems are discussed.

# CORRELATIONS BETWEEN MICROMECHANICAL FAILURE PROCESSES AND THE DELAMINATION TOUGHNESS OF GRAPHITE/EPOXY SYSTEMS

by

Michael F. Hibbs and Walter L. Bradley

Texas A&M University

College Station, Texas 77843

## INTRODUCTION

Because of their very high strength to weight and stiffness to weight ratios, graphite/epoxy composite materials are now used in a wide variety of aerospace, automotive, and sporting goods applications. The first generation resins developed for use in graphite/epoxy systems optimized stiffness and high glass transition temperatures (Tg) by using a very high crosslink density. Unfortunately, such resins are quite brittle. Recent developments have centered on how to increase resin toughness with a minimum penalty in stiffness and Tg. As tougher resins have been developed, it has been shown [1] that increased resin toughness does not lead to a commensurate improvement in composite toughness. Three possible reasons for this are (1) premature failure due to weak resin/fiber adhesion, (2) fibers providing constraint which changes the local state of stress and limits the ductility of the resin [2], and (3) fibers acting as rigid fillers and there by reducing the volume of material available for deformation in the yield zone around the crack

tip.

In the case of delamination of a graphite/epoxy composite, the fracture surface is characterized by the amount of fiber pullcut, interfacial debonding, and the extent of the resin deformation or microcracking. One of the most common fractographic features that results from microcracking of the resin are 'hackles'. These hackles appear as lacerations or scallops in the resin that form regular saw tooth or wave like patterns. Several attempts have been made to relate the orientation of the hackles to the direction of crack propagation [3]. Results to be presented in this paper clearly show that the hackles slant in opposite directions on the top and bottom surfaces of the crack face, making it impossible to infer crack growth direction from the hackle slant alone.

To develop an accurate interpretation of fractographic results observed on delaminated components, a systematic experimental program of delamination fracture of composite coupons with varying percentages of mode I and mode II loading is needed. This paper summarizes the results of such a study in which the effects of state of stress, resin ductility, and resin/fiber adhesive strength have been correlated with resulting fracture surface characteristics. In particular, the formation of hackles and their potential use as a reliable predictor of crack growth direction has been studied. The fractographic information has been collected using scanning electron microscope (SEM) observations of the delamination fracture surfaces of unidirectional split laminate specimens (DCB). These split laminate specimens have been fractured under mode I, mode II, and mixed mode I&II loading conditions. To clarify the interpretation of the post-mortem fractography, in-situ SEM observations of delamination

fracture of small DCB specimens loaded in mode I and mode II conditions have been made.

## EXPERIMENTAL METHODS AND MATERIALS

### RESIN AND COMPOSITE SYSTEMS

The four graphite/epoxy composites used in this study were comprised of Hercules AS4 graphite fibers combined with resins having both different degrees of toughness and interfacial bonding strength. The brittle Hercules resin 3501-6 was used with fibers that were unsized. The composite systems AS4/Dow-P6 and AS4/Dow-P7 were comprised of a somewhat more ductile Novolac epoxy resin with sized fibers to increase the interfacial bonding. The AS4/Dow-P7 resin was modified with rubber particles to increase resin toughness along with another second phase additive to enhance interfacial adhesion. The fourth system AS4/Dow-06 uses a much tougher crosslinkable thermoplastic epoxy with sized fibers. Unidirectional 14 ply laminate panels were made from the prepreg of these systems provided by Dow Chemical. A teflon strip 0.03mm in thickness was inserted along one edge of the panel between the mid-plies to provide a starter crack. The panels were then cured in an autoclave press at Texas A&M University using the temperature/pressure/time cycle specified by Dow Chemical for each system.

### FRACTURE TOUGHNESS

Delamination fracture toughness measurements for opening mode ($G_{Ic}$), shear mode ($G_{IIc}$), and mixed mode were made by using

25 cm. by 2.5 cm. double cantilever beam specimens (DCB), as shown in Figure 1. These specimens were tested using a MTS system at room temperature (24° C) in stroke control at a rate of .0085 cm/sec. A partial unloading compliance measurement was made after each approximate 1 cm. of crack growth. Stroke, displacement and load were recorded continuously as a function of time, while crack length was measured discretely using visual measurements on the edge of the specimen.

## ANALYSIS OF FRACTURE TOUGHNESS

A complete description of the analytical proceedures used for calculating the composite mode I, mixed mode, and mode II energy release rates for these systems can be found in Tse et al. [4]. In summary, the mode I critical energy release rate $G_{Ic}$ was calculated from the measured data by three methods, linear beam theory as described by Devitt et al. [5], the change of area under the load-displacement curve method suggested by Whitney [6], and the change in compliance method using an analysis suggested by Wilkins [7]. All three methods gave similar results. Thus, an average value obtained from these three methods is reported in this paper. For the mixed mode loadings, the total energy release rate was calculated by combining the mode I and mode II energy release rates, each calculated assuming linear beam theory. Because of the large loads and resulting large deflections needed for mode II crack propagation, the requirements needed for a linear beam theory analysis were not met. Thus, the mode II energy release rate was determined by measuring the area under the load-displacement curve bounded by the load-crack extension-unload and dividing this energy by the increase in crack

area which occurred during this load-unload cycle. It is worth noting that the area method used for the mode II calculations of $G_{IIc}$ assumes all damage occurs in the crack tip damage zone rather than in the far field. Thus, it is an upper bound estimate of mode II energy release rate which equals $G_{IIc}$ when no significant far field damage occurs. The fracture toughness of the neat resin material was determined using compact tension specimens (CT) tested according to ASTM-E399. Because of the relative brittleness of the resin studied, it was not possible to fatigue-precrack the specimens. Thus, a razor blade was used to pop in a very sharp crack at room temperature.

FRACTOGRAPHY

Specimens of suitable size for observation in the SEM were prepared by sectioning the delaminated DCB specimens with a jeweler's saw. Cutting debris on the fractured surface was minimized by cutting the samples before the delamination surfaces were separated. Any loose debris that did occur was blown away using compressed air. The surface was then coated with an approximately 200 Å thick layer of gold-palladium to avoid charging and improve imaging . The photographs were made on tri-X film, on a JEOL JMS-25 Scanning Electron Microscope at accelerating voltages of 12.5 and 15 Kv.

Real-time mode I and mode II delamination tests of the AS4/3501-6, AS4/Dow-P7, and AS4/Dow-06 systems were observed in JEOL JMS-35 scanning electron microscope using a JEOL 35-TS2 tensile stage. Mode I delamination was achieved by pushing a wedge into the precracked portion of a small DCB type specimen. The wedge tip was sufficiently blunt to insure that the wedge remained well behind the crack tip allowing mode I opening rather than wedge cutting of the

composite. A three-point bend fixture was used to provide the mode II loading in an end notch flexure (ENF) test arrangement [8]. For both loading conditions, the crack propagation was observed by viewing a polished edge of the specimen in the region of the crack tip. These observations were recorded with video tape and tri-X film. The edge of the specimens to be observed during delamination were carefully polished using standard metallographic techniques and coated with a 200 Å layer of gold-palladium.

## EXPERIMENTAL RESULTS

### FRACTURE TOUGHNESS RESULTS

A summary of the mode I ($G_{Ic}$), mixed mode ($G_{I,IIc}$), and mode II ($G_{IIc}$) composite fracture toughness are presented in Table 1 along with the fracture toughness values for the neat resin material obtained from the compact tension specimens. The delamination fracture toughness for mode I loading was found to be greater than the neat resin for the brittle system AS4/3501-6 and similar to the neat resin fracture toughness for the tougher systems (AS4/Dow-P6, AS4/Dow-P7,and AS4/Dow-06).

For all of the systems of this study an increase in the fraction of mode II loading resulted in an increase in the total energy release rate for crack growth, with the most dramatic increase in fracture toughness occuring in the more brittle systems; namely, AS4/3501-6 and AS4/Dow-P6.

### FRACTOGRAPHIC RESULTS: BRITTLE AND MODERATELY DUCTILE COMPOSITE

SYSTEMS (AS4/3501-6, AS4/DOW-P6, AND AS4/DOW-P7)

Post-mortem fractography of the delaminated DCB specimens (Figures 2, 3, and 4) indicates that the primary mode I fracture mechanism for the AS4/3501-6 and AS4/Dow-P6 systems was debonding at the fiber/resin interface or fracture through the interphase region. High magnification fractographs of these systems clearly reveal the texture of the fibers indicating at the most a thin sheathing of resin adhering to the fibers. The resulting fracture surface was similar to a flat corrugated roof which has the effect of increasing the surface area compared to a flat, or planar fracture surface. In the resin rich regions between fibers, a smooth brittle cleavage type fracture was exhibited with a limited number of shallow hackles. Occasional fiber pull out and breakage is also seen. The fracture surface of the AS4/Dow-P7 system reveals much more resin deformation and damage with some resin adhering to the fibers, indicating better interfacial bonding. The surface also is highly pock marked. These holes (approximately 1 - 5 microns in diameter) that gives rise to the pot marked appearence are apparently the result of volatiles trapped during the fabrication of the laminate panel (see Figure 4b). The AS4/Dow-P7 system also exhibited areas where large sheets of resin and fibers were pulled out as the delamination crack jumped back and forth between adjacent fibers (see Figure 4a).

In all of these systems, qualitative observations indicate the number of hackles and their angle of orientation with reference to the macroscopic fracture plane increased as the percentage of mode II or shear loading increased. This increase in hackle number and orientation is most conspicuous for mode II loading greater than 43% (see Figures 2,3, and 4). At near pure mode II loading, the hackle

are observed to be nearly perpendicular to the plane of the plies, and their edges sometimes appeared drawn and "tuffed". For the most part, the orientation or slant of the hackles remains constant on a given fracture surface (i.e., for a given ratio of mode I to mode II loading). They appear to slant towards the direction of crack growth on one fracture surface and in the direction opposite of crack growth on the matching fracture face (see Figure 5). Comparisons of the mode I fractography to the mode II fractography for the two brittle systems AS4/3501-6 and AS4/Dow-P6 shows that the amount of resin/fiber debonding as exhibited by the amount of resin adhering or coating the fibers does not seem to be affected by the increase in mode II loading (Figure 6). This would seem to indicate that interfacial debonding for these systems is insensitive to the loading conditions.

## FRACTOGRAPHIC RESULTS: DUCTILE RESIN SYSTEM (AS4/DOW-06)

The fracture surfaces of the ductile system AS4/Dow-06 were characterizied by resin fracture and deformation, with resin completely coating the fibers, indicating good fiber/resin adhesion. Fractography revealed no distinct hackles (Figure 7). Only at near pure mode II loading conditions were any even ill defined hackle-like features seen. These features are chaotic with no clearly defined orientation.

## REAL-TIME DELAMINATION FRACTURE OBSERVATIONS

Mode I Loading - In-situ observations in the SEM of fracture of the composite systems are seen in Figure 8. For mode I loading of the brittle AS4/3501-6, the primary crack is seen to proceed by interfacial debonding. A limited amount of microcracking is seen to

occur in the resin behind the primary crack tip and is normally associated with fiber bridging and eventual pullout.

The mechanisms for crack advancement in the delamination fracture of AS4/Dow-P7 were seen to be both resin/fiber debonding and resin deformation and microcracking. In the mode I fracture of the ductile AS4/Dow-06 system, crack propagation occurs primarily by resin deformation and fracture, with only occasional interfacial debonding. Considerable resin deformation and microcracking is seen in the regions outside the resin rich area between the plies.

Mode II Loading - In-situ mode II delamination observations were made for the AS4/3501-6 and AS4/Dow-P7 systems. In these systems a series of sigmoidal shaped microcracks are seen to develop in the resin rich region between the plies well ahead of the crack tip (see Figure 9). The primary crack extension occurs by the growth and coalescence of these microcracks. Normally this coalescence occurs near the fiber/resin interface at the upper or lower extent of the resin rich region between plies.

## DISCUSSION

### FRACTURE SURFACE CHARATERISTICS OF MODERATELY DUCTILE AND BRITTLE RESIN SYSTEMS AND THE FORMATION OF HACKLES

In mode I failure, the in-situ observations indicate that the primary micromechanism of delamination is by interfacial debonding for the AS4/3501-6 and AS4/Dow-P6 systems. Because the delamination crack takes the path of least resistance which in these systems was along the resin/fiber interface, resin fracture in the regions between

fibers was only observed occasionally. Significant resin deformation or microcracking leading to hackle formation was limited to the few isolated areas where good resin adhesion and/or fiber pullout occurred. Thus, only a relatively few, shallow hackles are seen in the mode I fractography. The composite fracture toughness of the brittle AS4/3501-6 system was seen to be twice that of the neat resin material. This may be explained [9] in terms of a greater fracture area due to the corrugated roof fracture surface in the composite as compared to a mirror smooth fracture surface in the neat resin. This greater fracture area along with fiber bridging and subsequent fiber breakage apparently compensates for the premature failure by resin debonding. However, the AS4/Dow-P6 system whose neat resin has twice the toughness of Hercules 3501-6 had a very similar delamination toughness. Assuming the interfacial bonding in each system is similar, this might be expected, since the failure mechanism for the AS4/Dow-P6 system was also principally resin/fiber debonding. Therefore, fiber bridging and breakage along with increased fracture surface was also responsible for providing most of the resistance to delamination. Delamination toughness for the AS4/Dow-P7 system seems to be derived from a combination of the better resin toughness, a better extraction of this resin toughness resulting from the increased resin/fiber adhesion, increased fracture surface area due to a "corrugated roof" fracture surface topography, and fiber bridging and breakage.

The fractography for both the brittle system AS4/3501-6 and the somewhat more ductile resin system AS4/Dow-P6 and AS4/Dow-P7, clearly shows that the number of hackles as well as their orientation or angle with respect to the ply plane increase as the percentage of

shear loading is increased (Figures 2,3, and 4). As the percentage of mode II loading is increased, the angle of the principal normal stress monotonically increases from being parallel to the ply plane in mode I to 45 degrees to the ply plane for pure mode II loading. The hackles which form only in relatively brittle systems are apparently the result of microcrack nucleation in advance of the crack tip and subsequent propagation in a brittle fashion through the resin rich region on the principal normal stress plane until they are stopped by the graphite fibers (Figure 10). The coalescence of these microcracks constitutes growth of the primary crack. Confirmation of this explanation is seen in both the fractographic evidence of increasing hackle angles as the shear loading is increased and the formation of sigmoidal shaped microcracks in front of the crack tip observed in in-situ mode II delamination of AS4/3501-6 and AS4/Dow-P7 (Figure 9).

In all of the graphite/epoxy composite systems of this study, the delamination toughness is seen to increase with higher percentages of mode II shear loading (see Table 1). The value for the mode II critical energy release rate found in this study for AS4/3301-6 was noted to be 2 to 3 times higher that reported in previous mode II fracture toughness studies of AS4/3501-6 [8,10]. No comparisons were possible for the four other systems studied, but the large $G_{IIc}/G_{Ic}$ ratios may indicate an apparent larger than expected mode II delamination toughness in these systems as well. Whether the higher mode II delamination toughness values reflect differences due to such variables as processing or if they are an artifact of the experimental or analytical procedure is still unclear. However, the general trends between mode of loading and delamination

toughness indicated by Table 1 are consistant with other published data, and will be used to describe qualitatively the relationship between failure mechanism and fracture toughness. The most dramatic increase in fracture toughness as the percentage of mode II loading was increased was seen in the systems that failed primarily by interfacial debonding under mode I loading conditions. For these brittle systems, AS4/3501-6 and AS4/Dow-P6, the increase in delamination toughness appears to be associated with the formation of the hackles and the change from continuous to discontinuous crack growth it represents. Both the increase in fracture surface area generated through the formation of these hackles and the more tortuous path of crack growth (sigmoidal shaped microcracks inpingement on fibers, etc.) would suggest greater resistance to crack growth for increasing mode II loading. When interfacial adhesion is improved, as in the AS4/Dow-P7 system, the resistance to crack growth in mode I loading is improved by resin microcracking and deformation. Therefore, the effective increase in delamination toughness under high mode II loadings that result from the development of regular microcracks and the formation hackles is greatly reduced. It is also worth noting that the more ductile AS4/Dow-Q6 system had no hackle formation and therefore a $G_{IIc}/G_{Ic}$ ratio which was much lower than for the more brittle systems that failed by debonding under mode I conditions (Table 1).

While the idea that mode II or mixed mode loading of a relatively brittle resin composites gives microcracking on the principal normal stress plane and subsequent coalescence gives rise to hackle formation seems qualitatively correct, there must be more to the story. The post-mortem and in-situ results for the pure mode II

delamination fracture (mode II fractography in Figures 2,3, and 4) clearly indicate a final hackle orientation much greater than the expected 45 degrees to the plane of the ply one would predict based on a simple stress analysis. The more nearly vertical overall orientation of the hackles for pure mode II loading could result from hackle rotation due to shear loading just prior to microcrack coalescence (see Figure 10). This rotation would not only orient the microcrack more vertically but could also open up the microcrack near the boundary where coalescence occurs. This opening of the microcracks gives the impression of material lost, which might correspond to matching hackles on the opposite surface. However, the mating fracture surfaces has for a hackled region are found to be flat, dish shaped regions which correspond to hackle coalescence on that surface.

The mode II in-situ results of the AS4/3501-6 (Figure 9) clearly show that the slant direction of the hackles depends on whether the coalescence of the microcracks occurs at the upper or lower boundary. Since the number of hackles pointing in the direction of crack growth on one fracture surface appears to be the same as the number of hackles pointing in the opposite direction on the other fracture surface, no preference as to whether coalescence takes place at the top or bottom of these microcracks is indicated. Once the microcrack coalescence begins on either the upper or lower boundary of the resin rich region between plies, it will continue on that same boundary. The stress redistribution that accompanies the coalescence of the first two microcracks will favor continued coalescence on this same boundary.

Bascom [11] has recently indicated that resin flow or yielding

may be an important mechanism in the formation of hackles. The amount of resin flow in the development of hackles in the AS4/3501-6 and AS4/Dow-P7 under 43% mode II loading was evaluated by noting changes in the fracture surface details before and after annealing the fractured specimen 15° C above the resin Tg for 4 hours to see the extent of recovery (Figure 11). No visible recovery in terms of change of shape or size of the hackles in these systems was observed, indicating that resin flow is not an important mechanism in the formation of the hackles. However, careful examination suggests that there may have been some change of hackle orientation. After annealing, the angle with respect to the ply plane seems to have decreased very slightly, supporting the idea that rotation of the hackles, which would increase the hackle inclination, may take place due to the mode II component of loading on the upper and lower boundaries of the sigmoidally microcacked region before final coalescence occurs. One might expect the greatest amount of hackle rotation to occur under pure mode II loading conditions, and therefore, a significant change in the hackle inclination with respect to the ply plane after annealing would be observed. At the time of this writing, tests to evaluate the effects of annealing on the mode II fracture specimens have not yet been conducted.

## IMPLICATIONS FOR FAILURE ANALYSIS

The above observations have important application to failure analysis. First, a very hackled surface on a unidirectional laminate clearly indicates a relatively brittle resin with significant mode II loading. The more nearly vertical the hackles, the greater was the mode II component of the service load which caused the failure.

Delamination of multiaxial composites such as [0,+ 45, 90] would be expected to show general hackling even for nominally macroscopic mode I loading due to the development of interlaminar shear stresses through the differential Poisson's contraction.

As mentioned before, some authors have suggested that hackles may be useful in determining the direction of crack growth. This study has clearly shown that this is only true for one of the fracture surfaces. On the other fracture face, the hackles point away from the crack growth direction. There does not seem to be any direct way to infer anything about crack growth direction from the hackle orientation. However, a more careful examination of the detailed river patterns on the individual hackles may allow crack growth direction to be determined. Individual river patterns may be misleading if interpreted to be more than the local microcrack growth direction but the resolved direction of many such river marks should point in the direction of crack extension. We found these river patterns more distinct and easy to map on relatively flat hackles (i.e., for relatively low fraction of mode II loading).

## FRACTURE CHARACTERISTICS OF DUCTILE SYSTEMS

The large amount of resin deformation and the lack of any distinct hackle formation indicates that the processes of fracture in the ductile A54/Dow-06 system are different from those in the more brittle systems. This is confirmed by the in-situ mode I delamination observations (Figure 8) that show that failure is by resin yielding and deformation. The good fiber/resin adhesion allowed the shear loads to be effectivly transferred to the resin and results in a deformation and damage zone of up to 3 or 10 fiber diameters across.

The mode II fractography of AS4/Dow-06 system showed an increase in resin deformation compared to that seen in mode I failure, with little or no hackle formation. Because there was no significant change in failure mechanism between mode I and Mode II delamination (see Figure 7), only a moderate increase in delamination toughness would be expected as one changed the loading from mode I to mode II. This hypothesis is supported by a $G_{IIc}$ to $G_{Ic}$ ratio of 3.4, as previously noted. Hackles are not developed because of the resin ductility (i.e., no brittle microcracks) failure from yielding occurring in lieu of the development and coalescence of a regular system of microcracks.

## SUMMARY

The results of this study show that in brittle AS4/3501-6 (resin $G_{Ic}$ = 0.07KJ/Sq.m.), the slightly more ductile AS4/Dow-P6 (resin $G_{Ic}$ = 0.14 KJ/Sq.m.) and AS4/Dow-P7 (resin $G_{Ic}$ = 0.32 KJ/Sq.m.) composite systems the number of hackles and their angle with respect to the ply plane monotonically increase with the percentage of mode II loading. In-situ delamination observations under mode II loading show that these hackles develop from the coalescence of sigmoidal shaped microcracks that form in a brittle fashion on the principal normal stress plane in the resin rich region ahead of the crack tip. However, under high percentage mode II loading conditions, the final orientation of the hackles with respect to the ply plane is often much greater than the 45 degrees expected from brittle cracking along the principal normal stress plane. This increased inclination

may result from rotation of the hackles due to the shear loading before final coalescence of the microcracks occurs. In the AS4/3501-6 and AS4/Dow P-6 systems where mode I delamination was dominated by interfacial debonding, the increase in delamination fracture toughness as the loading conditions are changed from pure mode I to pure mode II corresponds to the formation of these hackles. Both the increased surface area and the more tortuous path of crack growth that these hackles represent seem to be responsible for the observed increase in fracture toughness. In the AS4/Dow P-7 system where there was enhanced interfacial bonding, at least some of the mode I delamination toughness was obtained through resin deformation and microcracking. Therefore, the microcracking and formation of hackles associated with higher precentages of mode II loading produced a much less drastic increase in the delamination toughness.

In the tougher composite system AS4/Dow-06 (resin $G_{Ic}$ = 0.73 KJ/Sq.m.), hackles do not form under high mode II loading conditions. This is because in this ductile resin system, yielding and ductile fracture occur before the development and coalescence of a regular system of microcracks can take place. Since no change in failure mechanism (i.e. no formation of hackles) takes place as the loading conditions change from mode I to mode II, a less substantial change in the delamination fracture toughness occurs.

In failure analysis, hackles can be used to identify a state of shear loading at the crack front during failure. However, care must be taken in using hackles to identify the macroscopic state of the applied loading, since in multidirectional laminates, shear loading at the crack tip can result from differential Poisson's contractions where nominally pure mode I loading conditions exist

macroscopically. Since there is no preference on whether the coalescence occurs at the upper or lower boundary of the microcracks, the direction of crack growth cannot be determined from the direction of hackle slant alone.

REFERENCES


1. Hunston, D.L., Bullman, G.W., "Characterization of Interlaminar Crack Growth in Composites: Double Cantilever Beam Studies", 1985 Grant and Contract Review , NASA Langley Research Center Materials Division, Fatigue and Fracture Branch , Vol. II, February 13-14, 1985.

2. Chakachery E.A., Bradley, W.L., "A Comparison of the Crack Tip Damage Zone for Fracture of Hexcel F185 Neat Resin and T6T145/F185 Composite", Presented at the ACS International Symposium on Non-Linear Deformation, Fatigue and Fracture of Polymeric Materials, Chicago, IL., September 8-13, 1985.

3. Morris, G.E., "Determining Fracture Directions and Fracture Origins on Failed Graphite/Epoxy Surfaces", Nondestructive Evaluation and Flaw Criticality for Composite Materials , ASTM STP 696 , American Society for Testing and Materials, 1979 pp. 274-297.

4. Tse, M.K., Hibbs, M.F., and Bradley, W.L., "Delamination Fracture Studies of Some Toughened Graphite/Epoxy Composites, Including Real-Time Fracture Observations in the Scanning Electron Microscope", Presented at the ASTM Symposium on Toughened Composites, Houston, Texas, March 13-15, 1985.

5. Devitt, D.F., Schapery, R.A., and Bradley, W.L., "A Method for Determining the Mode I Delamination Fracture Toughness of Elastic and Viscoelastic Composite Materials", Journal of Composite Materials , Vol. 14, October, 1980 pp. 270-285.

6. Whitney, J.M., Browning, C.E., and Hoogsteden, W., "A Double Cantilever Beam Test for Characterizing Mode I Delamination of Composite Materials", Journal of Reinforced Plastics and Composites , Vol. 1, October 1982 pp. 297-313.

7. Wilkins, D.J., Eisenmann, J.R., Cumin, R.A., and Margolis, W.S., "Characterizing Delamination Growth in Graphite/Epoxy", Damage in Composite Materials: Basic Mechanisms, Accumulation, Tolerance and Characterization , ASTM STP 775 , American Society for Testing and Materials, 1982 pp. 168-183.

8. Russell, A.J., and Street, K.N., "Moisture and Temperature Effects on the Mixed-Mode Delamination Fracture of Unidirectional Graphite Epoxy", ASTM STP 876 , American Society for Testing and Materials, 1985.

9. Bradley, W.L., Cohen, R.N., "Matrix Deformation and Fracture in Graphite Reinforced Epoxies", Presented at the ASTM Symposium on Delamination and Debonding of Materials, Pittsburg, PA., November 8-10, 1983.

10. Jordan, W.M., "The effect of Resin Toughness on the Delamination Fracture Behavior of Graphite/Epoxy Composites", Ph.D. Dissertation, Texas A&M University, College Station, Texas, 1985.

11. Bascom, W.D., "Fractographic Analysis of Interlaminar Fracture", Presented at the ASTM Symposium on Toughened Composites, Houston, Texas, March 13-15, 1985.

TABLE 1

RESIN AND COMPOSITE ENERGY RELEASE RATES

| System | Resin $G_{Ic}$ | Composite $G_c$ Mode I | 43% Mode II | Mode II | Composite $G_{IIc}/G_{Ic}$ Ratio |
|---|---|---|---|---|---|
| AS4/3501-6 | 0.07 | 0.137 | 0.695 | 1.292 | 9.43 |
| AS4/DOW-P6 | 0.14 | 0.165 | 0.334 | 1.806 | 10.95 |
| AS4/DOW-P7 | 0.32 | 0.340 | 0.629 | 1.325 | 3.90 |
| AS4/DOW-Q6 | 0.73 | 0.848 | 0.969 | 2.836 | 3.34 |

Energy release rates given in KJ/Sq.m.

## FIGURE CAPTIONS

Figure 1. Schematic showing how asymmetric loading of a split laminate (DCB) can introduce a mixed (mode I & mode II) state of stress at the crack tip.

Figure 2. Fractographs of AS4/3501-6
Note, as the percentage of mode II loading is increased, both the number of hackles and their angle with respect to the fracture surface is increased. Arrows indicated the direction of crack growth.
a) pure mode I loading
b) 12% mode II loading
c) 43% mode II loading
d and e) pure mode II loading

Figure 3. Fractographs of AS4/Dow P-6
The number of hackles and their angle with respect to the fracture surface increase as the percentage of mode II loading is increased. Under pure mode II loading conditions the hackles appear nearly vertical. Arrows indicate the direction of crack growth.
a) pure mode I loading
b) 43% mode II loading
c and d) pure mode II loading

Figure 4. Fractographs of AS4/Dow P-7
The number of hackles and their angle with respect to the fracture surface increase as the percentage of mode II loading is increased. Under pure mode II loading conditions the hackles appear nearly vertical. The 'pock marked' surface may be the result of trapped volatiles during the curing of the laminate panel. Arrows indicate the direction of crack growth.
a) pure mode I loading - large sheets of fibers and resin are seen to be pulled out.
b) 43% mode II loading
c and d) pure mode II loading

Figure 5. Hackles slant in the direction of crack growth on the upper fracture surface and in the opposite direction on the lower fracture surface. Arrows indicate the direction of crack growth.

Figure 6. Clean fibers indicating fiber/matrix debonding in both mode I and mode II loading conditions for the AS4/3501-6 system.

Figure 7. Fractographs of delamination fracture of the ductile AS4/Dow 0-6 system
In the AS4/Dow-06 system the fibers are completely coated with resin indicating good resin/fiber adhesion. Note, that in this ductile system distinct hackles are not observered even at pure mode II loading conditions. Arrows indicate the direction of crack growth.
a) mode I loading
b) 43% mode II loading
c and d) pure mode II loading

Figure 8. Mode I in-situ delmination. Arrows indicate the direction of crack growth.
a) AS4/3501-6 failure is seen to be primarily by debonding at the fiber/matrix interface.
b) In the mode I delamination failure of the AS4/Dow 0-6 system extensive resin yielding is observed.
c and d) In the AS4/Dow P-7 system, mode I delamination failure occurs by a combination of fiber/resin debonding and resin yielding. Partial resin coating of the fibers indicates improved resin/fiber adhesion.

Figure 9. Mode II in-situ delamination. Arrows indicate the direction of crack growth.
a) development of the sigmoidal microcracks in the resin rich region between fibers in front of the crack tip in the AS4/3501-6 system
b) Sigmodial microcracks in the AS4/Dow P-7 system under pure mode II loading conditions. Note, the fiber/resin interfaces are not clearly distinguishable in this fractograph
c and d) Hackles resulting from the coalescence of the microcracks developed in mode II loading of the AS4/3501-6 system.

Figure 10. a) The principal normal stresses that developed ahead of a crack tip in the resin rich region between plies under mixed mode loading conditions.
b) The development of sigmoidal microcracks along the principal normal stresss plane and the rotation of the hackles due to the shear loading before final coalescence of the microcracks. The direction in which the hackles slant depends on whether the microcracks coalesce at the upper or lower boundary.

Figure 11. The fracture surface before and after annealing 15 degrees C above the resin Tg. There is no observable change in size or shape of the hackles indicating resin flow is not an important mechanism in hackle formation.
a and b) AS4/3501-6 system - The angle of the hackles with respect to the fracture surface may have decreased slightly after annealing suggesting that rotation of the hackles due to the shear loading occurred before final coalescence of the microcracks.
c and d) AS4/Dow P-7

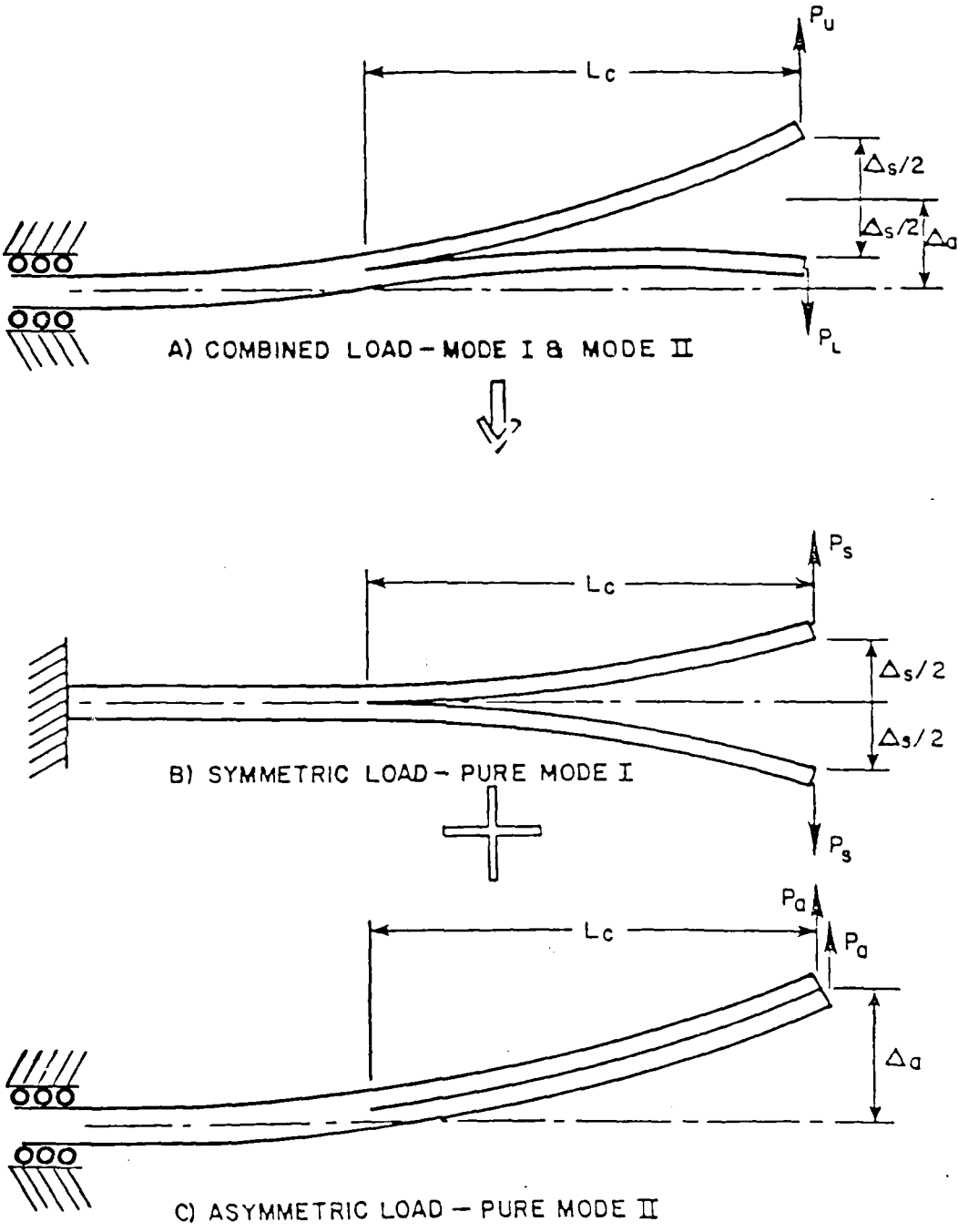


Figure 1. Schematic showing how asymmetric loading of split laminate can introduce a mixed mode I/mode II state of stress at the crack tip.

Figure 2.

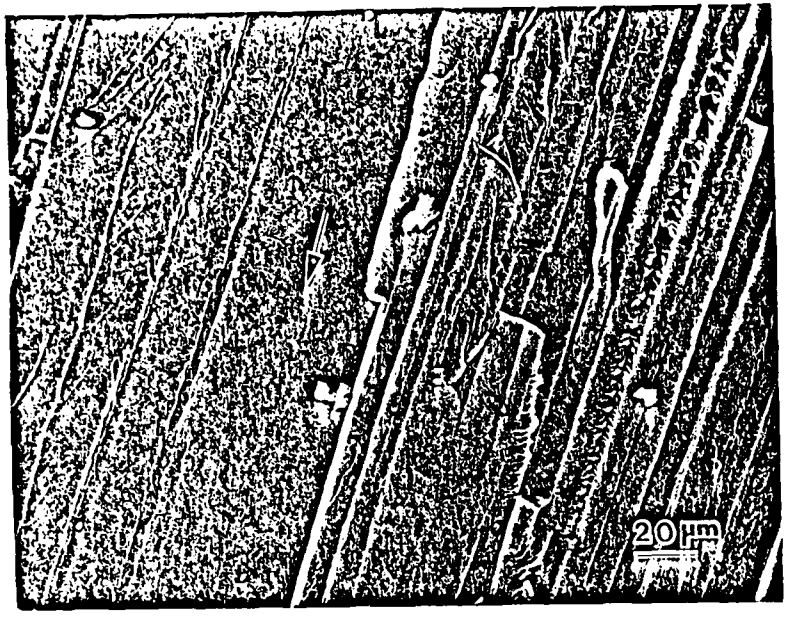


2a

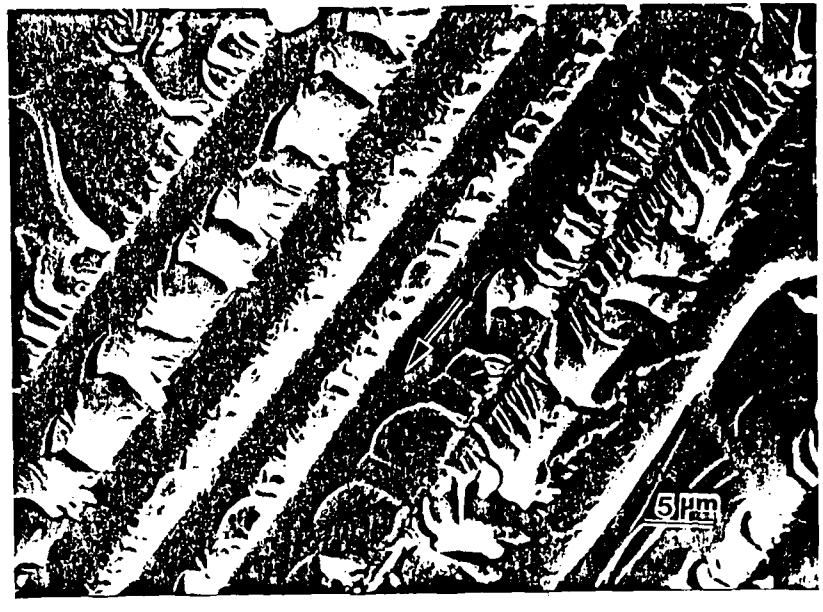


c

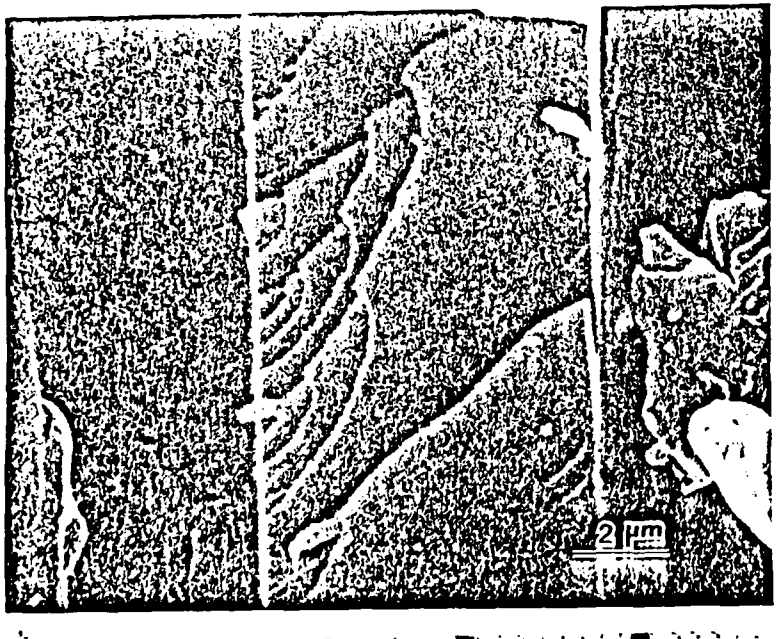



2 e

Figure 3.

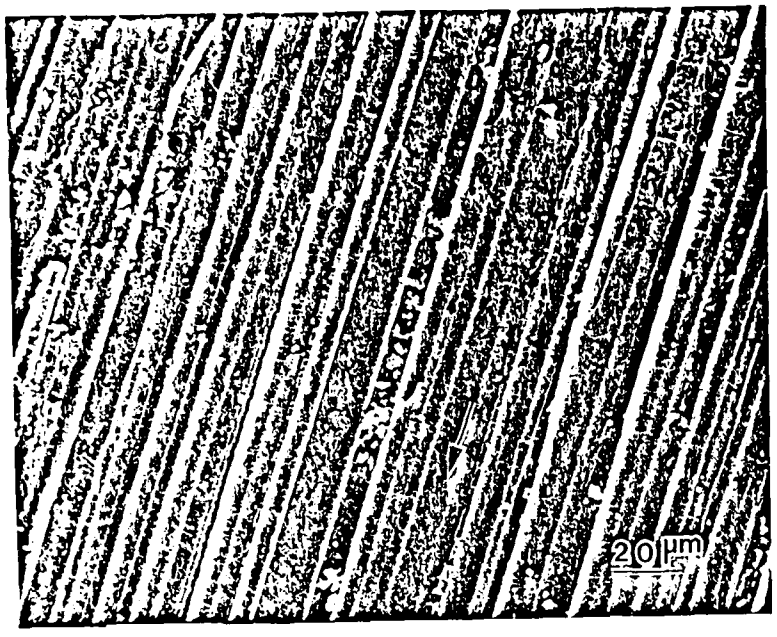


3a

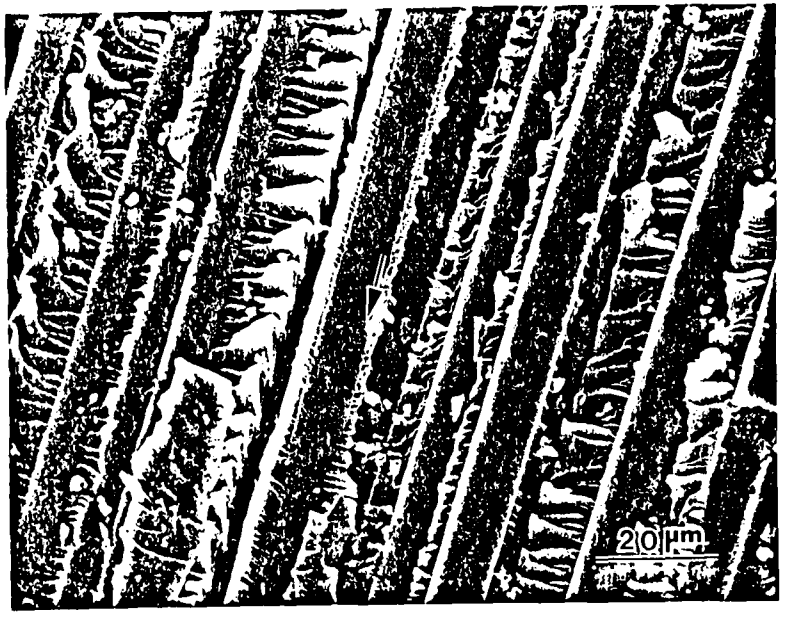


b

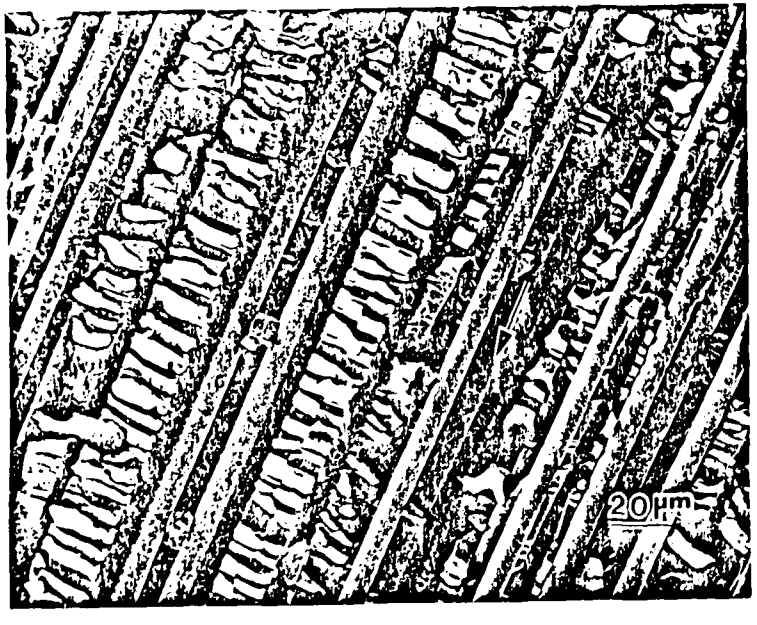


c

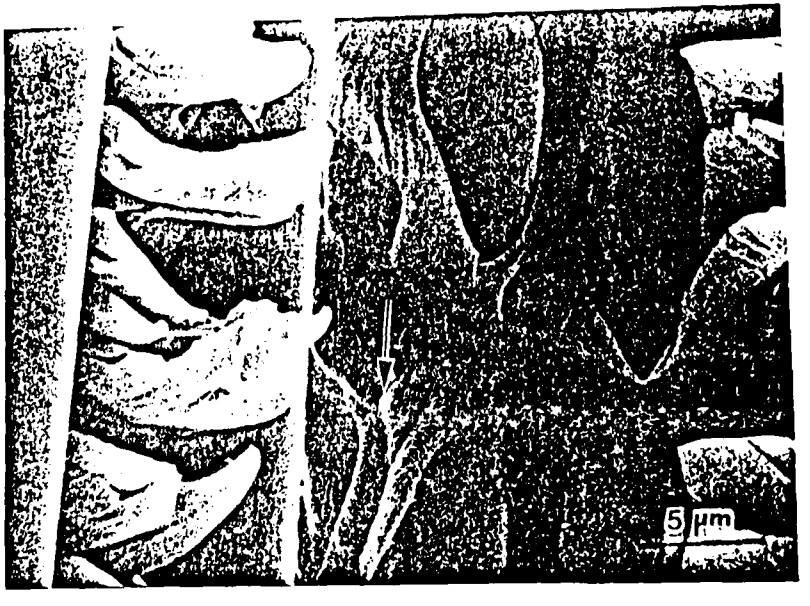


d


b


d


4 a

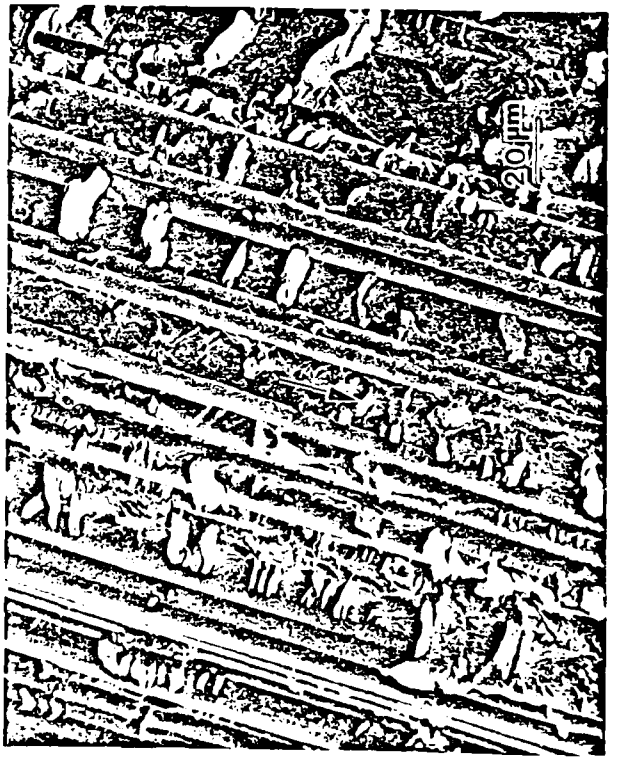


c

Figure 4.

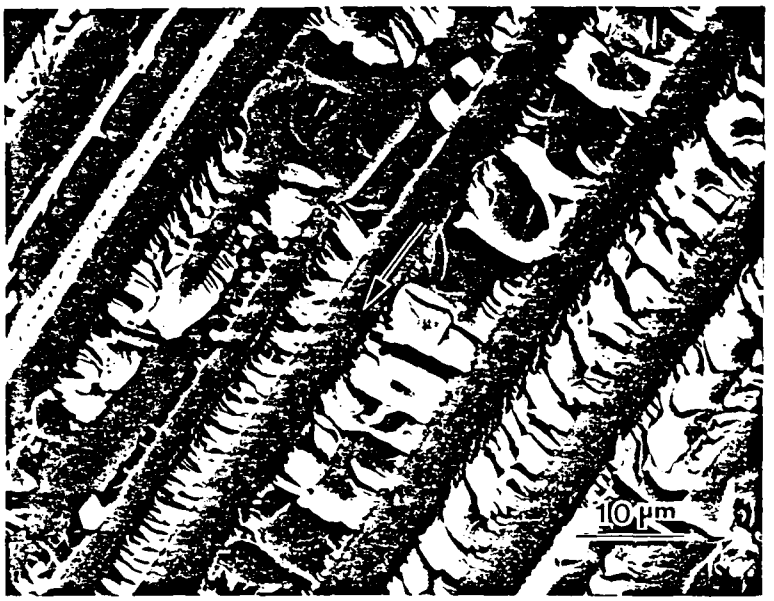


Lower Fracture Surface

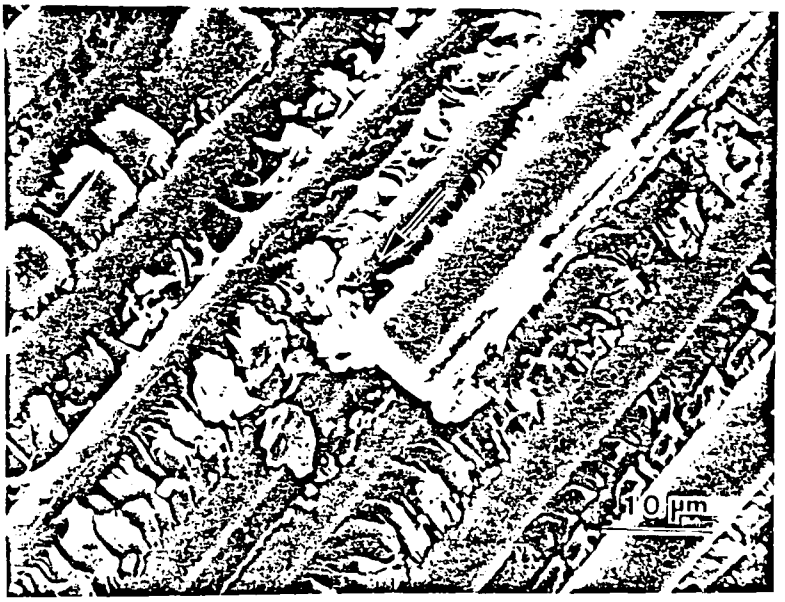


Upper Fracture Surface

Figure 5.

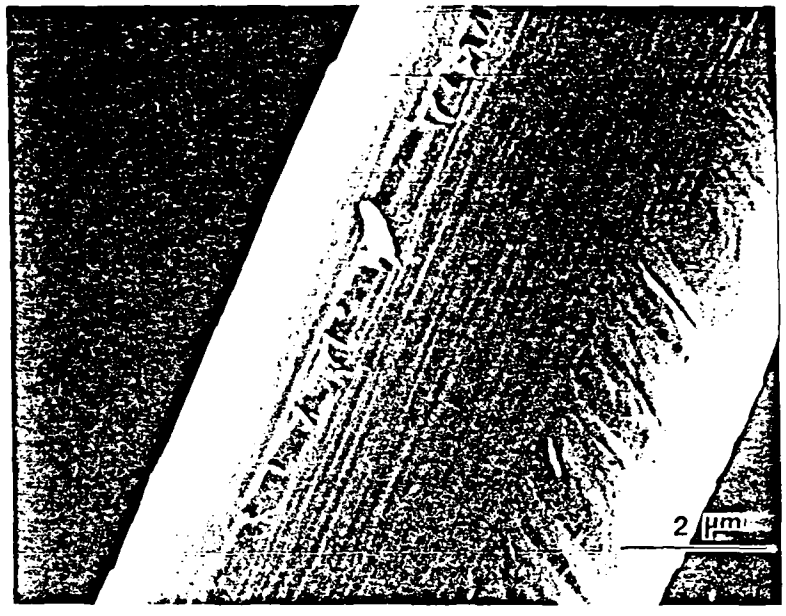


Mode I Loading

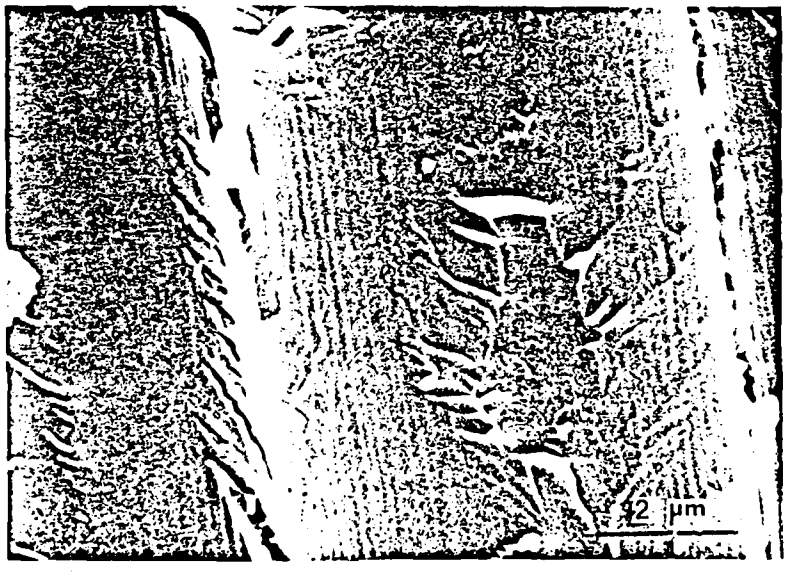


Mode II Loading

Figure 6.

Figure 7.

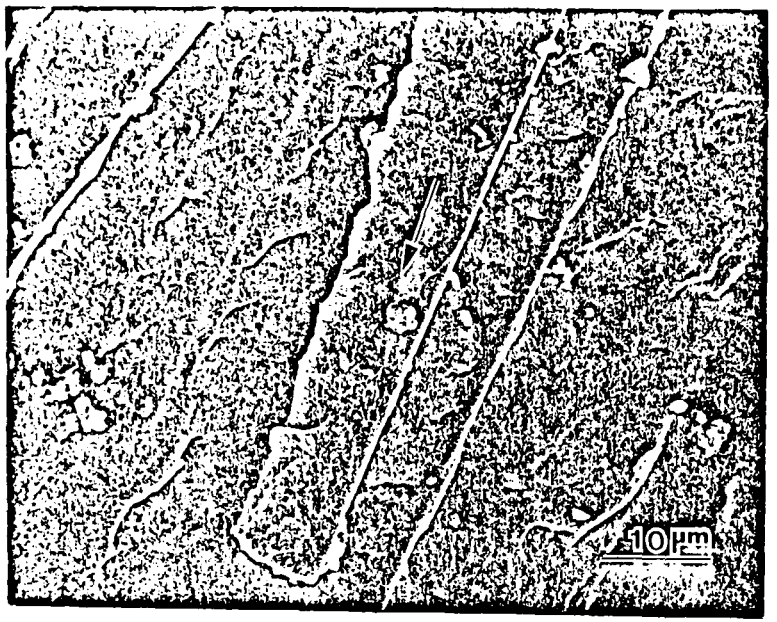


7 a

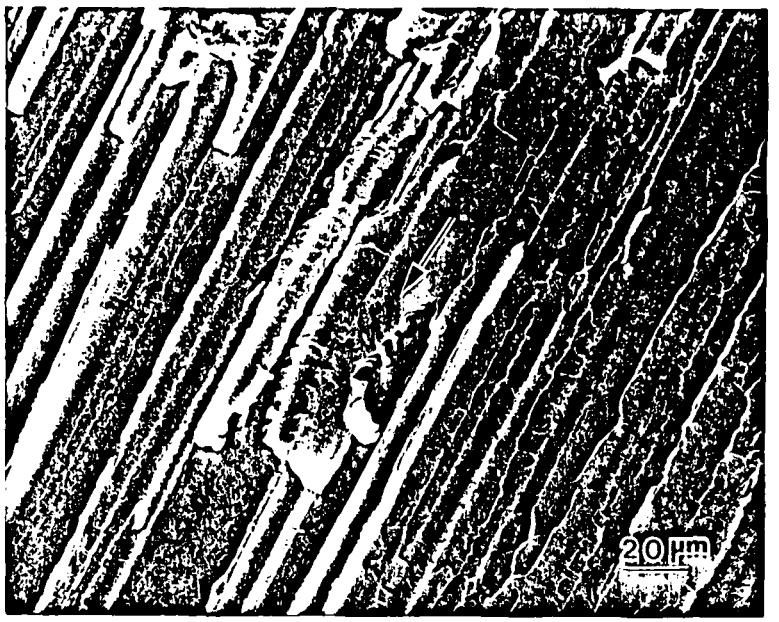


b

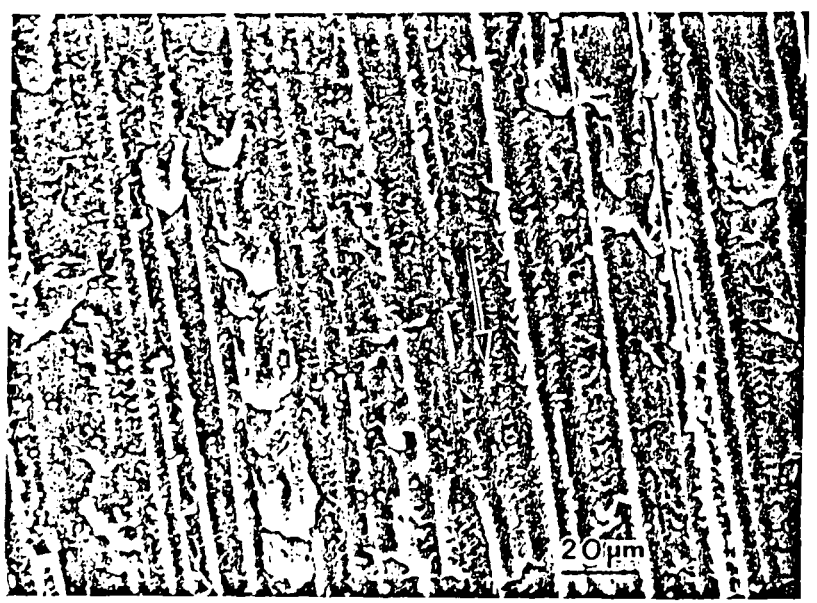


c

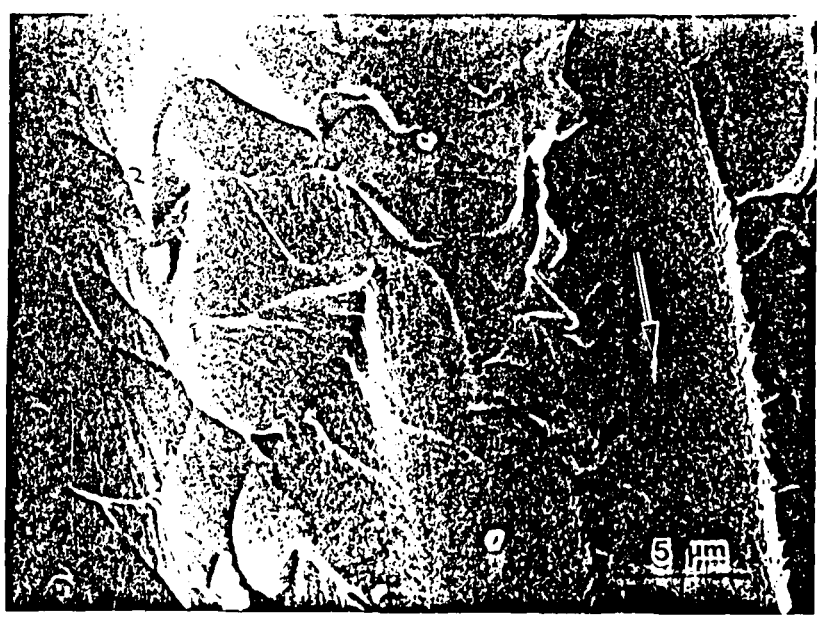


d


8 a


b

Figure 8.


8 c

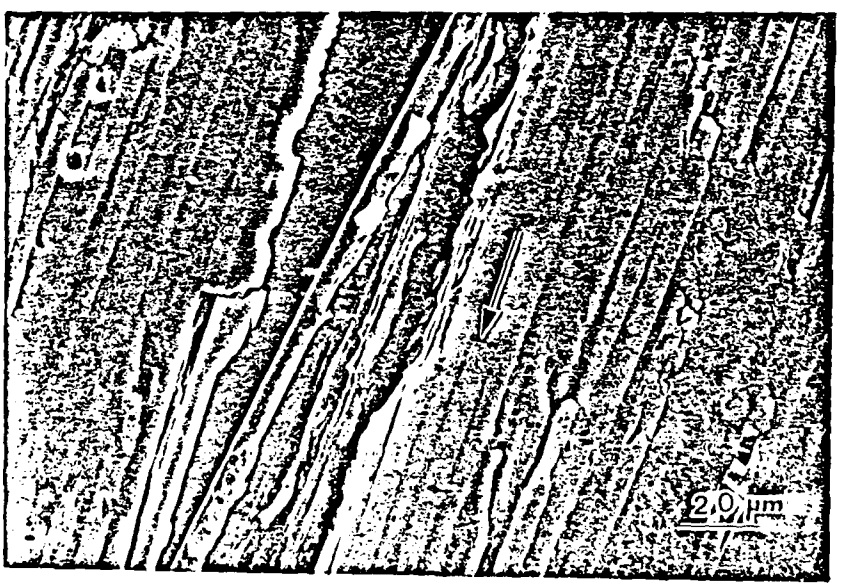


d

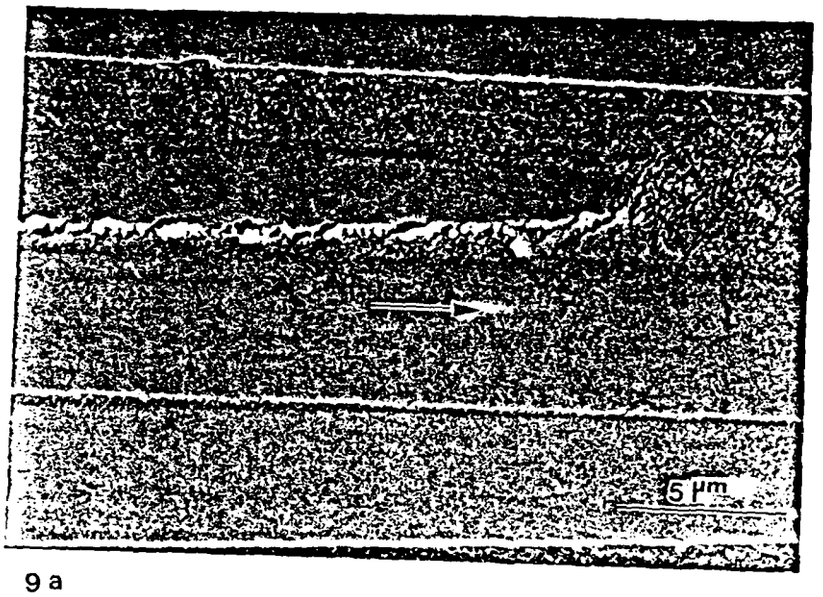


9 a

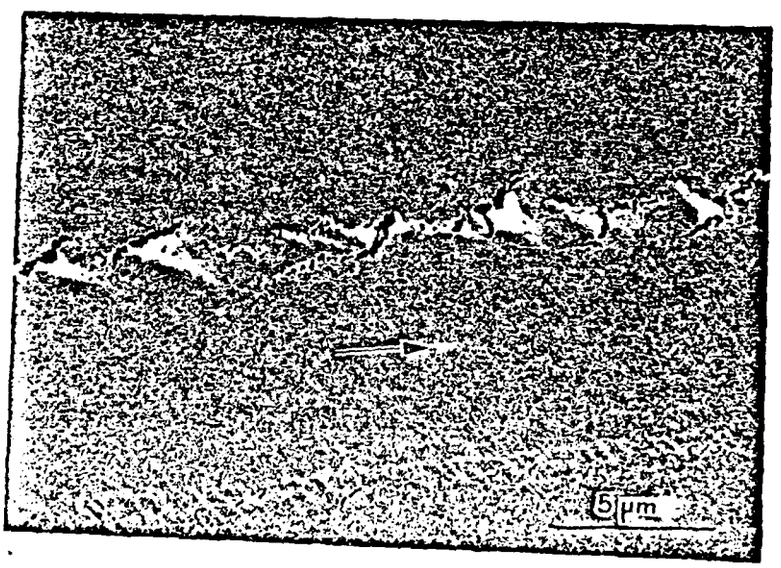


b

Figure 9.

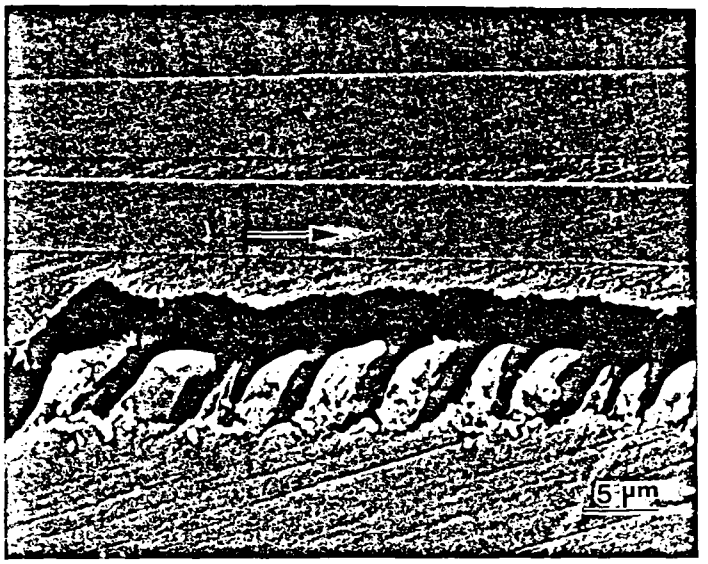


9 c

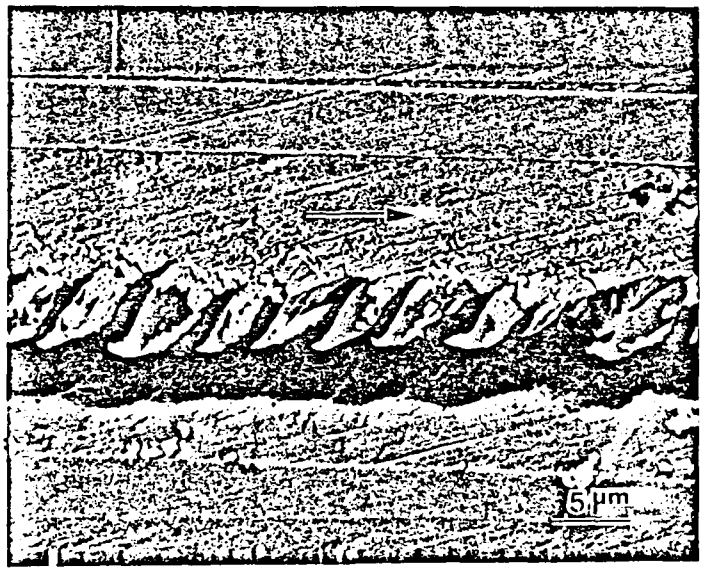


d

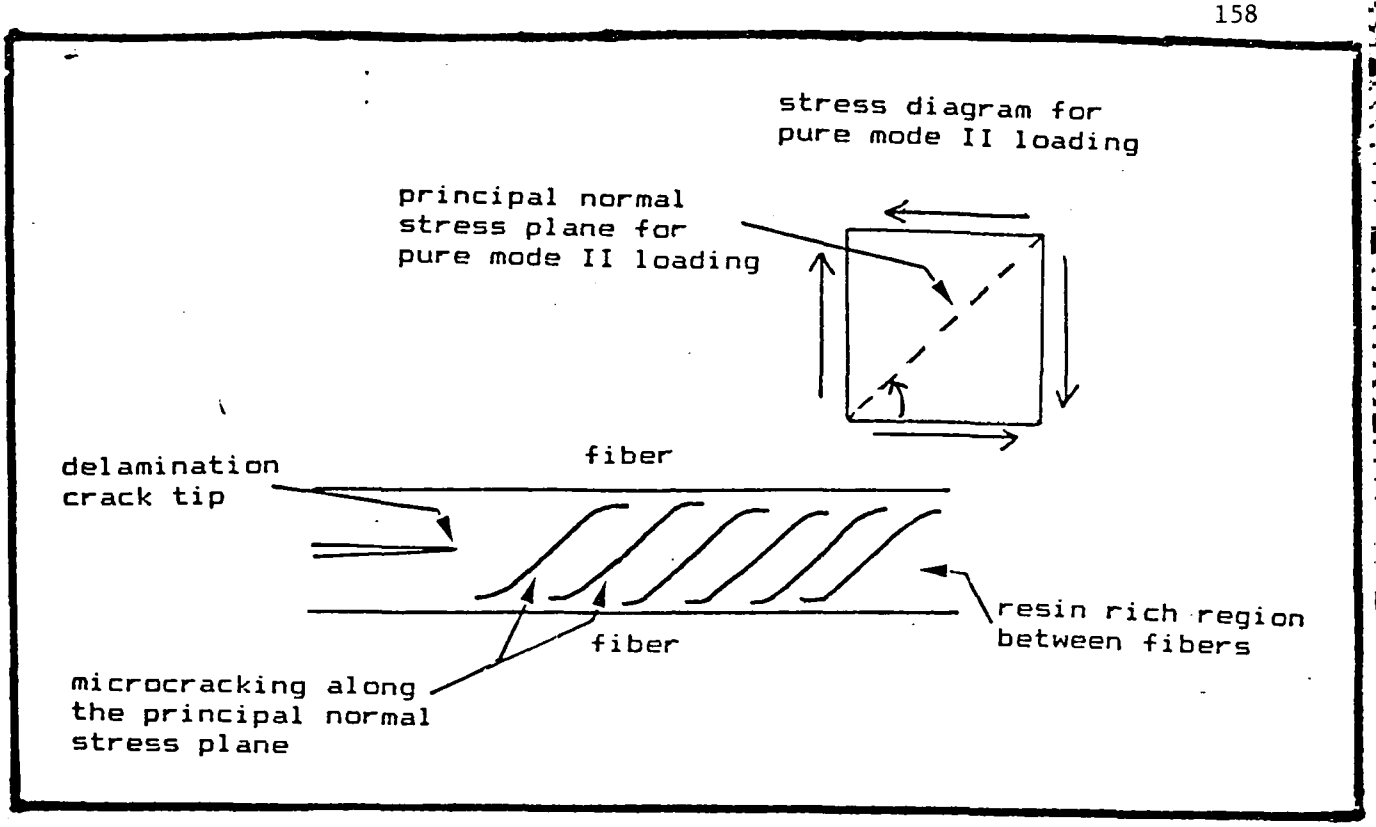


Figure 10a

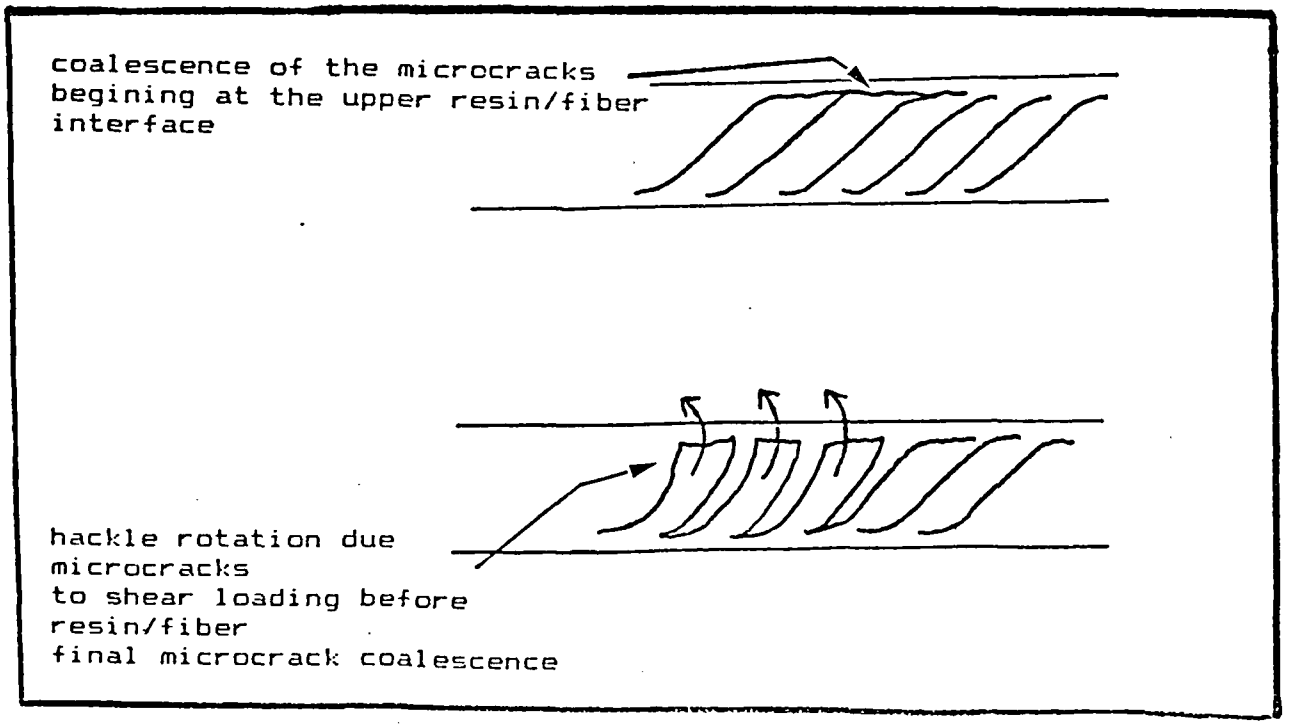


Figure 10b

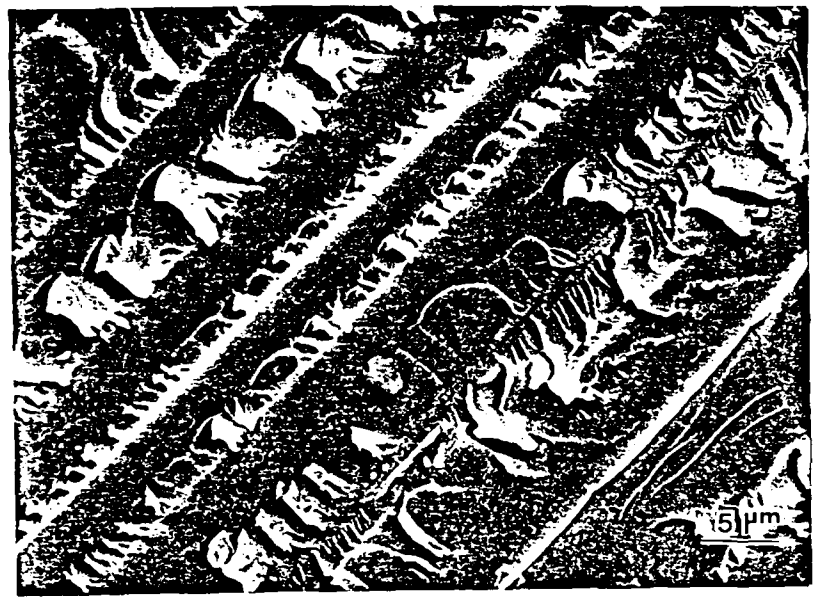


11a

Before Annealing

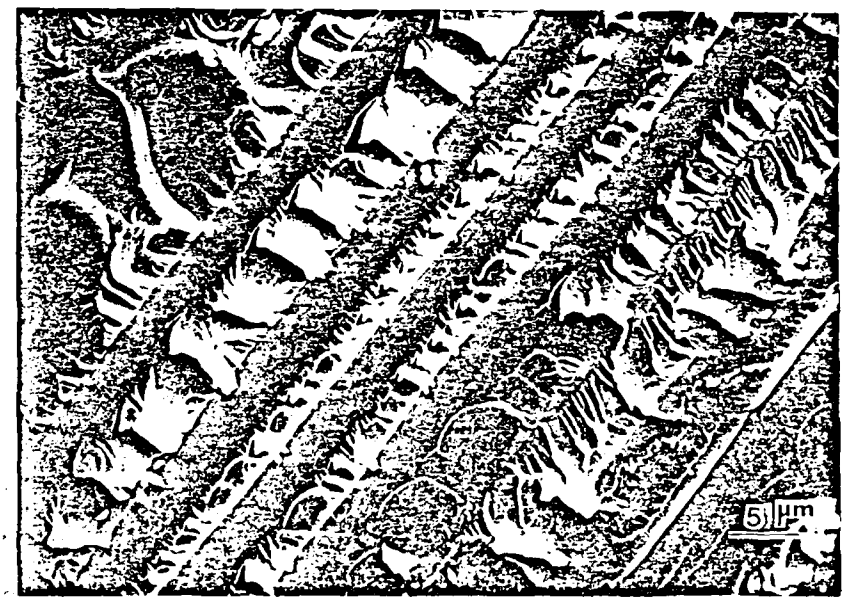


b

After Annealing

Figure 11.

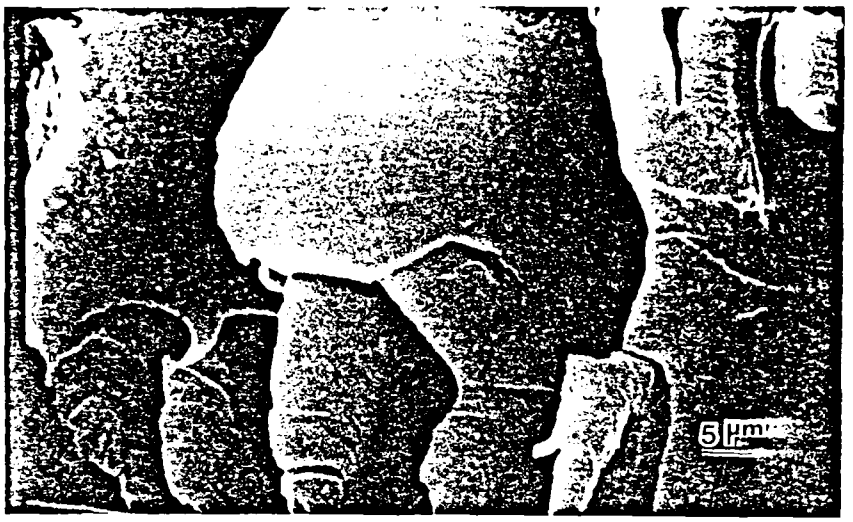


11 c

Before Annealing

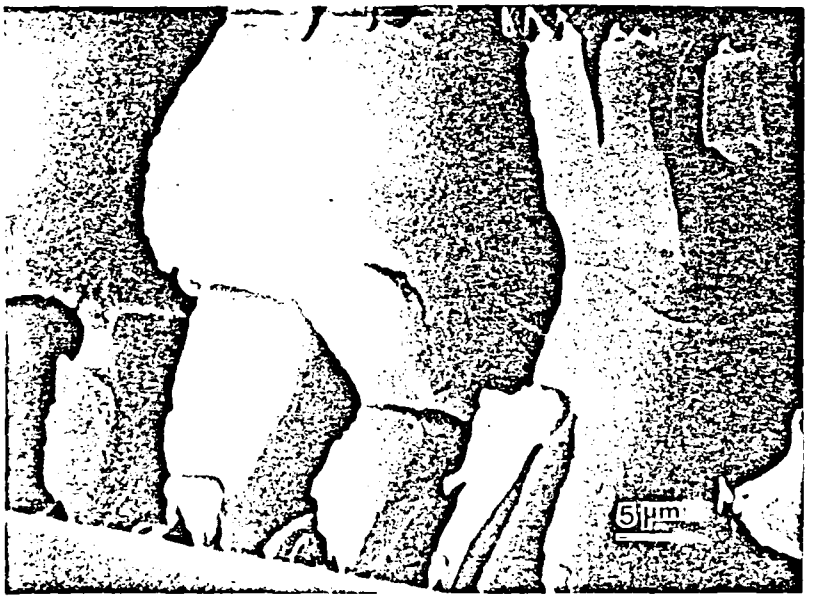


d

After Annealing

# "The Meaning and Significance of Hackles in Composite Materials Failure Analysis"

by

William Jordan, Michael Hibbs, and Walter Bradley

Texas A&M University

College Station, Texas 77843

published in proceedings of

International Conference: Post Failure Analysis Techniques for Fiber Reinforced Composites

held

July, 1985; Dayton Ohio

# The Meaning and Significance of Hackles in Composite Materials Failure Analysis

by

William Jordan, Michael Hibbs, and Walter Bradley
Texas A&M University
College Station, Texas 77843

## INTRODUCTION

The dramatic increase in use of graphite/epoxy composites in many diverse applications has brought about the need for reliable failure analysis techniques of these materials. For years, fracture surface morphology has been successfully used as means of identifying the fracture origin and direction of crack propagation in metals. There have been recent attempts by Hahn(1,2)and others to apply similar techniques to graphite/epoxy composites. In order to more easily use fracture surface characteristics as a tool in failure analysis, a better understanding of the micromechanical processes involved in failure in these materials is needed.

In the case of delamination of a graphite/epoxy composite, the fracture surface is characterized by the amount of fiber pullout, interfacial debonding, and the extent of the resin deformation or microcracking. One of the most common features of resin deformation have been identified as 'hackles'. These hackles appear as lacerations or scallops in the resin that form regular saw tooth or zipper patterns. The works of these authors and others (Hahn) have shown that, as the shear or mode II component of the state of stress

at the delamination crack front is increased, both the number and angle of the hackle with respect to the ply plane also increase. Several attempts have been made to relate the orientation of the hackles to the direction of crack propagation. Early works indicated that hackles slant towards the direction of crack growth (3,4). A more recent study has indicated that the hackles slant in opposite directions on the top and bottom surfaces of the crack face (5).

In this study, the effects that the state of stress, direction of crack growth, and resin ductility have on the formation of hackles in delamination failure will be explored. Evaluations will be made on the basis of scanning electron microscope (SEM) observations of the post-mortem fracture surfaces of unidirectional split laminate double cantilever beam specimens (DCB). These DCB specimens have been loaded in mode I, mode II, and mixed mode I & II conditions. Also, observations through the SEM of a mixed mode failure provided by unidirectional crack lap shear specimens (CLS), described by Wilkins, et al. (6) were made. These specimen gave approximately 75% mode II and 25% mode I loading.

To better understand the micromechanics involved in the formation of hackles and to help in the interpretation of the post-mortum fractography, in-situ SEM observations of delamination fracture of small DCB specimens loaded in mode I and mode II conditions were made.

Because, in most applications of composites, multidirectional laminates are used, a discussion of the resulting fracture surfaces from multidirectional laminates is also included.

## EXPERIMENTAL PROCEDURES

The graphite/epoxy composites used in this study were made from three resins, Hercules 3502, Hexcel 205 and Dow Chemical Q6 (a new experimental resin system). These three resins were chosen because they had very different toughnesses. In the case of the 3502 and Q6, pre-preg tape was obtained from the manufacturer and made into a 30 cm. square unidirectional panel with 24 plies. The panels were cured according to the manufacturers recommendations. A thin 0.03 mm teflon strip was placed between the center two plies to provide a starter crack. Hexcel provided unidirectional laminate made from prepreg of HX205 resin and graphite fibers. Test specimens 2.5 cm. by 25 cm. were cut from each panel. Double cantilevered beam specimens were tested on an MTS system in stroke control. Small specimens (2 cm x 0.4 cm) were cut from the larger panels for testing in the scanning electron microscope.

A schematic of the loading for the various tests is shown in Figure 1. Mixed mode conditions are obtained by superimposing a pure mode II load upon a mode I load. Pulling down only on the lower surface gives 43% mode II conditions if the upper arm is unloaded. Note pure mode II loading is obtained by pulling down on the top surface. To remove as much as possible any rubbing together of the fracture surfaces, a teflon strip about .1 mm thick was placed between the ends of the top and bottom surfaces.

Crack lap shear tests with approximately 75% mode II were conducted using the test specimen shown by Wilkins. The samples were tested on an Instron test machine in stroke control.

Fractographs were obtained by sectioning the fractured coupons with a jeweler's saw. The amount of cutting debris was minimized by cutting the samples before the top and bottom surfaces were separated. Any loose

debris that did occur was blown away by compressed air. The surface was then coated about 200 A thick layer of gold-palladium. The photographs were made on Tri-X film, using a JEOL JSM-25 Scanning Electron Microscope at accelerating voltages of 12.5 and 15 kv.

A limited number of mode I and mode II delamination tests were observed in the scanning electron microscope using a specially designed stage capable of loading specimens in the SEM. These observations were recorded in video tape and on tri-X sheet film. The edge of the specimen to be observed during delamination was carefully polished using standard metallographic techniques and coated with a 200 A gold-palladium alloy.

## EXPERIMENTAL RESULTS

### Post-mortem Fractographic Examination

In this section post-mortem fractographic results for delamination of three graphite/epoxy composites will be presented.

Brittle resin composite AS4/3502 ($G_{1c}$ = 189 J/m$^2$) - Fractography of the post-mortem delamination surfaces indicates that the number of hackles increase as the percentage of shear loading is increased, with the most dramatic increase being between 43% and 100% mode II loading (Figure 2). Mode I fracture surfaces were characterized by a flat corrugated roof appearance with a limited number of shallow hackles. The angle or slant between these hackles and the plane of the fracture surface is seen to increase as the percentage of shear loading is increased. At near pure mode II loading, the hackle are observed to be nearly perpendicular to the plane of the plies, and their edges appeared drawn and "tuffed". For the most part, the orientation or slant of the hackles remains constant on a

given fracture surface and point in opposite direction on the matching fracture face.

Because the interfacial bonding is so poor in AS4/3502, almost all fracturing occurred at the interface for pure mode I loading. AS1/3501-6 shown in Figure 3 indicates the more typical corrugated roof appear of pure mode I fracture with fracture occurring primarily through the resin. It should be noted in Figures 2 and 3 that almost no hackles are observed in the brittle system for pure mode I loading.

Moderately ductile resin composite HX205 ($G_{1c}$ = 455 J/m$^2$) - The fracture surfaces of the more ductile resin composite system HX205 were similar in appearance to those seen in AS4/3502, except for a much greater degree of resin deformation (Figure 4). As the percentage of shear loading was increased both the number and slant of the hackles increased. As the mode II loading is increased the shape of the hackles appeared more pulled or drawn than those seen in the brittle AS4/3502 system.

Ductile resin system Dow Q6 ($G_{1c}$ = 850 J/m$^2$) - The fracture surfaces of the ductile system Q6 were characterized by considerable resin deformation with good fiber/resin adhesion. Fractography reveals no distinct hackles (Figure 5). Only at near pure mode II loading conditions were some ill defined hackle like features seen. These features seen to be random with no consistent orientation.

In-situ delamination fracture observations in SEM

In-situ observations of fracture in the SEM of the three composite systems are seen in Figure 6. For mode I loading, both the brittle system AS4/3502 and the moderately ductile system HX205, the primary crack is seen to proceed by interfacial debonding. A limited amount of microcracking

is seen to occur in the resin behind the primary crack tip, and is normally associated with fiber bridging and eventual pullout.

In the mode I fracture of the ductile Q6 system, crack propagation occurs primarily by resin deformation and fracture with only occasional interfacial debonding. Considerable resin deformation and microcracking is seen in the regions outside the resin rich area between the plies.

In the mode II delamination of the AS4/3502 system, a series of sigmodial shaped microcracks are seen to develop in the resin rich region between the plies, well ahead of the crack tip. The primary crack extension occurs by the growth and coalescence of these microcracks.

## DISCUSSION

### Hackle Formation in More Brittle Resin Systems

The fractography for both the brittle system AS4/3502 and the moderately ductile system Hexcel HX205 clearly shows that the number of hackles as well as their orientation, or angle with respect to the ply plane, increase as the percentage of shear loading is increased (Figures 2-4). In mode I failure, the in-situ observations indicate that the primary micromechanism of delamination is by interfacial debonding (Figure 6) or continuous growth of the microcrack through the resin rich region between plies. This brittle fracture as it occurs for debonding or resin cracking occurs perpendicular to the principal normal stress in the region of the crack tip.

As the percentage of mode II loading is increased, the angle which the principal normal stress at the crack tip makes with respect to the ply plane changes from being parallel to the ply plane in mode I to 45° to the ply plane in pure mode II loading. The hackles formed are apparently

the result of the cracking occurring in a brittle fashion on the principal. normal stress plane, giving a whole series of microcracks running through the resin rich region between plies until they are stopped by the fibers. Coalescence of these microcracks, usually by interfacial debonding gives macrocrack advance and leaves a zipper appearance to the fractured surface, as shown in Figure 2.

The above conclusions have important implications to failure analyst. If the state of loading is known, the direction of the principle normal stress can be calculated from the tensile and shear components of the load. By assuming that the hackles are oriented perpendicular to the direction of the principle normal stress, one should be able to estimate the fraction of mode I and mode II loading which caused the delamination. To accomplish this, one must measure the hackle angles by looking at their profiles. This may be done by nickel plating the fracture surface to preserve the hackles, sectioning and polishing one edge.

Bascom ( 7) has recently indicated that resin flow or yielding may be an important mechanism in the formation of hackles. Indeed, at a high percentage of the shear loading in the moderately ductile system HX205 or near pure mode II loading for the brittle AS4/3502, the shape of the hackles seems to indicate some resin drawing (Figure 4). This is probably due to resin flow before final microcrack coalescences takes place. The amount of resin flow in the development of hackles can be evaluated by annealing the fracture surface near the resin's Tg to see the extent of recovery but, at the time of this writing, annealing tests had not been performed on our specimens.

## Fracture Characteristics of Very Ductile Systems

The large amount of resin deformation and the lack of any distinct hackles indicates that the processes of fracture in the ductile Q6 system are different from those seen in the more brittle systems. This is confirmed by the in-situ mode I delamination observations (Figure 6) that show that failure is by resin cracking and deformation. The good fiber/resin adhesion indicates that the shear loads must be effectively transferred to the resin. Because of the resin's ductility, failure from yielding occurs before the development or coalescence of a regular system of microcracks can take place. Clearly the use of fracture surface topography in the failure analysis of any ductile system is much less instructive.

## SUMMARY

Hackles form in graphite/epoxy composite materials when the following requirements are met: (1) relatively brittle epoxy is used; (2) some regions of resin concentration are present (e.g., low fiber density in delamination plane between plies); and (3) some mode II loading must be present locally in the crack tip region. Such conditions are routinely met in laminates with a multiaxial layup since interlaminar shear stresses are always present in such laminates, even when they are loaded with only mode I loading conditions. Furthermore, fiber nesting is not possible in such systems, which means that regions of resin concentration are always present at the interface between adjacent plies. Thus, it is not surprising that hackles are a very dominate feature on the fracture surface of delaminated multi-directional laminates.

In a unidirectional laminate, hackles will be a common feature of the delamination fracture surface only when the macroscopic loading conditions give a significant fracture of mode II loading. Otherwise, hackles will only

be observed occasionally when local heterogeneities in the composite cause the crack tip to experience a significant mode II contribution even though the macroscopic loading conditions are pure mode I. Furthermore, fiber nesting in unidirectional layups give a smaller volume of resin concentrated regions where hackles may form.

Since hackles result from sigmodial shaped microcracks for unidirectional layups, we do not believe that crack growth direction can be deduced from the macroscopic orientation of the hackles, since they will point in the direction of crack growth on one fracture surface and in the opposite direction on the other fracture surface. Sometimes a more detailed examination of individual microcracks may indicate "river patterns", and these may be useful in accertaining crack growth direction. We believe that only the hackles angle of inclination with regard to the plane of delamination gives useful information, and this information has to do more with state of stress than crack growth direction.

Finally, a change in loading conditions during crack growth could give a change in crack growth direction which might be reflected in a change in hackle orientation in a multi-directional laminate. Thus, it might be difficult to determine crack growth direction from hackles for proportional loading; nonproportional loading and subsequent changes in crack growth direction could probably be accertained from changes in hackle orientation.

her-

ACKNOWLEDGEMENT

This work was performed at Texas A&M University through the support of the Air Force Office of Scientific Research under the direction of Major David Glasgow.

REFERENCES

1. Hahn, H. T. and Johannesson, T., "A Correlation Between Fracture Energy and Fracture Morphology in Mixed Mode Fracture of Composites," presented at 4th International Conference on Mechanical Behavior of Materials, Stockholm, Sweden, August 15-19, 1983.

2. Hahn, H. T. and Johanneson, T., "Fracture of Unidirectional Composites: Theory and Applications," presented at Meeting of ASME, Bostom, MA, Nov. 13-18, 1983.

3. Richards-Frandsen, R. and Naerheim, V., "Fracture Morphology of Graphite/Epoxy Composites," J. of Composite Materials, Vol. 17, March 1983, pp. 105-113.

4. Morris, G. E., "Determining Fracture Directions and Fracture Origins on Failed Graphite/Epoxy Surfaces," in Non Destructure Evaluation and Flaw Critically for Composite Materials, ASTM STP 696, 1979, pp. 274-297.

5. Liecht, K. M., Masters, J. E., Ulman, D. A., and Lehman, M. W., "SEM/TEM Fractography of Composite Materials," report no. AWAL-TR-82-4085, report by General Dynamics, Fort Worth, for Materials Laboratory, AFWAL, 1982.

6. Wilkins, D. J., Eisenmann, J. R., Camin, R. A., Margolis, W. S., and Benson, R. R., "Characterizing Delamination Growth in Graphite-Epoxy," in Damage in Composite Materials, ASTM STP 775, 1982, pp. 168-183.

7. Bascom, W. D., personal communication.

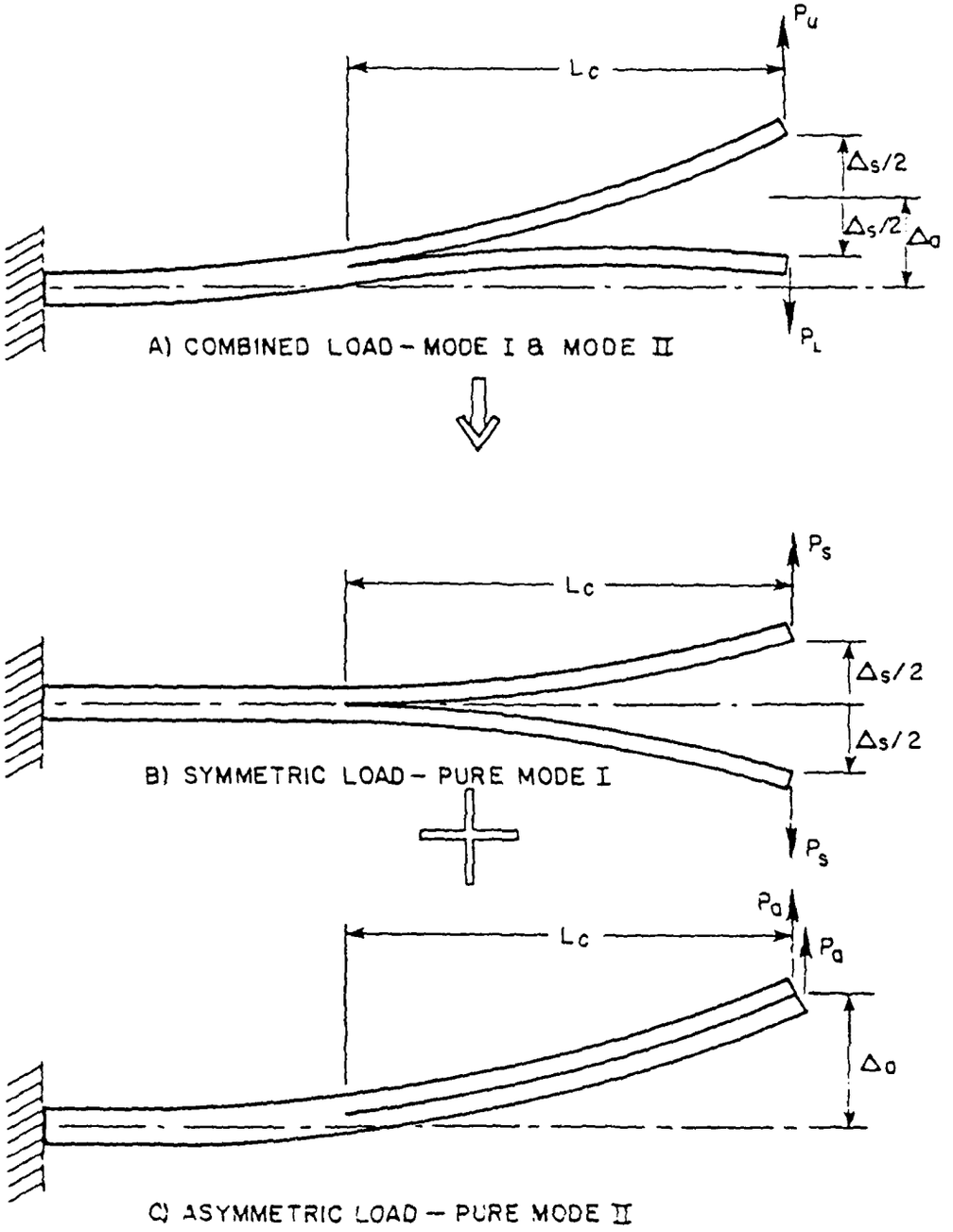


Figure 1. Schematic showing mixed mode test conditions obtained by asymmetric loading of a double cantilevered beam test specimen.

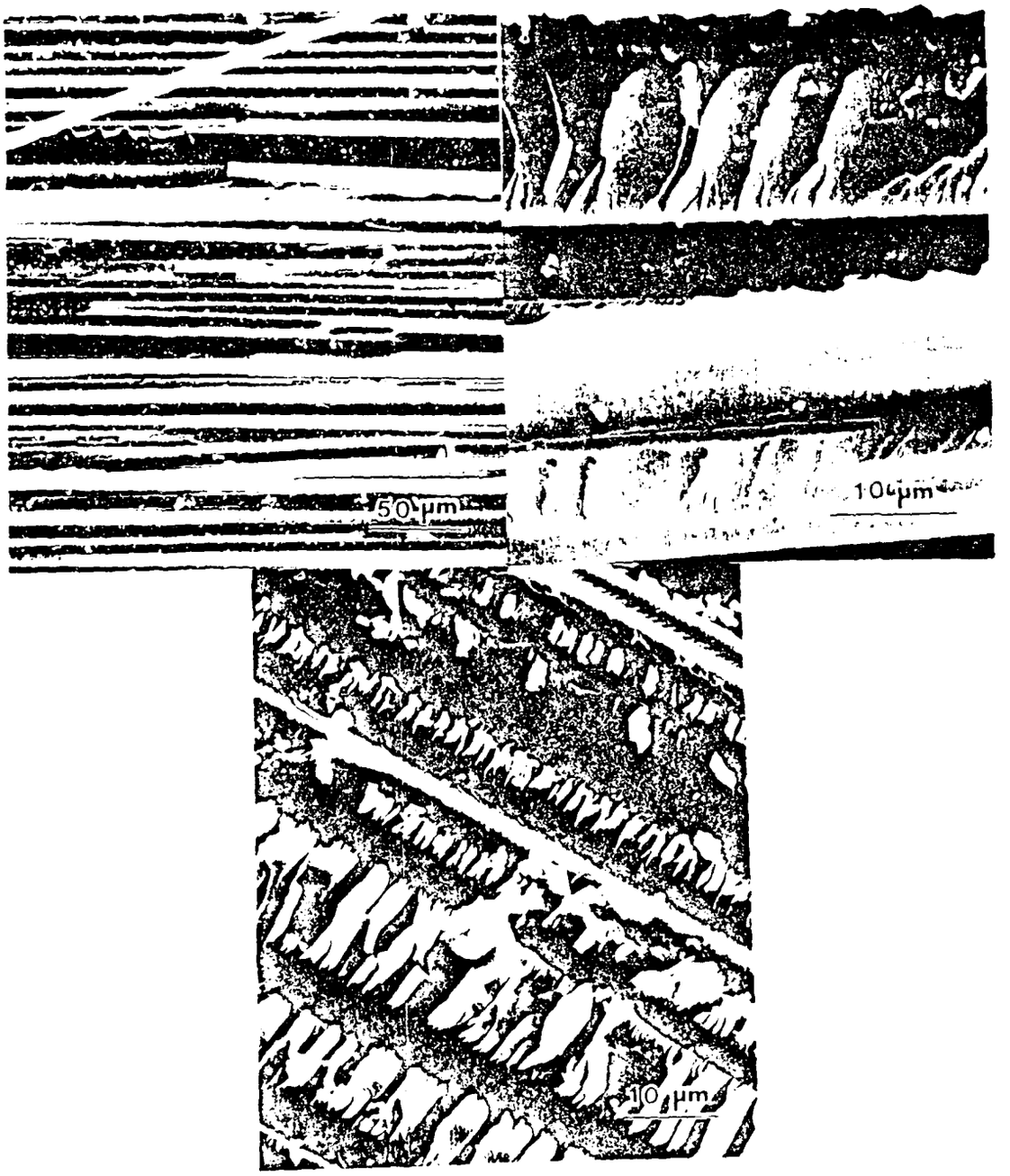


Figure 2a. Fracture surface of AS4/3502 system fractured in mode I conditions (left, 300 x).

Figure 2b. Fracture surface of AS4/3502 system fractured in 43° mode II conditions (right, 4500 x).

Figure 2c. Fracture surface of AS4/3502 system fractured in mode II conditions (bottom, 1500 x).

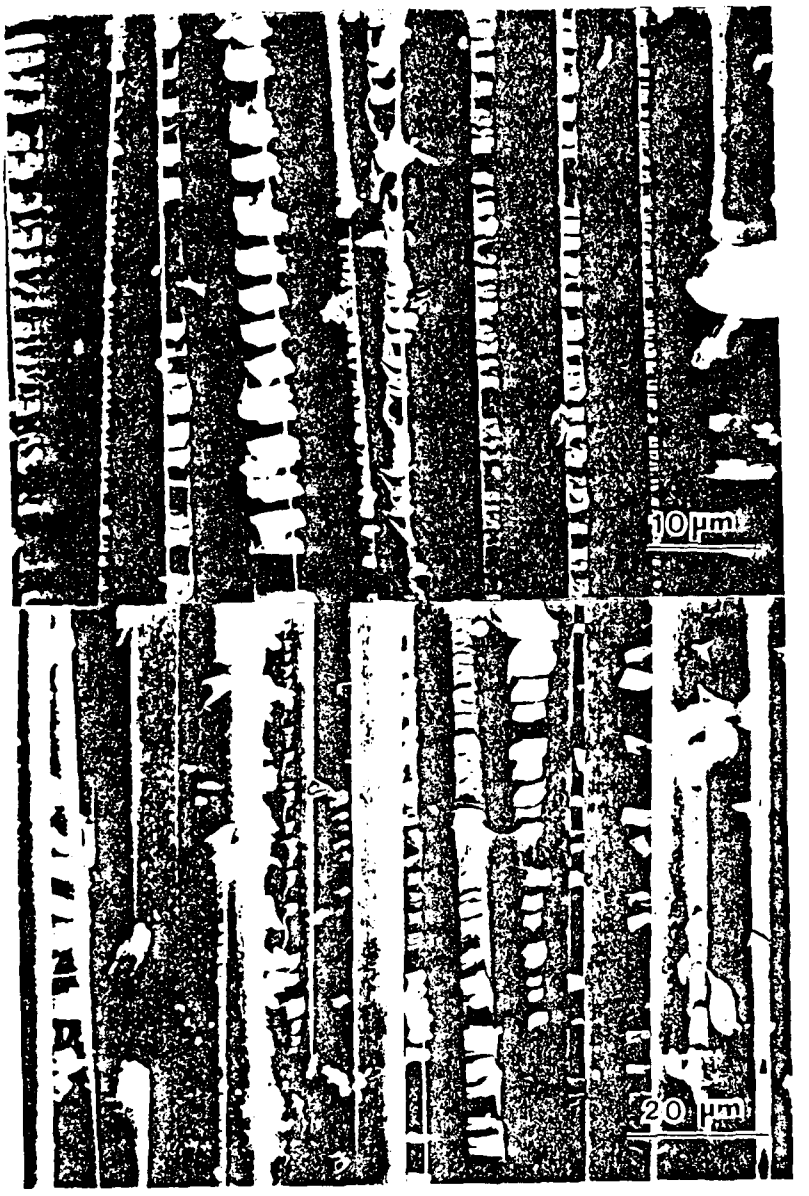


Figure 2d. Fracture surface of AS4/3502 system fractured in mode II conditions showing how on top surface (top, 1500 x) and bottom surface (bottom, 1000 x) the hackles point in opposite directions.

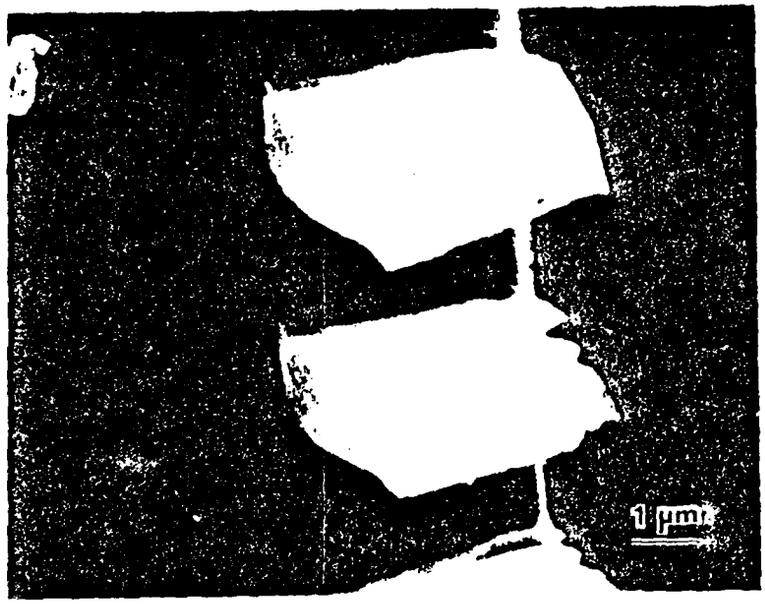


Figure 2e. Enlarged view of hackle in AS4/3502 mode II test showing sigmoidal shape of hackle surface (10,000 x).

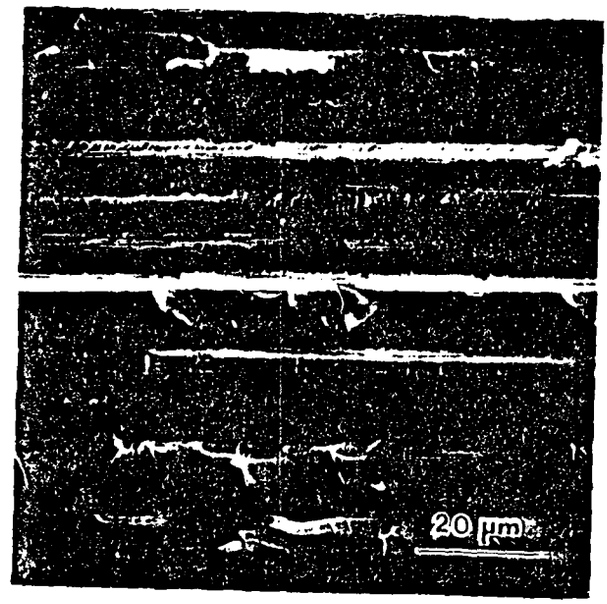


Figure 3. Fracture surface of AS1/3501-6 system fractured in mode I conditions (1000 x).

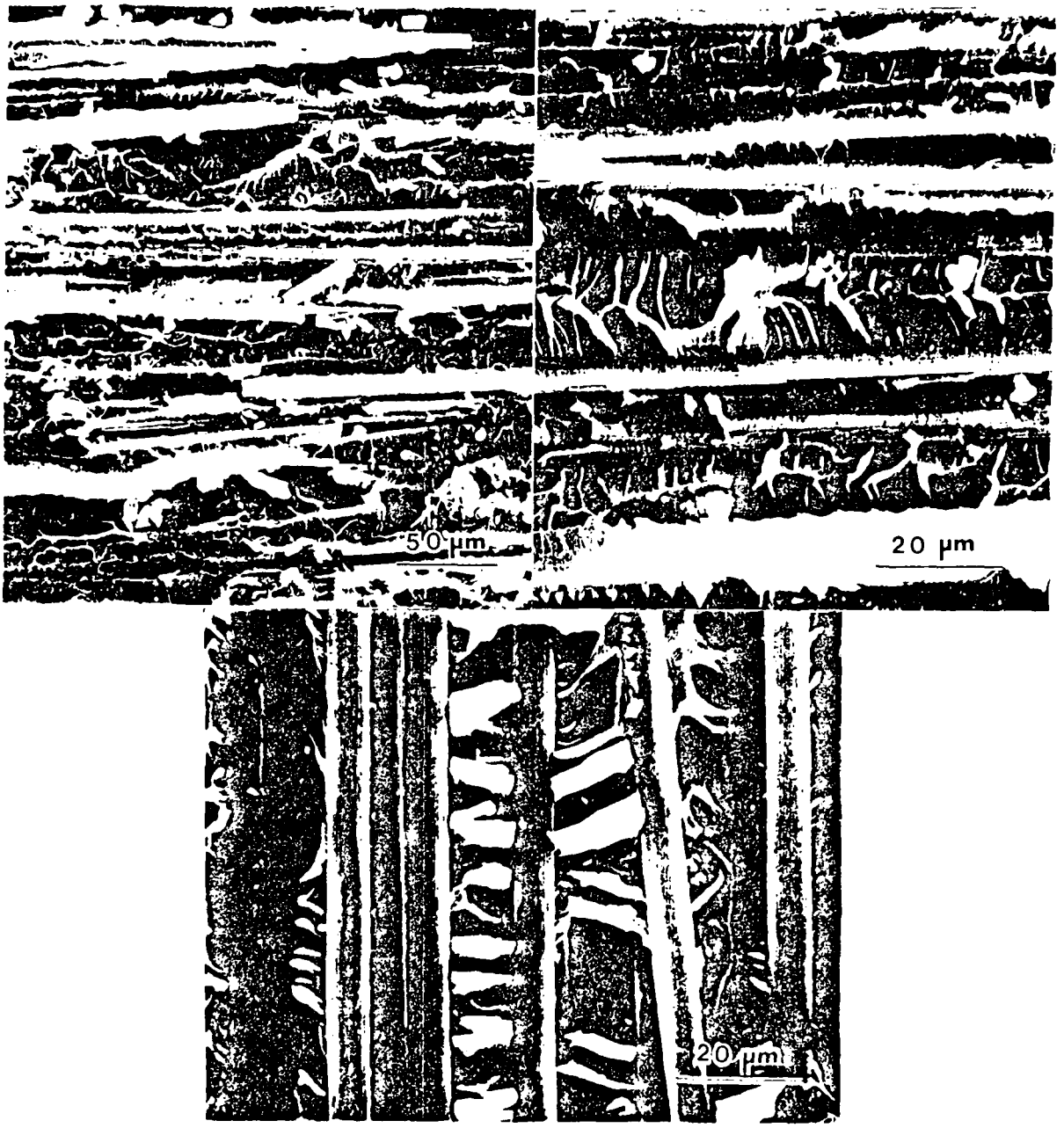


Figure 4a. Fracture surface of Hx205 system fractured in mode I conditions (left, 300 x).

Figure 4b. Fracture surface of Hx205 system fractured in 43° mode II conditions (right, 1000 x).

Figure 4c. Fracture surface of Hx205 system fractured in mode II conditions (bottom, 1000 x).

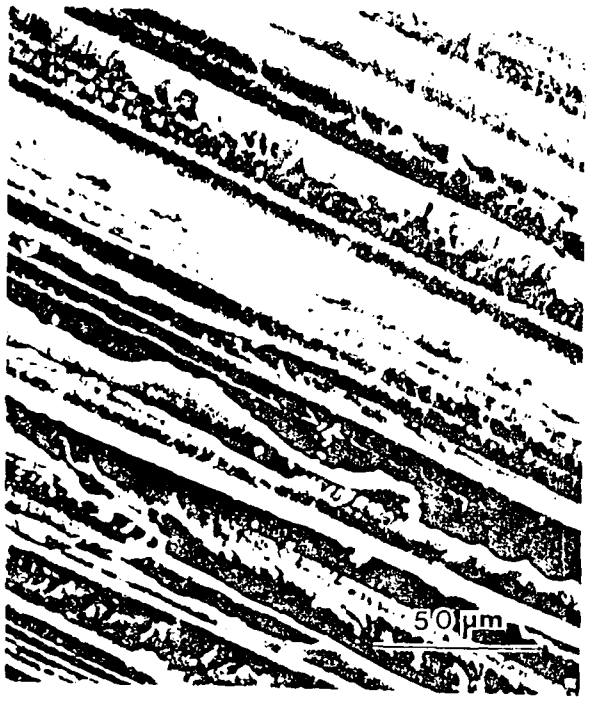



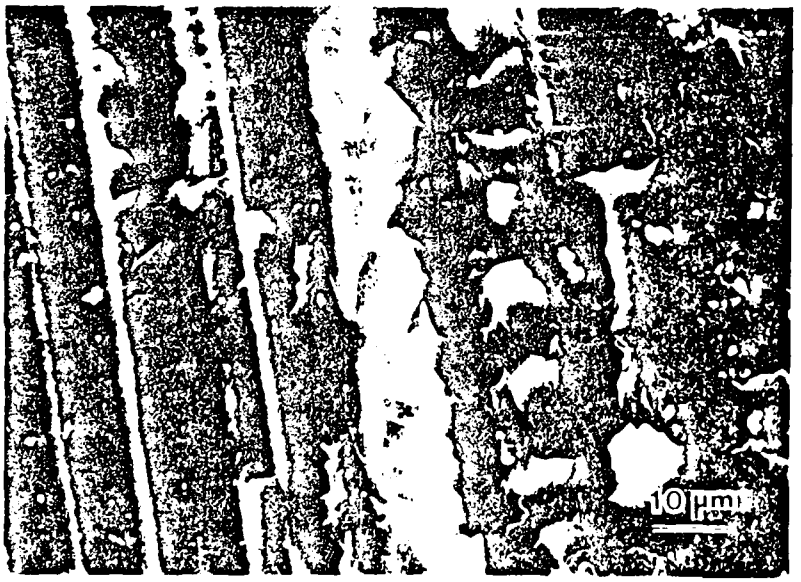


Figure 5a. Fracture surface of Q6 system fractured in mode I conditions (left, 450 x).

Figure 5b. Fracture surface of Q6 system fractured in 43 mode II conditions (right, 1500 x).

Figure 5c. Fracture surface of Q6 system fractured in mode II conditions (bottom, 1000 x).

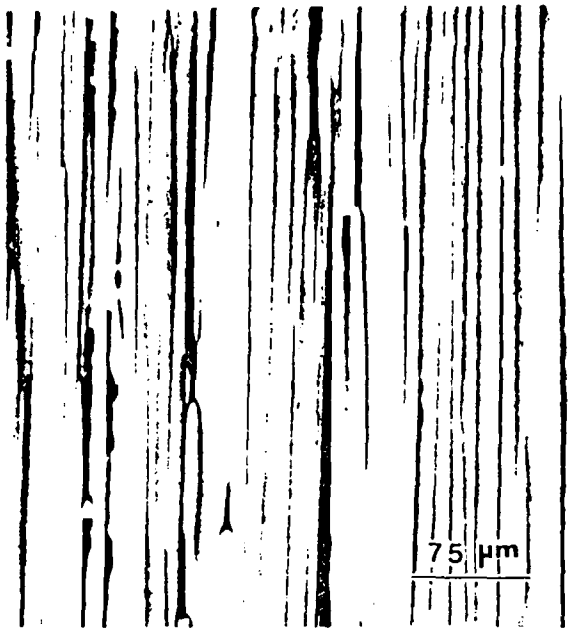



Figure 6a. Insitu delamination of AS4/3502 system (top, 220 x).

Figure 6b. Insitu delamination of Hx205 system (bottom, 1000 x).

END

12-86

DTIC